Methods for improving data acquisition and signal processing for monitoring the ECG

Henry J Dore

Submitted for the degree of Doctor of Philosophy

University of Sussex

September 2022

Declaration

I hereby declare that this thesis has not been and will not be submitted in whole or in part to another University for the award of any other degree.

Signature:

Henry J Dore

Contents

List of Abbreviations:

ADC	Analogue to digital converter
ASIC	Application-specific integrated circuit
AWGN	Additive white Gaussian noise
DWT	Discrete wavelet transform
ECG	Electrocardiogram
EMD	Empirical mode decomposition
EMG	Electromyogram
EPS	Electric potential sensor(s)
FFT	Fast Fourier transform
FRA	Frequency response analysis
GUI	Graphical user interface
HR	Heart rate
HRV	Heart rate variation
IMF	Intrinsic mode function
INAMP	Instrumentation amplifier
MSE	Mean square error
NICU	Neonatal intensive care unit
NNECG	Neonatal electrocardiogram
PO	Pulse oximetry
PP	Peak-to-peak
PPG	Photoplethysmography
PSD	Power spectral density
SPI	Serial peripheral interface
SQI	Signal quality indicator

List of Figures:

List of Tables:

Preface

Abstract

The electrocardiogram (ECG) is a recording of the electrical activity of the heart and is widely used by clinicians as a diagnostic tool and during life-saving resuscitation efforts. The traditional 12-lead silver chloride ECG remains the gold standard in healthcare, despite promising advances in sensor technology and signal processing that have the potential to improve quality and ease of recording.

The primary aim of this research is to improve the data acquisition and signal processing of the ECG. To achieve this, methods were developed to improve the utility and range of applications for non-contact electric potential sensors (EPS). These sensors allow for rapid, high resolution ECG recording and can be incorporated into passive monitoring systems and wearable devices. Dry flexible textile electrodes and hardware/software filtering systems were developed for use with EPS. These were characterised using simulated and pre-recorded ECGs, cardiac phantoms, and real world data through live human recording.

Firstly, dry flexible textile electrodes were developed and characterised for EPS ECG sensing. These electrodes were shown to have the capacity to for the rapid acquisition of high quality ECG suitable for the calculation of heart rate, with an accuracy within ±1 beat per minute, and a 99% beat detection confidence compared to reference electrodes. Secondly, a novel adaptive filtering technique was developed and validated using a novel neonate phantom developed for EPS testing. Using the noise profile from the injection of a known signal, an algorithm for an adaptive ECG filter was generated. This filter was highly effective in removing the predominant mains power line noise that EPS sensors are particularly susceptible to, with average of 22 dB reduction. Additionally, this filtering method introduced no significant alteration of the ECG morphology, with a mean square error equal to that of traditional filtering techniques.

This work advances the development of applications for EPS technology by demonstrating and characterising textile electrodes and novel filtering methods. Textile electrodes allow for the integration of these devices into convenient and comfortable devices, as explored in the proof of concept for a smart ECG sensing mattress for use in the neonatal intensive care unit. The novel filtering techniques displayed here are tailored to the characteristics of EPS sensors, and provide ECG signal quality that can compete with the high standards required in clinical practice.

List of publications

This thesis is based on the work described in the following papers:

1. Conference Poster: *"Neo-Sense: a real time data processing & acquisition unit for monitoring neonatal ECG in the delivery room"* 2019, UK Circuits and Systems Conference (UKCAS), Proceedings. Authors: **Dore H**, Aviles-Espinosa R, Anton O, Rabe H, Rendon-Morales E.
2. Conference Publication: *"Neo-SENSE: A non-invasive smart sensing mattress for cardiac monitoring of babies"* 2019, IEEE Sensors Applications Symposium (SAS), Proceedings. Authors: Aviles-Espinosa R, Rendon-Morales E, Luo Z, **Dore H**, Anton O, Rabe H, Prance RJ.
3. Conference Publication: *"Evaluation of screen-printing techniques for embedding ECG sensors in medical devices"* 2020, 27th IEEE International Conference on Electronics, Circuits and Systems (ICECS), Proceedings. Authors: **Dore H**, Aviles-Espinosa R, Luo Z, Anton O, Rabe H, Rendon-Morales E.
4. Journal paper: *"Characterisation of textile embedded electrodes for use in a neonatal smart mattress electrocardiography system"* 1 Feb 2021, Sensors (Switzerland)21(3):1-20 Authors: **Dore H**, Aviles-Espinosa R, Luo Z, Anton O, Rabe H, Rendon-Morales E
5. Conference Publication: "*Evaluation of a combined approach for denoising ECG measurements using unconventional sensors*" 2022, Computing in Cardiology Conference (CinC), Proceedings. Authors: **Dore H**, Aviles-Espinosa R, Luo Z, Anton O, Rabe H, Rendon-Morales E

Author contributions

The author made the following substantial contributions to the included papers:

1. *"Neo-Sense: a real time data processing & acquisition unit for monitoring neonatal ECG in the delivery room*": Design, construction & programming of 1st NeoSense prototype; presentation of poster at conference; poster main author.
2. *"Neo-SENSE: A non-invasive smart sensing mattress for cardiac monitoring of babies"*: Presentation of paper at conference.
3. *"Evaluation of screen-printing techniques for embedding ECG sensors in medical devices"*: Design & construction of analog front end; Experimental design & testing; data processing & visualisation; paper main author.
4. *"Characterisation of textile embedded electrodes for use in a neonatal smart mattress electrocardiography system"*: Design, construction & programming of 2nd NeoSense prototype; Design & construction of test setup; experimental investigation; data processing & visualization; paper main author.
5. "*Evaluation of a combined approach for denoising ECG measurements using unconventional sensors*": Lead investigator; Experimental work; neonate phantom conceptualisation, design & construction; hardware & software design & fabrication; data processing & visualization; initial author paper (revised later for conference submission).

Chapter 1: Introduction

1.1 Motivation

The first minutes of a child's life outside the womb are fraught with danger. The transition from intrauterine to extrauterine life is an extremely complex physiological adaptation [1] requiring the clearance of fetal lung fluid, the onset of breathing, and rapid changes in blood flow, metabolism, and thermoregulation as the child becomes self-sufficient. Key amongst these adaptations is the delivery of oxygen to the brain. Even mild oxygen deprivation can cause serious and lasting damage [2], and in the most severe cases results in infant mortality. In a study carried out to assess the response to resuscitation of the new born [3], it has been reported that out of 591 births all of which required resuscitation, 30% of the infants experienced some level of brain injury due to oxygen deprivation, of which 30% died in the first week following birth.

Given the many challenges and potential hazards associated with childbirth it is only through the dedication and hard work of clinicians that infant mortality during birth has more than halved since 1990 [4]. Medical intervention is required in around 10% of births and can range from simple stimulation to more severe resuscitation procedures such as positive pressure ventilation and chest compressions [5]. According to the World Health Organization, globally there are 13.5 million resuscitations, and still 4 million newborns are affected by brain injuries and nearly 2.5 million potentially avoidable deaths occur [6].

These interventions are crucial to improving outcomes for newborns and are guided by careful and structured monitoring of vital signs and infant progress using a range of methods. Sensor-based technology for clinical monitoring such as the electrocardiogram (ECG) and pulse oximeter have supplanted the use of manual methods for infant assessment in the delivery room as well as providing continuous post-partum monitoring of vulnerable infants in the neonatal intensive care unit.

From the inception of the ECG at the end of the 19^{th} century to the widespread clinical adoption in the latter half of the 20^{th} century electrocardiogram sensor technology has been constantly evolving and improving. In addition to recording the heart rate, the ECG now serves as a powerful diagnostic tool capable of diagnosing conditions such as abnormal heart rhythms and coronary artery disease, amongst others. This increased functionality is due to incremental advances in sensor and electrode technology, as well as signal processing techniques. ECGs no longer require invasive and bulky electrodes attached to the patient and can be comfortably sensed from the wristband of a smartwatch. Modern ECGs also employ sophisticated digital data acquisition at high frequency and resolution displayed on smart devices and interpreted by automated algorithms - a far cry from hand annotated analog paper and ink.

This thesis presents a range of methods for improving the speed, comfort and quality of ECG acquisition, and increasing the resultant signal quality. These include the use of novel electric potential sensing technology, comfortable & conformal textile electrodes, and novel filtering techniques. The advances presented here are applied in the context of the development of a smart mattress concept for the monitoring of the neonatal electrocardiogram (NNECG).

1.2 State of the art

ECG sensing is a broad topic that touches on many different disciplines and research areas, beginning with the theory of biopotential monitoring and clinical practice, then encompassing hardware considerations such as electronics and materials science, finally leading to information technology fields such as digital signal processing and AI powered ECG classification. A complete state of the art of ECG technology would be no small task, therefore the core of this work largely encompasses two key subject areas:

- Textile electrodes

- ECG signal processing

The choice of these two subject areas came from the development of a smart mattress ECG system in the formative stages of this PhD (see section 1.3 for more detail). Work on this prototype system identified areas and methods where there were exciting and novel opportunities for investigation, and strongly influenced the direction of this research.

There now follows a description of electric potential sensing as a novel technology, and in depth description the two key subject areas, including the state of the art, the identification of gaps in knowledge and a justification for further investigation considering the previous works.

1.2.1 Electric potential sensing

The traditional silver chloride electrocardiogram is undoubtably a powerful diagnostic and monitoring tool, but just as the ECG improved upon the stethoscope for early cardiac assessment, so other novel sensor technologies can offer benefits and overcome the limitations of previous devices and techniques. The morphological variation between the adult and infant ECG as well as the potential for injury and infection involved with electrode attachment and interface gels have led to interest in a range of novel sensors for recording the ECG in infants and neonates. One such candidate is the electric potential sensor (EPS).

The electric potential sensor is a non-contact sensor that measures spatial electric potential. The fundamental physical theory behind its operation is well described elsewhere [7], but a short electrical description follows. Figure 1 shows a simplified structure of the EPS:

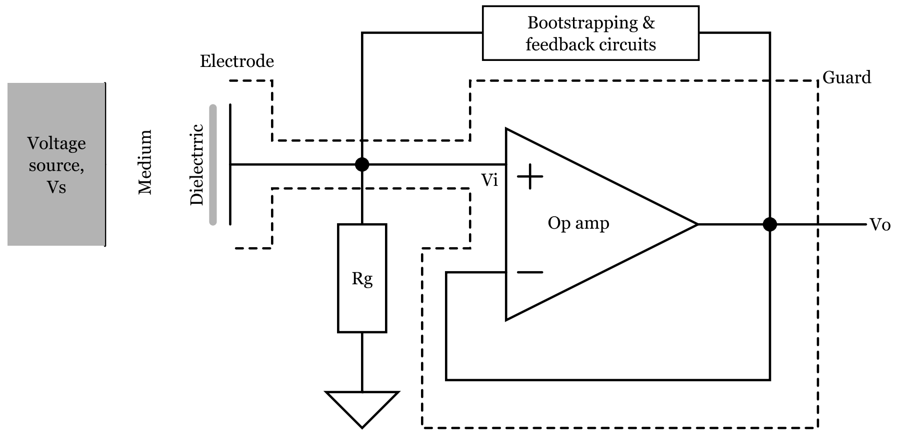

Figure 1: The electric potential sensor

The EPS is an active sensor based around a high accuracy electrometer grade operational amplifier (op amp). This op amp is arranged as a voltage follower, and serves as a high impedance input for the output of an insulated electrode. The high input impedance of the op amp causes the voltage at Vo to be a close approximation of the ambient electric potential at Vs. The insulated electrode measures displacement current, as opposed to traditional ECG electrodes that measure conduction current through a conductor. As the input electrode is insulated this sensor operates in non-contact mode, where no charge current is applied. Whilst the active portion of the sensor is insulated, a passive reference electrode in contact with the patient's skin is employed for voltage referencing to the EPS sensor.

High input impedance active sensors such as these have been studied in many forms since the 1970s [8]. These early examples used stainless steel conducting electrodes, but later implementations moved towards using insulated electrodes, such as those published by Richardson [9], whose work was of particular interest to NASA [10] who were keen to experiment with novel and less invasive astronaut monitoring systems. Later insulated high impedance active electrodes were proposed for use at nonconducting interfaces such as in severe burn patients [11] where petroleum-based burn ointments prevented the use of traditional ECG recording.

The modern EPS device is a result of the incremental advances in electronics and semiconductor research and fabrication improvements. Guarding, bootstrapping and active feedback techniques are employed to improve the input characteristics and sensor performance. By way of comparison the Richardson sensor had an input resistance of 4 GΩ, and capacitance of 5000 pF whereas the EPS has 20 GΩ and 15 pF respectively [12]. EPS tailored for biosignal recording exhibit a flat phase response and a flat amplitude response in the band 0.5 to 500 Hz in contact mode as shown in Figure 2 (reproduced from [13]):

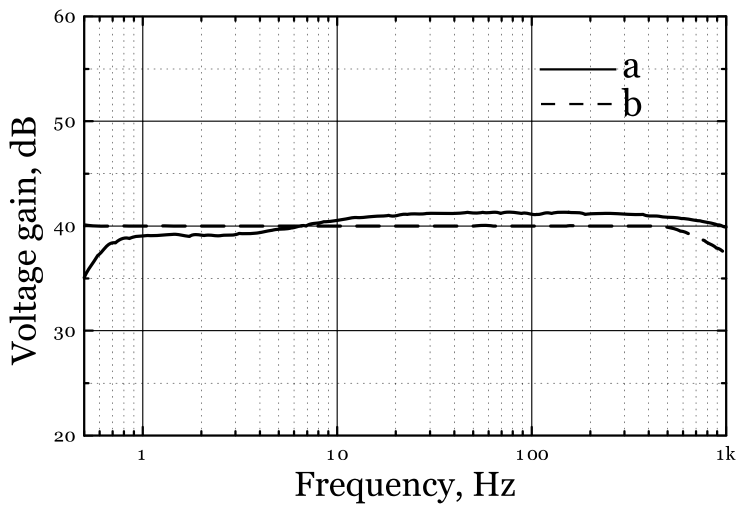

Figure 2: Typical measured frequency response plots for the electric potential probes for (a) remote off-body and (b) contact on-body sensing

The majority of the ECG signal power lies in the range 0-40 Hz, as shown in Figure 3:

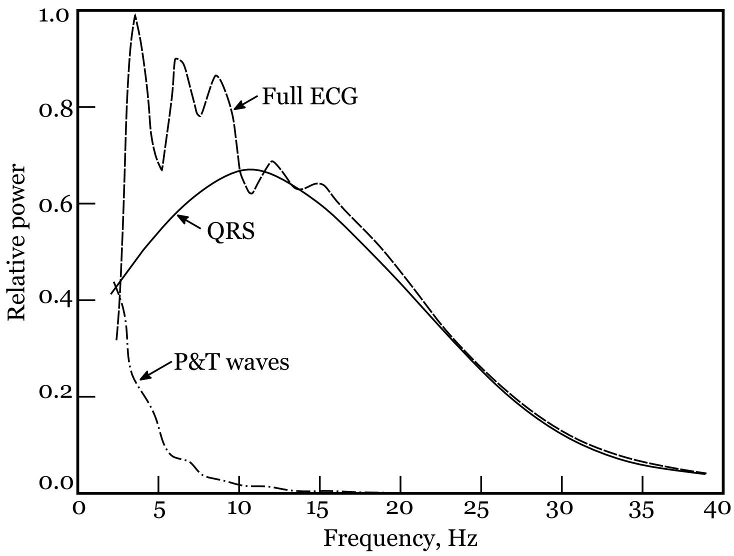

Figure 3: The components of the ECG in the frequency domain, reproduced from [14]

This gives these sensors favourable frequency and phase characteristics suitable for the measurement of the ECG, being within the bandwidth of the majority of the ECG signal power.

Although significant clinical trials have been performed with these sensors in adults [15] and infants [16], they have not achieved widespread adoption. The medical community is wisely reticent to adopt new technology, especially in critical care applications, without the most rigorous demonstrations of clinical excellence and a device's suitability, reliability and safety [17]. Recent interest in eHealth home monitoring driven by connected smart devices has renewed interest in novel sensor designs, although regulatory approval for such devices falls under the less stringent categories for low-risk fitness monitors [18]. Any ECG devices based on EPS technology that would be used to make medical decisions would require the most rigorous proofs of efficacy and the highest levels of regulatory scrutiny.

In operation ECG systems employing EPS sensors are generally more susceptible to noise than traditional ECGs using AgCl electrodes. Large capacitive coupling impedances, in the GΩ range for ECG frequency ranges (typically 0.5 to 250 Hz), make the signal prone to corruption with ambient environmental noise, predominantly 50/60 Hz powerline interference which couples to the bulk mass of the body [19]. This form of environmental interference can also include the body's electrical activity in response to a nerve's stimulation of the muscle, known as the electromyogram (EMG). Examples of two common sources of EPS noise are shown in Figure 4:

a)

b)

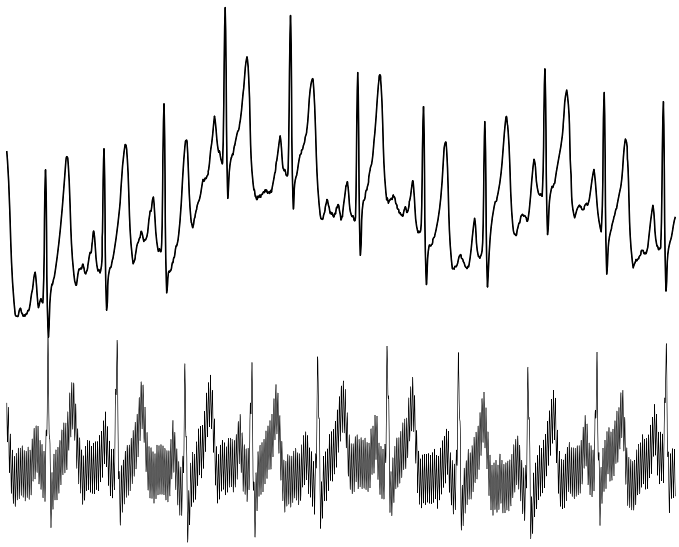

Figure 4: examples of a typical noisy ECG recorded by EPS sensors for: a) baseline wander, b) 50 Hz power line interference

Ambient environmental noise presents as frequency specific noise at an amplitude which can completely occlude the ECG signal in the worst cases, as seen in Figure 4b. Additionally, EPS sensors are often integrated into garments or wearable technologies, to leverage the benefits of non-contact and electrolyte free sensing, and so are particularly susceptible to motion artefacts (MA). These are caused when the patient's body moves in relation to the sensor, either from physical activity (running, walking etc.) or simply from the motion of the chest in the process of breathing. MA interference in EPS ECG recordings presents as a large baseline wander, as seen in Figure 4a. At small amplitudes this baseline wander can be used to determine the breathing rate of the subject, but in the cases of large amplitude shifts this will saturate the amplifier of the EPS device and cause a loss of signal. As shown in Figure 4 the amplitude of both the baseline wander and the 50 Hz noise can easily occlude the ECG signal of interest. Whilst the R peak feature is still visible, MA interference causes the amplitude threshold of the peak to vary which can affect HR measurements. For the power line interference, the amplitude of this noise can often exceed that of the P and T waves, and the Q & S features of the QRS complex, obscuring these features and making this signal unsuitable for diagnostic purposes. Additionally, the rapid successive peaks of the 50 Hz noise can be registered as R peaks by HR calculation software, reducing the accuracy of RR measurements and therefore giving inaccurate HR readings.

In order to extract the small biosignals from these much larger noise components EPS devices can be used in pairs with a common ground reference electrode, as seen in Figure 5:

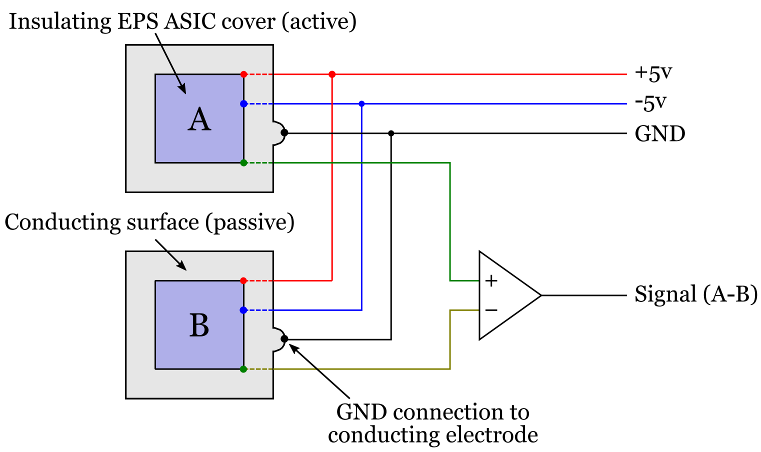

Figure 5: Connections for hybrid mode operation of the EPS

EPS are application-specific integrated circuits (ASIC) in a plastic surface mount package. 4 connections are present on the ASIC for a bipolar power supply (+5v and -5V), a voltage signal output and a ground. The term "hybrid mode" comes from the use of both insulating and conducting electrodes. In Figure 5 the insulating EPS ASIC cover is a dielectric material covering the active sensor is shown. There is an additional passive electrode in contact with the patient's body and connected to the system ground that acts as a ground reference for zero potential. The signal from both sensors is fed into an instrumentation amplifier (INAMP). These devices ensure high accuracy and stability by the use of input buffer amplifiers, providing low noise and drift, and high open-loop gain & input impedance. The subtraction of the two EPS signals reduces the noise common to both sensors, providing an initial signal filtering [7]. Cardiac readings from different areas have different morphologies, but the noise (particularly the power line noise) is considered to be homogenous across the body, therefore the noise is removed but not the ECG signal. In an ideal scenario the subtraction of the two EPS sensors would provide a completely clean ECG signal, with only the morphological differences due to sensor placement providing the ECG trace but this is not sufficient alone to provide a clean ECG signal. Differences in placement of the sensors, coupling and frequency/amplitude response characteristics due to manufacturing variations lead to differing levels of noise and signal in each sensor, therefore further signal processing is required in the form of analog and digital filtering. In order to perform this subtraction operation, the individual sensors must share a common system ground, hence the need for the reference ground electrode. This common ground is also required as zero potential for analog filtering circuitry. These electrodes do not require interface paste like a traditional AgCl electrode, as they do not carry signal information [20], so they can be made of conductive flexible or textile materials to improve conformity and comfort, as described in the next section.

Operating as a transducer to convert displacement current into electron current, the EPS works in non-contact mode as an insulated electrode, not requiring electrical contact with the skin. Whilst it has been shown that these sensors are sensitive enough to detect the perturbation in the ambient electric of a person walking on the other side of a brick wall, or a droplet of water at 1 m distance [21], the voltage output of the EPS sensor is directly proportional to the distance from the source. It has been shown they have the capacity to record respiration and heart rate information across a 40 cm air gap [22] but the optimal mode for high resolution EPS ECG recording is in so called “hybrid” mode, as introduced in Figure 5. The close contact of the sensors with the patient's body minimises the sensing distance therefore improving signal to noise ratio and the addition of a common ground reference electrode enables signal subtraction and filtering. In order for a fully realised EPS system to be comfortable to wear and quick and easy to apply, a flexible electrode without a chemical paste or gel electrolyte is preferable as this reference electrode.

1.2.2 Textile electrodes

Dry and flexible electrodes have seen a resurgence in development in the last decade, driven by interest from the wearable electronics market. The market for wearable electronics is expanding rapidly and is projected to grow from $115 billion in 2021 to $265 billion by 2026 [23]. Whilst this is largely driven by consumer electronics such as fitness trackers and smartwatches, these are more often being integrated into clinical practice for diagnosis and biosignal monitoring [24]. The implications of this huge investment in research and development for novel clinical devices therefore cannot be understated.

The electrical activity at the electrode-skin interface consists of the interaction between the electron charge transport of the measurement system (in this case the ECG front end) and the ionic charge transport of the human body, which combine to form a half cell [25]. This half cell consists of an electrode (the conductive material of the electrode) and an electrolyte. From this half cell a potential difference is formed by charge redistribution due to the movement of ions into solution in the electrolyte. The main difference at the electrode-skin interface between the wet and dry electrode is the electrolyte. For wet electrodes the electrolyte consists of the applied electrolytic paste and the patient's skin (the epidermis and dermis layers). For dry electrodes the electrolytic paste is omitted, and the electrolyte consists of the patient's skin and a relatively poorly defined layer consisting of skin, hair, air gaps and sweat in various concentrations and configurations depending on a multitude of factors. The models of the two systems are described in Figure 6:

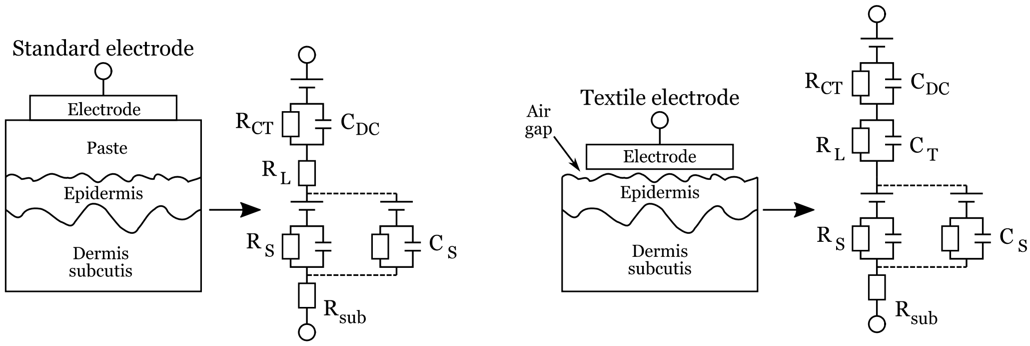

Figure 6: Skin electrode interface for Standard AgCl electrode (a) and Textile electrode (b), reproduced from [25]

In Figure 6a the homogenous electrolytic paste layer is modelled as a simple resistance, R_L, and therefore the impedance for this stage is also R_L, as Z=R for a perfect resistor with no reactance. In Figure 6b the contrasting dry electrode model show a capacitive component modelled as C_T as the absence of the electrolytic paste layer causes an air gap. Dry contact with the skin in the presence of sweat or other skin contaminants is modelled as the conductive path R_L in parallel with the capacitance C_T. For ECG recording the key difference between dry and wet electrodes is the impedance of the skin electrode interface. This impedance can be calculated for the models shown in Figure 6 above as Equation 1 and Equation 2:

$$Z_{standard} = \frac{R_C T}{1 + j\omega R_{CT} C_{DC}} + R_L + \frac{R_S}{1 + j\omega R_S C_S} + R_{SUB}$$

Equation 1

$$Z_{Textile} = \frac{R_C T}{1 + j\omega R_{CT} C_{DC}} + \frac{R_L}{1 + j\omega R_L C_T} + \frac{R_S}{1 + j\omega R_S C_S} + R_{SUB}$$

Equation 2

Although the capacitive and resistive properties of human tissue are well studied [26, 27] measurement of these individual components is not generally performed for the skin electrode interface due to instrumentation difficulties. The capacitance of the air gap C_T is highly variable, being subject to many different variables including skin composition, sweat, ambient humidity, subject movement, and contact pressure/air gap. Coupling capacitances of 10 pF to 200 nF and resistance from 1 GΩ to infinity are typical of this component [28]. Therefore, the skin electrode interface is considered as an ensemble, with electrode impedance being specified as a resistance in parallel with a capacitance as “R Ω || C F”. Considering typical values for the complete skin electrode interface for wet electrodes as 100k Ω || 10 nF, and dry electrode as 1M Ω || 10 nF (as measured in [29]) the impedance of dry and wet electrodes can be estimated using Equation 3, the results of which are shown in Figure 7:

$$\frac{1}{Z} = \frac{1}{R} + j\omega C, where\ \omega = 2\pi f \quad \therefore \quad |Z| = \frac{1}{\sqrt{\left(\frac{1}{R}\right)^2 + (\omega C)^2}}$$

Equation 3

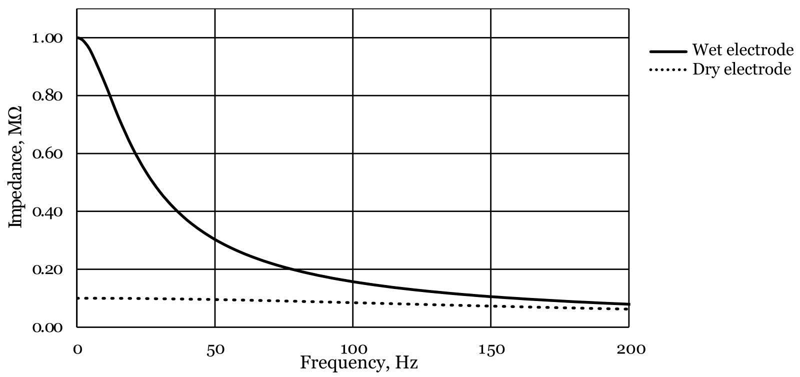

Figure 7: Comparison of typical wet and dry impedances for EPS in contact mode

The majority of the power of the ECG is in the frequency band 5 to 40 Hz, therefore in the region of interest in Figure 7 the impedance of dry electrodes is between 3 to 10 times that of the wet electrodes.

As previously stated, EPS style and capacitively coupled sensors perform best in hybrid mode, with a common ground reference. There is considerable interest in the use of comfortable, conformal textile materials for these ground references. There is a vast range of materials available for this purpose, from the simplest types of threaded conductive textiles to exotic micro/nano structures. Here follows a description of various implementations of dry flexible electrodes as ground reference for an EPS style/capacitively coupled biosensor, and potential applications for this technology.

There are many implementations of textile electrodes in standalone electrode/sensor packages (i.e., not integrated into a device or garment), and these studies tend to focus on a single property of the textile. One detailed investigation considered the transmission characteristics of a range of commercially available conductive textiles though paper and cotton [30]. This study employed an isolating Faraday cage to remove the predominant 50 Hz noise that EPS style sensors are susceptible to, showing detailed transmission characteristics at a range of frequencies for their sensor design, and later demonstrates the suitability of the sensor with a human volunteer. Other studies focused on surface resistivity [31], nothing that low surface resistivity is preferable in textile electrodes, and a conductive textile woven with stainless steel wire was tested with a robust surface resistivity test regime (AATCC Test Method 76-2005) and gave a value of 1.25 Ω/sq, in line with that of typical AgCl electrodes. Another study considered the degradation of SNR on a range of textile electrode materials after 50 cycles in a domestic washing machine [32]. Aside from these granular investigations into specific properties of materials for textile electrodes, application focused works tend towards considering the textile electrode in a specific application. These application focused studies take into account multiple material considerations as the specific application requires and tend towards a broader evaluation of the textile electrode in terms of received signal quality and signal quality indexes, rather than individual characteristics (such as resistivity) which can be difficult to quantify when the system contains real biosignals and the variations of human physiology.

One common application of textile electrodes for capacitive ECG is in the form of a belt or band. This design is simple to produce, and is often used as the first step after standalone electrode validation, and as proof of concept in a human volunteer before moving towards a more complex application. The use of an elasticated belt or band holds the sensors in place on the subject, reducing the relative movement of sensor and skin therefore reducing movement artefact and baseline wander in the ECG signal. An example of such a belt developed for use with EPS sensors is shown in below:

Figure 8: Flexible elasticated belt developed for use with EPS sensors with conductive fabric reference electrodes

A range of materials have been investigated in this form. Embroidered silver/titanium electrodes were integrated into an ECG belt with a novel humidified design [33] where low impedance and the effect of water charging provided high quality ECGs at rest and in motion of the subject. Conductive Ni/Cu covered foam has also been integrated into a capacitively coupled ECG belt to be worn around the chest [34]. In this implementation the foam can deform, adapting to the curvature of the chest and proving a more solid mechanical as well as electrical connection. Often these belt/band implementations are presented as a first step towards implementation of ECG sensors into a garment. By way of example, graphene clad nylon [35] has been shown to be suitable for use as both sensing and reference electrodes in wrist or neck bands, with the next logical step being the implantation of these electrodes in the collar of a shirt of the cuff of a jacket.

Many fully realised wearable implementations of capacitively couple ECG systems have been presented in literature in the past decade. An early example of this is shown using capacitively coupled graphene clad nylon textile electrodes integrated into a vest with onboard data acquisition and telemetry via Bluetooth [36]. This implementation employs a "large breathable reference electrode" made of stretchable conductive yarns performing as a conductive reference in direct contact with the skin. The reference electrode is also shown to work capacitively through a layer of cotton (when the vest is worn over other clothes) albeit with increased movement artefact noise. This device is aimed at recording the ambulatory ECG, potentially as a sport tracker, so priority is given to the robustness against MA noise, however other wearable implementations seek to target the clinical ECG market. A 12 lead capacitively coupled ECG using commercially available conductive fabric (Shieldex™) is presented in [37]. This aims to recreate the complete 12 lead ECG (the gold standard ECG, widely used in diagnosis of arrythmia) with capacitively coupled active electrodes instead of the standard AgCl electrodes. This implementation showed extremely high correlation for PQR and S waves (correlation > 0.9) and reasonable correlation for P & T waves (correlation approx. 0.8) across 3 different subjects in the lying (supine) position, sitting and whilst walking. This particular work is strong evidence of the suitability of capacitively coupled ECGs for clinical diagnosis.

As well as employing textile electrodes in wearable technology there is a branch of research that aims to opportunistically monitor patients in situations where they will likely be at rest for a period of time. Implementing ECG sensors in furniture, where people will routinely sit without movement, allows for periodic ECG recording which can be compared against baseline values to check for arrythmias or other morphological changes that may indicate a health problem, and therefore provide data to guide intervention. Recording the ECG from a seated patient has the advantages of reducing or eliminating MA noise, and providing a likely location for the position of sensors for optimal ECG recording. An early version of such a system employed ECG sensors implanted into a seat using a copper mesh electrode [38] and later improvements in conductive textiles lead to the development of an armchair with woven silver and polymer fibre electrodes [39] providing greater comfort and washability.

This concept of monitoring the ECG when the patient is at rest with sensors embedded in furniture is exemplified by the concept of a smart mattress. Capacitively coupled active electrodes can be embedded in a mattress (or mattress topper), and the ECG can be acquired through the back from a patient lying in the supine position. In a clinical setting this can allow for constant, long term monitoring of the patient without the need to attach the typical 12 lead AgCl ECG electrodes, increasing patient comfort. This technology also allows for the ECG recording in patients where attaching such electrodes might cause damage or infection to the skin, particularly in the case of burn victims and neonates where the skin is delicate.

One implementation of this concept is described in [40] where silver electrodes printed on PES knitted substrate are demonstrated as a complete continuous monitoring system for a hospital visit. To begin, sensors are embedded in a stretcher to record ECG at admission, then in a mattress for monitoring during treatment & recovery, and finally in a hospital wheelchair for monitoring during patient discharge. The smart mattress concept can also be shown to derive the respiratory rate of a patient from the baseline wander of the ECG caused by the movement of the patient's abdomen during breathing [41] using a Ni/Cu conductive fabric electrode, detecting the frequency and also cessation of breathing which could be used to raise an alarm. Outside of the hospital, the smart mattress concept is also well suited to a home monitoring system, as it is unintrusive and requires no external sensors to be connected.

The smart mattress concept has clear benefits for polysomnography (sleep studies). As the patient is generally not in motion for the majority of the sleep period, high quality ECG as well as the respiration rate (as described in [41]) can be recorded. This has led to such studies as the comparison of heart rate variability during sleep [42], where the different sleep stages (rapid eye movement, light, deep, etc.) can be derived from the capacitively measured ECG. The susceptibility of the capacitively coupled ECG to movement artefacts cannot be ignored, even during sleep, and it has been shown that large movements such as position change can cause disconnection events (due to the capacitively coupled ECG becoming saturated), and even small subconscious limb movements will adversely affect the signal quality [43, 44].

The deformation of the ECG signal by movement of the subject to different sleeping positions has an unexpected benefit, as the capacitance of the sensor under load from a patient lying on top of it increases, and in a multiple sensor array this information can be used to derive the orientation of the subject [45]. This positional data could then be used to decide which sensors in a multiple sensor array were located in the optimum position to record the ECG. As the subject might lie in one of several positions during sleep, the problem of positioning the sensors correctly for the patient must be addressed. Some approaches favour multiple sensors distributed over a large area such as in [46] where an array of 128 capacitively coupled ECG sensors were embedded in a mattress, and a sensor selection algorithm developed to select the optimal ECG signal. Another method to tackle this problem was to vary the pattern of the textile electrode on the mattress to optimise coverage [47].

In the case of the newborn infant movement is minimal. The average newborn spends about 16 hours a day asleep, and when awake their movements and activity are small and uncoordinated, being mainly involuntary reflex responses. There is, therefore, considerable interest in the use of the smart mattress non-contact ECG in the neonatal intensive care unit (NICU), as well as in the delivery room. A capacitive

ECG sensing array embedded in a neonatal mattress with a conductive textile reference electrode was tested with 15 preterm neonates in the NICU [48]. This study showed that when good sensor coverage was attained the results for instantaneous heart rate were largely in agreement with traditional ECG in terms of sensitivity and positive predictive value, and that the ECG signal shape was described as “encouraging”. As with previous mattress implementations described above, the smart mattress for neonates has also been shown to be capable of determining the preterm infant sleep states using ECG and HRV features [49]. Another application for capacitive ECG sensing with neonates using electrodes inserted into infant underwear [50] showed promising ECG waveforms but with little spectral analysis and no comparison to an AgCl ECG it is difficult to quantify the signal quality.

1.2.2.1 Conclusions and knowledge gap 1

Comfortable, non-invasive, diagnostic standard, high-resolution ECG can be provided by employing EPS sensors as described in [37]. The potential for non-contact ECG recording is of particular interest to the paediatrician, where traditional AgCl ECG with electrolytic pastes and adhesive electrodes could cause damage to delicate infant skin [51]. Optimal EPS operation for ECG acquisition is in hybrid mode with the use of a common reference electrode. By employing dry flexible textile electrodes as this common reference electrode, EPS sensors can be integrated into garments or devices for HR acquisition and ECG recording.

This suggests that EPS sensors with a textile reference electrode could form the basis of a smart mattress system. Drawing on sources described in section 1.2.2 above and others, the current state of the art in smart mattress systems and prototypes is described in the table below:

Reference	Description	Sensing technology	Notable features	Limitation
Peng et. al. 2021 [52]	Flexible electrode based smart mattress	Capacitive ECG	Wireless Bluetooth transmission. ECG recording in multiple positions.	Tested in adults only
Atallah et al. 2014 [48]	Neonatal mattress with integrated sensors	Capacitive ECG	Multiple channel, adaptive selection. ECG and vectorcardiogram reconstruction.	Signal dependent on subject position
Takano et. al. 2018 [53]	Integrated fabric-sheet sensing scheme	Fabric-sheet unified sensing electrode inc. capacitive ECG	Additional respiratory and ballisto-cardiographic sensing from a single sensor.	Low sensitivity and accuracy in ECG. Adult testing only.
Werth et. al. 2019 [49]	Incubator mattress with eight capacitive sensors	Capacitive ECG	Sleep state determination from heart rate variability analysis.	Small study size. Susceptible to noise.
Joshi et. al. 2019 [54]	Bedding embedded sensors	Thin film pressure sensors	Ballistographic analysis robust to noise.	Respiration only, no ECG.
Cay et. al 2022 [55]	E-Textile sensing system for NICU monitoring	Piezoresistive	Embroidered signal traces.	Respiration only, no ECG.

Table 1: comparison of current smart mattress prototypes

Investigations such as that described by Peng et al. [52] show strong results albeit with limited signal quality assessment and a focus on the adult ECG. The large surface area allowed for high quality ECGs to be recorded in a range of subject positions. Takano et. al. 2018 [53] describe a similar device with a mattress integrated capacitive ECG, ballisto-cardiography and respiratory sensor. These three bio measurements are taken from a single large sensor, again allowing for large variations in subject position. This device is also tested using an adult volunteer so the particular difficulties in recording the infant ECG are not explored, particularly low signal amplitude and therefore low signal to noise ratio (as the standard background ECG noise is generally ubiquitous).

Smart mattress implementations for use with newborns are more rare in literature. The results of a previous smart mattress systems described by Atallah et al. [48] whilst extremely high quality, only considered one material for the textile electrode, and did not aim to characterise this material (referred to only as "a conductive textile") or optimise signal quality by the choice of material. Further work on this device leads to the implementation described in Werth et. al. 2019 [49]. Here the high resolution ECG readings allowing for extremely accurate heart rate variability analysis, and the subsequent determination of sleep state from multiple infant subjects. These devices, despite having multiple channel adaptive sensor selection are still susceptible to external noise. Another key work in the area of capacitive ECG sensing for newborns is the device proposed by Kato et al. [50] which, by contrast, shows good textile material consideration and characterisation, but is not a complete system and lacks a human trial.

The devices described in Joshi et. al. 2019 [54] Cay et. al 2022 [55] do not record the ECG, however these are included in the smart mattress category as they integrate simple and affordable piezoresistive and thin film pressure sensors into neonatal mattresses. Such techniques would be relatively simple to integrate into capacitive

ECG mattresses to provide additional patient information at little extra cost or complexity. Notably, the work by Cay et. al. includes a well characterised and described integration of embroidered sensors with conductive textile power and signal traces. Such techniques are key to the construction of a conformal and compliant mattress that is safe to use with infants.

The shortcomings of these works describe a gap in knowledge, where a single proposed work could contrast and characterise the choice of material for a textile reference electrode within the larger context of a complete smart mattress prototype aimed specifically at newborns. This research area forms the first half of this thesis.

1.2.3 ECG signal processing

The electrical activity of the healthy human heart is a repeating analog continuous time signal. The earliest electrocardiograms recorded this data using arc lamps gradually exposing a complicated arrangement of moving photographic plates [56]. The next major developments were the first tabletop versions of Einthoven's string galvanometer (1900s) were large bulky machines weighing in excess of 250 kg [57] but were rapidly superseded by portable suitcase devices such as those manufactured by the Cambridge Scientific Instrument Company in the 1930s [58], the new devices weighing around 10 kg and at a fraction of the cost, and allowing for the recording of the ECG by ink printing onto a paper reel. This trend towards smaller devices is epitomised by the ubiquitous Holter monitor, a device weighing less than 1 kg and widely regarded as the first wearable ECG device, capable of continuous ambulatory recording of the ECG for 24 hours [59].

The 1960s saw the beginnings of the development of computerised ECG machines. ECG data could be recorded on magnetic tape and digitised; however, the computing limitations of the day required these ECG records to be sent to a central processing installation for digitisation, meaning these were unsuitable for live recording and too costly for mass adoption. One of the first examples is a 3-lead ECG digitised at 1 kHz in 8 bit resolution in 1959, a sample rate and resolution comparable with modern ECG machines [60]. It was not until the development of microelectronics in the 1980s that the digital ECG would come to be widely employed.

As with the development of the early analog ECG machines, the trend towards smaller devices continued in the digital age. Early digital ECG machines were bulkier and more expensive than their analog cousins, but advances such as the integrated circuit and semiconductor technology (particularly operational amplifiers) quickly led to a drop in size and price [61]. the advent of increased computing power expanded the capacity of data analysis, to the point where by 1988 more than 50% of recorded ECGs were interpreted by computer [62]. Present-day digital ECG machines are affordable, portable and ubiquitous in healthcare systems worldwide, and ECG monitoring is employed in the vast majority of surgical procedures and during patient observation [63]. An increase in features and reliability has offset the reduced costs of device manufacture, keeping the price of clinical ECG machines largely unchanged since 2000 at anywhere between £2000 and £10 000 GBP depending on specification [64]. In contrast, some low-cost direct to consumer devices such as smartwatches and mobile phones can now incorporate non-clinical ECG recording sensors. One such device, the Apple iWatch, costs under £400 and provides a high resolution single lead ECG with moderate to strong reliability and validity in comparison to lead 1 of a traditional 12-lead ECG, and have subsequently been approved by the US Food and Drug Administration (USFDA) for the detection of atrial fibrillation [65]. Profiting from the drop in manufacturing prices, these widely available devices are reaching maturity and are beginning to be integrated into traditional healthcare systems, albeit cautiously [66]. With the advent of the digital ECG the power of digital signal processing can be harnessed to offer improved noise reduction.

The electrical activity of the heart is a low level biopotential within a body containing other biosignals. The body is constantly in motion, even when the subject is at rest, due to respiration and the muscular activity of the heart. In addition, the human body exists in an ambient environment with other unknown signals which can be coupled to the body or otherwise cause interference, and the ECG is susceptible to contamination from many of these noise sources. This is especially true in the case of EPS sensors, which can be more sensitive than traditional AgCl ECGs due to the weak capacitive coupling, lack of interface paste, and an air or cloth gap between sensor and skin [21]. The four main sources of noise in the ECG are base line wander, power line interference, muscle artefact (aka electromyogram) noise, and additive white Gaussian noise.

Base line wander (BW) is a low frequency component noise in the range 0.05 to 3 Hz [67]. It is predominantly caused by motion of the patient through respiration as the chest rises and falls. The movement of sensors relative to the body due to this respiration causes a slow amplitude shift in the baseline of the ECG. BW noise can make the interpretation of the ECG difficult and can in cases of extreme movement (such as coughing) lead to saturation of input stages in the analog front end causing loss of signal.

Power line interference (PLI) is a frequency specific noise (50 or 60 Hz) caused by the electromagnetic radiation from electronic devices [68]. PLI lies in the middle of the ECG power spectrum, and due to its amplitude and pervasiveness is often the largest noise component in the ECG. Unshielded or poorly designed electronic devices such as switch mode power supplies and mains LED lighting contribute to this noise and are exacerbated by the tendency of the human body to act as an antenna and couple to PLI sources, increasing the amplitude of PLI interference in the ECG.

Muscle artefact (MA) noise caused by the electrical activity of the muscles can be picked up both by traditional AgCl sensors and EPS sensors alike, and manifests in the range 0.01 to 100 Hz and typically these events are short in duration (~50 ms) [69]. This form of ECG noise is most present in ambulatory / exercise ECG, being largely absent in the resting ECG. Large amplitude MA noise can obscure features such as the T wave, and as the spectral content of MA noise overlaps that of the ECG, filtering aimed at MA noise can often alter the morphology of the ST segment, making clinical diagnosis impossible. The electroencephalogram (EEG) and electrooculogram (EOG) are biosignals similar to the EMG, both of which are records of the electrical activity of the human body (from the brain and eye muscles respectively) although the amplitude of these signals is comparatively small (0.001-0.01 mV for EOG/EEG, compared to 1-10 mV for the EMG) and therefore do not normally affect ECG recordings.

Additive white Gaussian noise (AWGN) covers a range of noise sources, the majority of which occur as a result of the electric properties of the ECG recording device employed and the quality of the signal transmission lines. These sources are typically low amplitude and broad band, and comprise mostly and shot and thermal (aka Johnson–Nyquist) noise [70]. Careful design of electronics and cable shielding can mitigate the effects of these noise sources on ECG recording.

Noise that lies within the ECG bandwidth of interest (1-150 Hz) can manifest as morphological distortion, which can lead to mis-diagnosis of arrythmias [71], whereas broad band noise or high amplitude frequency specific noise can occlude the R peak, causing inaccurate HR calculation [72]. For ECGs to be useful for accurate HR monitoring and clinical diagnosis these sources of noise must be identified and removed by filtering and denoising methods. Some examples follow of filtering methods, as applied to EPS and similar capacitive style ECG sensors.

Despite the advances in digital signal processing, most ECG sensors still employ some form of analog signal processing, often in the analog front end for signal conditioning. This often takes the form of a low pass (LP) filter at ½ f_s (sample rate) for antialiasing, and a high pass (HP) filter to reduce baseline wander and keep the signal in range of the ADC [73]. Standard analog front end hardware filters comprised of discrete R and C components with op-amp buffers and are well studied, and indeed have been applied in to capacitive sensors both as LP filters for the removal of high frequency noise [74] and as a bandpass filter from 0.2 Hz – 80 Hz [75]. These filters have the advantage of being simple to construct but are limited in their noise attenuation and offer no adaptive features. The digital domain therefore offers more scope for denoising, and various advanced methods are available for ECG signal processing post digitization.

Finite impulse response (FIR) and infinite impulse response (IIR) are traditional DSP filtering methods, and have been widely applied to non-contact EPS style sensors [76]. These numerical methods can be scaled in complexity and effectiveness by the increasing the filter order (or length of impulse response) to match the available hardware of needs of the application. FIR filters have a linear phase, meaning no phase distortion is introduced into the filtered signal, and have no feedback and are therefore stable for any input signal. IIR filters require fewer co-efficients and therefore require less resources to implement, however they have non-linear phase characteristic which may induce signal distortion especially at the cut off frequencies, this makes IIR filters unsuitable for use in certain applications, for example narrow notch filters for 50/60 Hz PLI removal, where FIR filters would be preferable. FIR filters have employed as a band pass (0.4 – 40 Hz) filter for wearable capacitively coupled ECG systems [77] show strong PLI suppression due to the high complexity (64th order) and therefore steep rolloff at the HP filter cutoff frequency. Being programmatically defined, these DSP methods can be optimised adaptively, and a method using a least squares algorithm to define the optimum filter order has been shown to be effective in ccECG MA removal [78].

Statistical filtering methods such as the Bayesian or Kalman filter estimate the state of a linear dynamic system from a noisy ECG, given an understanding of the expected form of the noise free signal. Both extended [79] and adaptive [80] Kalman filters have been applied to capacitive ECGs, and perform well in the reduction of Gaussian noise, but have been shown to mistakenly ascribe beat to beat ECG variation to measurement noise.

Empirical mode decomposition (EMD) is an adaptive separation filtering method. It commonly utilises the Hilbert–Huang transform to decompose signals into their various components called intrinsic mode functions (IMFs), although other decompositions such as Karhunen–Loeve can also be employed. This method can be applied to nonlinear and nonstationary processes making it suitable for use with the ECG. EMD is effective in removing high frequency components such as random noise, however the determination of IMF order is heavily influenced by window length [81] and incorrect selection can lead to loss of ECG morphological information. EMD is suitable for HR calculation, and applied to noisy ECG signals from wearable capacitive sensors provided an average error of 0.23% in HR calculation [82] compared to the AgCl ECG.

Another complex spectral filtering method similar to EMD is the discrete wavelet transform (DWT). This method decomposes the ECG signal into sets, where each set is a time series describing the signal in a specific frequency band. Several DWT methods exist, but the one most commonly applied to the ECG is the Daubechies wavelet, where careful selection of wavelets and scaling function is critical to avoid loss of information or alteration to the ECG waveform. Early implementation with capacitively coupled ECGs showed promise in low frequency noise removal (BW) [83] but struggled with HF noise. It has been shown more recently that employing a moving window wavelet transform provided a signal predominantly free of noise [84] but with some deformation to the T wave.

The bleeding edge drive to find applications for artificial intelligence (AI) models such as neural networks and deep learning computational methods has also shown interest in the ECG. Using a traditional AgCl ECG LEAD I trace as a reference source, a 3 channel capacitively coupled ECG was de-noised of motion artefacts using a deep learning network [85]. The large variation in ECG morphology, amplitude and HR frequency between patients is a barrier to the applicability of this method, and it is unclear as to whether selected training data is sufficient to prepare the network for use across a wide variation of patient electrocardiogram morphology. Other promising applications for AI include QRS feature detection [86] and the classification of signal quality to determine body position during sleep from multiple capacitive electrodes [87].

1.2.3.1 Conclusions and knowledge gap 2

Provided above are several examples of filtering methods applied to capacitively coupled and EPS style sensors for denoising the ECG. Some of these methods do not consider the case of these novel sensors, and employ methods transferred from traditional AgCl ECG filtering such as in [76], and work such as in [77] considers a frequency band too narrow (0.5 to 40 Hz) to be acceptable for clinical diagnosis quality ECGs. This suggests that there is a research gap in surrounding methods specifically tailored to the EPS ECG.

Of the literature surveyed, the majority number of these considered only data from adult ECGs [79, 82, 84, 85] and another was evaluated using only simulated data [81], suggesting a lack of investigation specifically into the filtering requirements of the low amplitude neonatal ECG in the literature.

The ECG signal from an EPS device is different from that of a traditional ECG, and the susceptibility of EPS sensors to 50 Hz noise and MA makes signal processing more challenging than with traditional AgCl ECG. Traditional signal processing techniques such as the standard American Heart Association filtering recommendations [88] must be evaluated with this novel technology, and EPS specific filtering and signal processing techniques should be investigated where the standard methods are found to be lacking. Improvements in signal quality, reliability and acquisition time gained through improved filtering methods could improve the case for clinical adoption of the EPS.

1.3 Prototype development

As stated in section 1.2, the decision to focus on the two research areas of textile electrodes and signal processing arose from the early investigation of the smart mattress concept. This investigation led to the creation of several smart mattress prototypes, and as the creation of these devices and the lessons learned during this process informed the direction of this research, the concept and the prototypes are presented here for context.

The co-authored paper entitled "Neo-SENSE: a non-invasive smart sensing mattress for cardiac monitoring of babies" (see Chapter 2) sets out the basic premise of the concept, which I will summarise here now, and is shown in Figure 9 below.

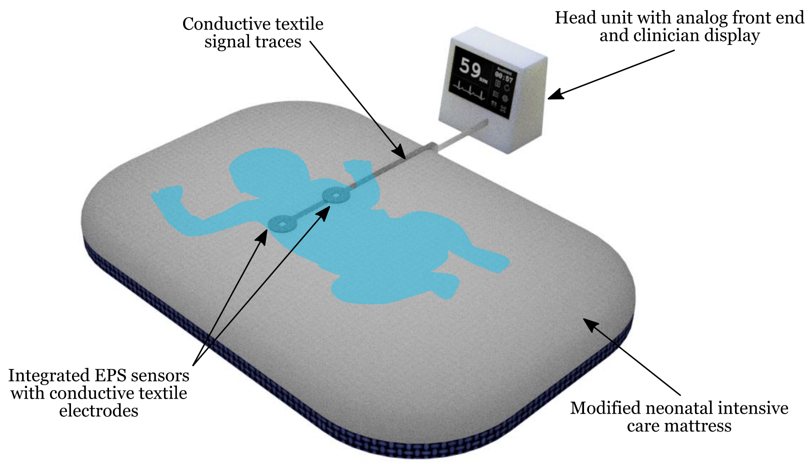

Figure 9: Overview of smart mattress concept showing key components

In the smart mattress concept, electric potential sensors are integrated into a modified neonatal intensive care mattress, with conductive textile reference electrodes. Conductive textile signal traces provide power and signal return for the active sensors to a clinician display, ensuring the mattress is soft and comfortable. The head unit contains an analog front end for signal conditioning, as well as a clinician visual display unit to provide a waveform display and instantaneous heart rate, as well as digital storage of the ECG and networking/wireless capacity.

This device requires no sensors to be attached, and no interface paste or electrolyte gel to be applied to the infant. The newborn is placed on the mattress, and it automatically begins collecting ECG data and calculating the HR.

The first prototype was designed as a test-bed for initial investigation into EPS sensors and textile materials, and was presented in the conference poster "Neo-Sense: a real time data processing & acquisition unit for monitoring neonatal ECG in the delivery room" (see Appendix 1). The first prototype was designed as a test bed for the investigation of analog front end topography, analog filtering techniques, data acquisition, display and storage techniques. A clinical trial involving a cohort of infants was initially planned (but later abandoned due to the Covid-19 pandemic restricting access to hospitals), and it was identified that as a development environment the first prototype was unsuitable for field use. Therefore, a second prototype based on National Instruments hardware was developed. This second prototype was also used to investigate the simplification of the filtering process, with the removal of the analog notch and low pass filters with only a low pass antialiasing filter, relying solely on digital signal processing to clean up the ECG signal. The technical details of these two prototypes are summarised below:

	Prototype 1	**Prototype 2**
Platform	Raspberry Pi 3 A+	National Instruments myRIO 1900
ADC	12 bit @ 1kHz	12 bit @ 1kHz
Analog filtering	Low pass (f_c 200 = Hz) notch (f_c 50 = Hz)	Low pass (f_c = 500 Hz)
Digital filtering	FIR (software)	FIR (FPGA)
Programming environment	C++	National Instruments LabVIEW

Table 2: Prototype specifications

The first prototype was developed as a low-cost platform where rapid development was possible using readily available components and software packages for the ubiquitous Raspberry Pi (Raspberry Pi Foundation, UK). The second prototype was based on the LabVIEW Ecosystem (National Instruments, TX, USA), with National Instruments hardware and software solutions. This offered higher quality data acquisition circuitry and leveraged the power of FPGA technology at the cost of a significant increase in price (roughly an order of magnitude).

Circuit diagrams for the analog front end, filtering, power supply and signal conditioning circuits are available in Appendix 2: Prototype #1 schematic and Appendix 3: Prototype #2 schematic.

1.4 Thesis overview

This thesis and the theoretical and practical investigation that it is comprised of concerns the implementation of novel electric potential sensing technology in electrocardiography. This thesis aims to improve the knowledge and characterisation around EPS sensing, acquisition, and filtering, both in the adult and the NNECG. Following from the two gaps in research knowledge, as identified in sections 1.2.2.1 and 1.2.3.1, two key areas are explored and developed in this thesis:

1. The use of textile electrodes for EPS sensors
2. Advanced signal processing techniques for EPS sensors

Incremental development in these areas is required if the EPS sensor and related technologies are to find regular use in future in novel ECG sensing systems.

The relationship between the prototype development, the published works, and this thesis is depicted in Figure 10 below:

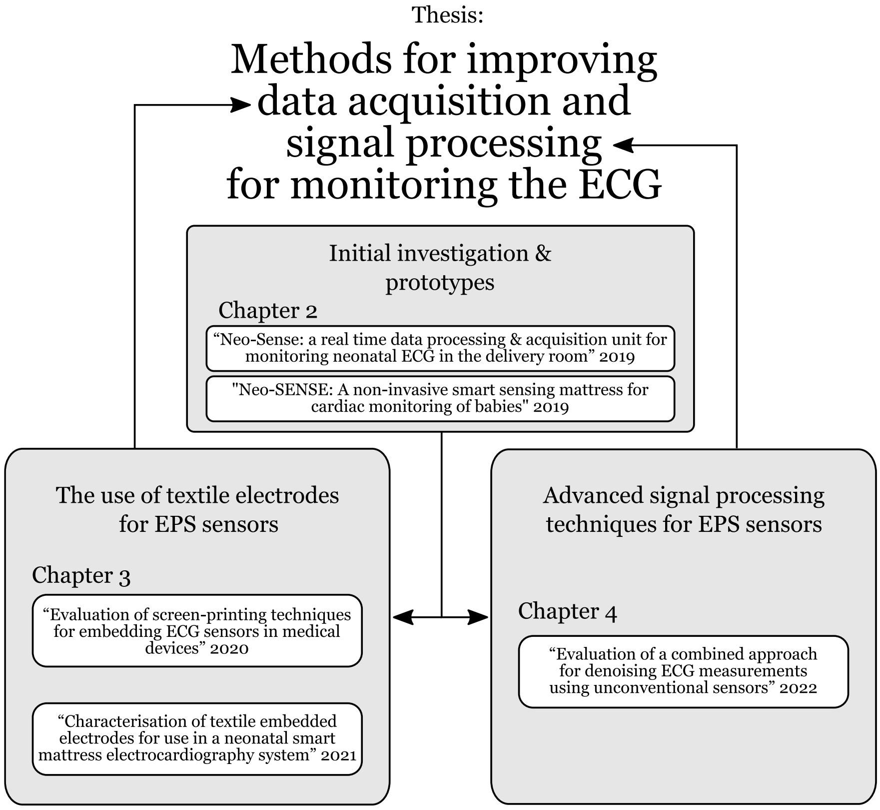

Figure 10: Thesis summary

The initial investigation described in Chapter 2 and in the conference poster presented in Appendix 1 identified these two key research areas. Chapters 3 and 4 then describe the subsequent investigation into these areas, and feed back to form the content and title of the thesis. These two research areas are outlined in the following sections.

1.4.1 The use of textile electrodes with EPS sensors

EPS sensors can provide high quality ECG with rapid HR acquisition. These sensors work best in hybrid mode, with a common zero potential reference for filtering and movement artefact reduction. The use of textile and flexible dry electrodes would allow these sensors to be built into textile devices, with one such proposed implementation being a smart mattress concept [89] for automatic HR assessment without the need to attach additional probes. Such a device could be used in the delivery room to monitor HR during resuscitation efforts, or in the neonatal intensive care unit for the long-term monitoring of vulnerable infants. For these devices to be viable the following questions regarding textile and flexible dry electrodes must be answered:

- How do dry electrodes affect the signal quality of an EPS ECG?
- Which methods and materials are most suitable for textile embedded dry reference electrodes?

The smart mattress concept is presented in Chapter 2 to provide context for the research, and the methods to characterise textile electrodes and to quantify signal quality are described in Chapter 3.

1.4.2 Advanced signal processing techniques for EPS sensors

There are substantial differences between traditional AgCl ECG and EPS ECG recordings. EPS sensors confer the benefits of rapid, gel free electrode application, and non-contact sensing, but incur additional noise due to their sensitivity. To better define this area the following research questions are proposed:

- What particular requirements and challenges apply to the acquiring the ECG with EPS sensors?
- What novel signal processing techniques can improve the quality of the ECG employing EPS style sensors?

The work presented in Chapter 4 in this thesis proposes a methodology for testing EPS sensors with a novel neonate phantom, improving repeatability and allowing the use of real world signal, and describes a novel adaptive filtering method.

Chapter 2: Neo-SENSE: a non-invasive smart sensing mattress for cardiac monitoring of babies

Please note: the thesis author was not the main author on this paper, this work and (along with the poster supplied in appendix 1) is presented as context for the basis of the further investigation.

2.1 Introduction

Within the first minute of life, a newborn must take its first breath to make the transition from life inside the womb to the outside world. Approximately 10% of these babies require assistance or intervention during this transition [6]. Current qualitative methodologies to evaluate the resuscitation procedure efficacy in the successful delivery of newborns such as palpation and auscultation rely on the experience of the neonatal staff attending the birth. Within the last two decades, technologies that allow measuring the heart rate (HR) of the newborns have been introduced. These technologies include pulse oximetry (PO), electrocardiography, Doppler ultrasound and forehead reflectance photo plethysmography (PPG). Among all these, ECG and PO have shown to be more precise than qualitative methodologies. However, multiple studies have shown that using PO [90, 91], the time elapsed after birth to the successful establishment of HR display often exceeds one to two minutes.

Moreover, a limitation of PO is that HRs <100 bpm in newborns especially preterm infants are not consistently detected due to the weakness of blood perfusion [92].

The current challenges of preterm infant monitoring combined with increasingly sophisticated scientific advancements, have driven the development of novel technologies to assess both new-born and infant HR in ways that seek to overcome the limitations of currently available devices [93].

This is also supported by Finn et al. [92] where it is concluded that in order to provide an enhanced monitoring of preterm infants during stabilization in the delivery room, the electrocardiogram (ECG) monitoring should be available as an adjunct to ongoing clinical assessment.

Based on this fact, a fast and reliable method to monitor HR immediately after birth does not currently exist. Today's technologies lack both, accuracy and rapid application, and have not been designed considering the human factors associated with either term or preterm babies. This includes the newborn skin vulnerability, size and weight, which could be less than 1 kg in preterm infants.

Based on this clinical need we propose a novel health care solution based on an innovative smart sensing device to assist midwives and neonatal staff during baby delivery.

2.2 Electric Potential Sensor

The EPS was invented at the University of Sussex as a non-invasive sensing technology [94]. Such sensor is feedback enhanced and stabilized electrometer-based amplifier that operates based on displacement current measurements. Technical details on the sensor characterization have been extensively described elsewhere [95-99].

The smart sensing device was built in a neonatal mattress employing bespoke EPS sensors that included associated feedback loops providing the functions of guarding, bootstrapping, and neutralization to enhance the input impedance, reduce the input capacitance, and maintain the electronic stability of the sensor [97]. The net effect of this combined with positive feedback techniques is to produce a broadband sensor (up to 100 MHz), with extremely high input impedance (up to 10^{18} Ω) and low effective input capacitance (~10-15 F) which is crucial for weak capacitive coupling with the baby. This new device produces a very low noise floor sensor at the operating frequencies of electrophysiological signals such as fetal and neonatal ECG. Its performance as a non-perturbative detector for measuring fields or voltages with high sensitivity level has proven a maximum sensitivity of ~2.6 μV/m and an associated accuracy of 2% [95, 98]. These details are summarised in Table 3:

Bandwidth	0 – 100 MHz
Input impedance	< 10^{18} Ω
Input capacitance	~10-15 F
maximum sensitivity	~2.6 μV/m

Table 3: Typical EPS sensor specifications

In our previous work, the EPS technology has been successfully tested for monitoring fetal ECG during early pregnancy [99] (starting from week twenty of gestational age) as well as recording ECG signals from micron sized living organisms such as Zebrafish [96]. This confirms that the sensor sensitivity and signal to noise ratio (SNR) is suitable to be used with preterm babies aged as early as 25 weeks having greater ECG amplitude given that the electrical signal does not need to propagate though maternal tissue.

2.3 Experimental Setup

The prototype described in this paper was built using an ultra-high input impedance EPS sensor with internal input bias current circuitry and guarding. The prototype was designed using a pair of dry EPS electrodes. The circuit design incorporates an electrometer and utilizes the electronic feedback techniques in order to increase the input impedance and maintain sensor stability. Figure 11 shows the schematic of the EPS sensor design along with the experimental setup designed to test the smart-mattress prototype for neonatal ECG monitoring.

We performed modifications on a mattress used in the neonatal intensive care unit (NICU) to include a pair of bespoke electro active EPS sensors. The voltage outputs from the sensors were sent to an analogue processing stage as shown in Figure 11, where signals were amplified, and conditioned by noise reduction (i.e., rejecting external noise at particular frequencies < 50 Hz) and bandpass filtering.

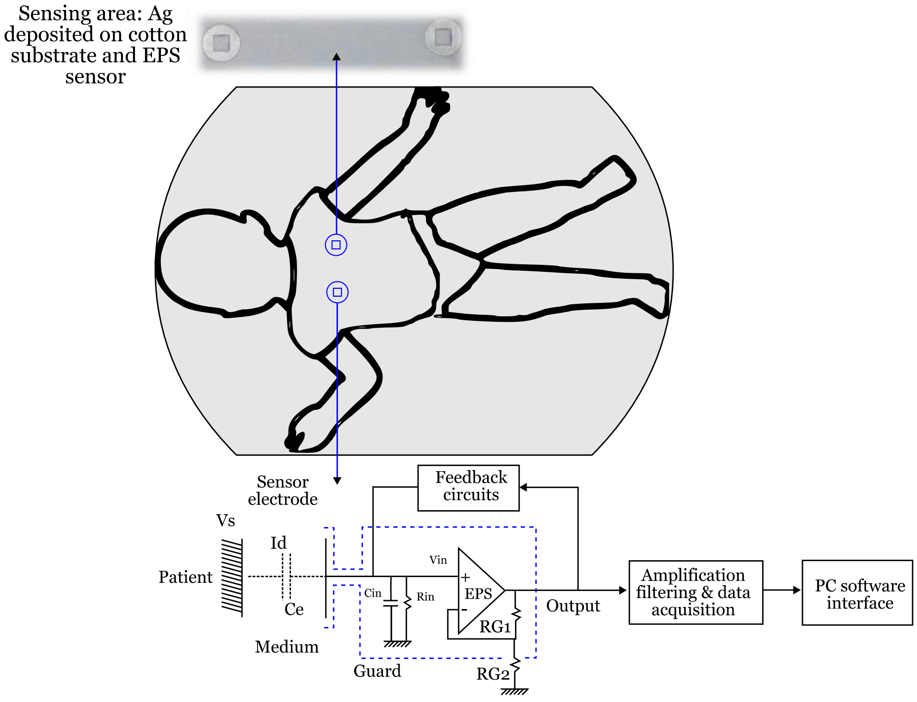

Figure 11: Schematic of the smart-mattress (top) and sensor design implementing the EPS sensor (bottom)

In this particular design, filters can be switched on/off for the detection of additional parameters such as breathing rates. The analogue output is digitized using a commercial National Instruments data acquisition system NI USB 6003 having a maximum sampling rate of 100kS/s. The data is then acquired using a laptop computer. Display and storage of the digital data is controlled using a custom-made graphical user interface based on LabVIEW software also incorporating digital filters and peak detection algorithms. Within this user interface, real-time parameters are displayed such as the ECG trace, the respiration trace and the instant HR values extracted using a peak detection algorithm.

2.4 Electrode interface

A crucial consideration for the design of the smart mattress's front-end is the electrode material interface. Currently, there are several types of electrodes used for recording electrophysiological measurements. The most common interface that has been extensively used is based on silver/silver chloride (Ag-AgCl). The main drawbacks of using Ag-AgCl electrodes are that it requires skin preparation (i.e.

removing skin oils) and the use of conductive gels as they require to make electrical contact with the sample [100].

In contrast, the EPS sensor only requires making physical contact with the patient without the need of any type of gel or skin preparation. Therefore, it is not affected by variations due to contact resistance in the same way that occurs within conventional electrodes. Figure 12 shows the electrode-sensing interface of the EPS sensor deposited (see 'though' representation) on fabric.

Figure 12: Close-up view of the EPS sensor front-end showing a see through view of the silver deposited electrodes (blue arrow)

Screen printing techniques were used to provide complete freedom for the design layout as it does not need to follow the fabric structure. The procedure was carried out by screen-printing several layers of silver conductive paste and a UV curable interface polymer paste onto the mattress's fabric. An interface layer was printed on the fabric before the silver ink was applied to improve the layer adhesion. The use of polymer interface layers have been proven to be able to effectively improve the durability of the electrode-sensing interface, in particular to withstand bending, stretching, abrasion and washing [101].

The interface paste UV-IF-1004 (smart Fabric Inks Ltd) creates a smooth surface on the fabric after solidification achieved by UV curing for a period of 30s after printing. Cotton was chosen as the fabric to avoid triboelectric charging effects that could affect the accuracy of the sensor, the silver ink used in this work is a screen-printable paste Fabink-TC-C4001 (Smart Fabric Inks Ltd.) which was cured at 120° C for 10 minutes to solidify and evaporate the unwanted solvents. This provided good conductivity to maintain the SNR performance. The silver ink mainly consists of silver flakes, vinyl resin and a solvent. Silver flakes have been proven to be biocompatible and suitable for skin according to [102].

In addition to the electrode-sensing interfaces, conductive tracks were also printed on the fabric to connect the EPS sensors and the analogue processing units. A UV-curable waterproof paste (UV-IF-1039) was printed on the conductive tracks for encapsulation. This provides benefits on the reusability of the device as the mattress could be cleaned using the approved wipes used at the hospital for hygienic purposes without affecting the stability of the sensor front-end.

The combination of screen printing techniques and the EPS hardware circuitry provides a reliable ECG sensor with excellent biocompatibility and comfort for the end user.

2.5 Experimental Procedure & Results

We evaluate the smart mattress design using two scenarios: a baby mannequin that was modified to produce an ECG signal output as shown in Figure 12, and a proof of principle demonstration with a single young infant aged 18 months.

Within the second scenario, the experimental protocol was explained to the infant parents, who gave written informed consent before the study took place. All experiments were performed in accordance with relevant guidelines and regulations. The protocol was approved by the Science & Technology Cross-Schools Research Ethics Committee (C-REC) University of Sussex with application ID number SOP/RGO/ER241/02.

The protocol was carried out in a private room and calm atmosphere to ensure recording stability. Recordings took place in one session, and the parents were asked to lay down the young infant on top of the sensor-integrated mattress. Ten ECG recordings lasting three minutes, where collected using our novel mattress design. Instant HRs, respiration rates and the ECG traces were recorded digitally for further analysis and representation. To validate the HR values obtained using our smart-mattress, parallel readings using a pulse oximeter (Nellcor, Minneapolis USA) were carried out.

As mentioned previously, PO measurements can take between 1 and 2 minutes to deliver a reliable reading once the sensor has been properly positioned [92], as well as not being suitable for preterm infants due to weak blood perfusion or whenever the HRs are below 100 bpm. In contrast with pulse oximetry, employing our proposed EPS device, we can reliably record additional functional parameters of the heart through the ECG trace and extract relevant data useful for diagnosing how cardiac chambers are behaving.

Figure 13 shows raw data of a single ECG pulse extracted non-invasively from the 18 months infant during the recordings.

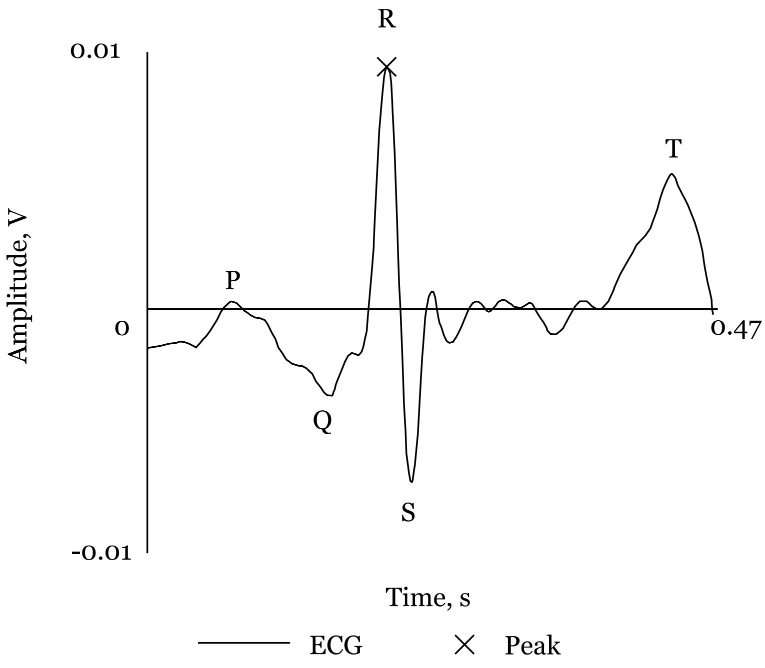

Figure 13: Raw data of a single pulse extracted from the young infant during the tests showing detailed ECG characteristics such as the PQRS and T waves

As it is shown, the ECG trace including the PQRS and T segments can be clearly observed without the requirement of further post processing. These waveform characteristics are useful for outlining the different stages of the heart functional activity such as atrial contraction (P wave), ventricles contraction (QRS waves) and relaxation of the ventricles (T).

Figure 14 shows ten seconds of an ECG recording carried out with the infant together with the respiration traces.

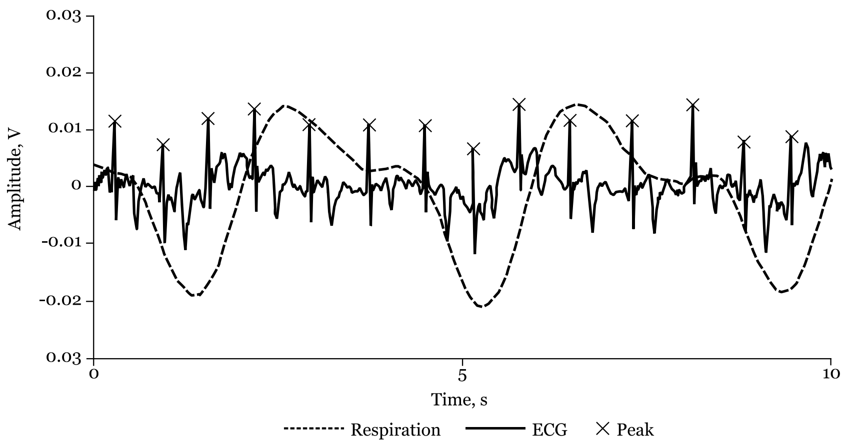

Figure 14: Example ECG and respiration trace of ten seconds

Recordings of the infant HR were manually notated for R peak extraction, then R-R intervals were calculated to generate an average HR. Results show that the mean heart rate of the infant was 93.12 ± 0.77 this being within the normal heart rates at rest according to [103] and the mean respiration rate was 16.3 ± 0.26 being in the lower limit of what has been reported in [104]. The parallel recordings using the pulse oximeter had an average value of 92.20 ± 0.71 falling within the range of measurements recorded using our sensing device. The data obtained is in agreement with the studies reported on [103, 104] for young infants HR and breathing rates at rest.

Our device provides accurate HR values in less than 30 seconds once the baby is placed on top of the mattress. This is especially required for resuscitation purposes. Our time to get an ECG trace is up to four times faster than pulse oximetry, which is crucial to avoid long term effects related with poor oxygenation of organs within the baby.

Employing our smart- sensing mattress the detection of baby respiration rate is also possible. This is a crucial parameter required by the midwife carrying out the ventilation procedure. The heart rate together with the breathing rate will enable clinical staff to assess the success of the procedure in order to make quick and informed decisions.

2.6 Conclusions

In summary, we have presented a new sensing platform development based on the EPS technology to monitor the ECG activity of babies. The proof of concept demonstration conducted with a young infant confirms the potential of our smart-sensing mattress to be used during resuscitation procedures for term and preterm infants directly after birth.

Highly sensitive detection of ECG was accomplished using the proposed bespoke EPS sensor, even in the presence noise sources such as the mains of 50 Hz and without heavy post-processing or signal averaging techniques, thus preserving its high SNR. Both HR and the respiration rates were acquired in real time in less than 30 seconds, this being up to 4 times faster than pulse oximetry. The proposed technology has the potential to be used for new-born stabilization at the delivery room as it reduces the time to obtain the vital signs required for assessing the success of resuscitation procedures. These details are summarised in a comparison with pulse oximetry below:

	EPS ECG	**Pulse Oximetry**
Mean heart rate	93.12 ± 0.77	92.20 ± 0.71
HR acquisition time	< 30 s	1 – 2 min*
Mean respiration rate	16.3 ± 0.26	N/A

(*characteristic, see [92])

Table 4: Comparison of EPS ECG and pulse oximetry

Additional applications include remote monitoring of infants in low-income countries implementing a telemedicine system as described in [105]. Here, the midwife can evaluate the HR for assessing the ventilation procedure evolution, while doctors can remotely assess ECG to determine possible congenital disorders, if present.

Future directions of this research are focused on testing the device at the NICU with a cohort of ten infants once the device is certified to be used at the hospital and ethical approval regulations are completed.

Chapter 3: Characterisation of textile embedded electrodes for use in a neonatal smart mattress electrocardiography system

3.1 Introduction

The predominant quantitative indicator of the health of a newborn is the heart rate (HR). Both the American Academy of Pediatrics [106] and the European Resuscitation Council [107] recommend assessing the newborn's heart rate within 1 minute of delivery. If the measured HR is less than 100 beats per minute (bpm) positive pressure ventilation should be administered, and if it is below 60 bpm chest compressions should be initiated [108]. The reliance of clinical professionals on HR data to inform intervention requires rapid and accurate HR acquisition. The most basic form of HR measurement is either done manually by feeling a pulse (palpation) or by listening to the heartbeat using a stethoscope (auscultation). The clinician counts the number of beats in 6 seconds and multiplies this by 10 to get the heart rate in beats per minute. These methods provide a rapid acquisition time of 7-19 seconds [109] and are used for the initial HR assessment. A member of clinical staff is required to administer these tests however, noise, stress and cognitive load can influence measurement. These readings can vary as much as 15 bpm from actual HR where errors in HR determination have been shown to occur in 26-48% of initial assessments [110].

It is critical that neonatal care providers have access to real-time, suitable and accurate diagnostic information to recognize deviations from typical neonate physiology and take the necessary steps to manage scenarios where intervention is necessary.

Clinical and technological advances in the neonatal intensive care unit (NICU) such as the introduction of the APGAR score in the 1950s and the recent widespread use of the pulse oximeter (PO) have been critical in informing interventions and improving infant outcomes [111, 112].

The two principal medical devices used in the delivery room to assess the HR are the pulse oximeter (PO) and the electrocardiogram (ECG). The pulse oximeter measures heart rate using a photodiode-based measurement of blood perfusion, and the electrocardiogram is an electrical measurement of heart activity. The silver chloride (AgCl) based ECG is considered the gold standard in the delivery room [113] and has been demonstrated to be both reliable and accurate in assessing HR, as PO has been shown to underestimate the HR compared to ECG struggling to obtain accurate HRs when the newborn suffers from low peripheral blood perfusion or the HR is less than 100 bpm [114].

Factoring in the time taken to attach the sensors, the device signal acquisition and HR estimation algorithm window length, the average time from birth to HR reading is > 70 seconds for ECG and > 110 seconds for PO [115]. This precludes these devices for use in the initial HR measurement under 1 minute. Additionally, there is the need to clean and prepare the newborn's skin to remove blood or other fluids that affect signal coupling, and the application of an electrolytic interface paste which can potentially become sites of infection. Rigid PO sensors and AgCl electrodes can also potentially cause abrasive damage to the delicate newborn skin. The delay in HR acquisition due to sensor application time, combined with the risks associated with AgCl electrodes to fragile newborn skin are both barriers to adoption. Given these drawbacks, alternative dry electrode technologies have been used for reducing the time required for taking a measurement while improving the skin biocompatibility. A study using dry stainless-steel electrodes [116] showed high quality and rapid signal acquisition in newborns after birth, however the electrodes are rigid and bulky (dimensions of 5 x 2.5 x 1 cm) thus still being a large and intrusive device. More recently novel silver nanowire dry electrodes [117, 118] show promise as substitutes for AgCl gel electrodes having a comparable performance to wet AgCl electrodes in terms of ECG signal to noise ratio for heart rate calculation. Fully organic conductive polymer composite (PEDOT:PSS) based dry electrodes [119] have shown to have excellent biocompatibility [120], self-adhesiveness, conformity and have also been shown to record high quality ECG waveforms with reduced noise interference (25 μV compared to 28 μV) compared to AgCl gel electrodes, thus being suitable for ECG based diagnosis. However, both silver nanowire and conductive polymer dry electrodes have not yet been tested in neonates.

Despite evidence that the electrocardiogram provides clear benefits over PO and palpation/auscultation and the recommendations are that ECG monitoring should be adopted in the NICU [108] for newborns requiring resuscitation, this technology has still not been fully developed. In this study we aim to provide a proof of concept system for ECG monitoring based on a full data acquisition and filtering system and two different materials suitable for use as fabric embedded textile based electrodes for use in the NICU delivery room. The device is capable of recording the HR within 6 seconds by embedding novel electric potential sensors into a smart mattress, in comparison with traditional ECG is (> 70 s) and pulse oximetry (> 110 s) [115].

The structure of the EPS sensor is described elsewhere [7]. Briefly, the electric potential sensor (EPS) is an electrometer-based amplifier insulating electrode that does not require galvanic contact with the body to acquire biopotential signals. Instead, it operates with displacement currents, and the traditional electrode-skin interface is replaced with a dielectric material. Here, a reference electrode in contact with the patient's skin is still required for voltage referencing to the EPS sensor. Please see Figure 1 for a schematic diagram of the EPS sensor structure, as well as the operating principle.

Electric potential sensing can be used in place of traditional AgCl electrodes to record high quality ECG signals without the need for electrolytic pastes or location specific sensor application [121]. Previous work using the EPS has shown that it can be used to provide a rapid and reliable ECG reading from a young infant [89]. Textile based conductive electrodes and signal traces can be used to embed these devices in a standard delivery room mattress facilitating the continuous measurement of the HR of a newborn (see Figure 15).

Figure 15: Delivery room mattress with embedded sensors

This work aims to investigate the use of textile conductive fabric and screen-printed textile conductive ink electrodes as the reference electrode in an EPS based ECG system. EPS sensors are commonly used with a rigid copper reference electrode. In this paper the three cases (a) copper reference, (b) conductive polymer ink and (c) conductive textile fabric reference electrodes are compared for suitability in recording HR using a custom front end, data acquisition and touchscreen graphical user interface prototype.

3.2 Materials and Methods

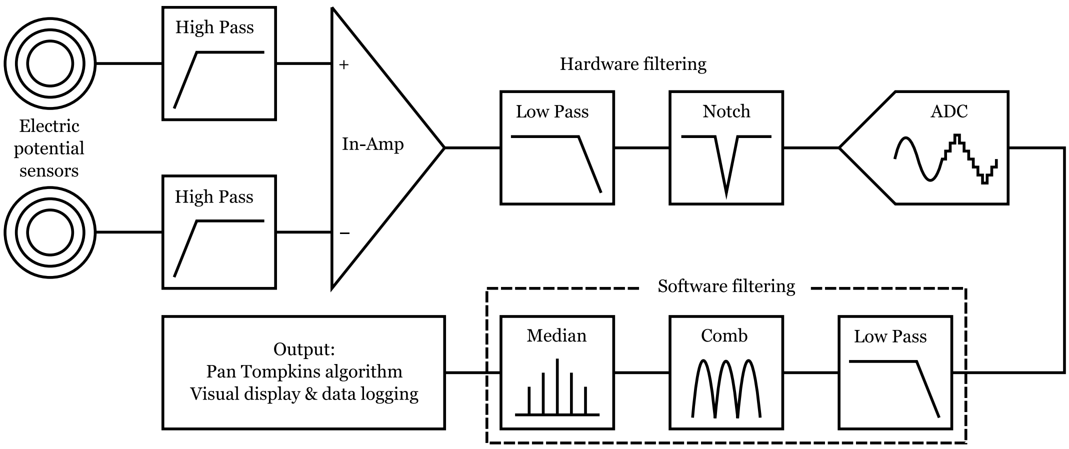

Figure 16: Prototype system signal path with input, filtering and output stages identified

Figure 16 shows an overview of the prototype system used to characterize the proposed textile based electrodes. The input stage reads the electrical signal of the heart with a pair of ultra-high input impedance EPS sensors [94] with internal input bias current circuitry and guarding. The voltage outputs from these sensors are sent to the filtering and analogue processing stage for signal conditioning. The resultant cardiac signal is then digitized, and additional digital signal processing is performed by an embedded microprocessor. Finally, in the output stage HR calculation is performed by the system and displayed on a 7” touchscreen, along with a representation of the signal waveform. The graphical user interface allows for control of the data acquisition and storage methods, as well as filtering and peak detection options.

3.2.1 Input stage

The EPS devices are application specific integrated circuits (ASICs) contained in a land grid array (LGA) style package measuring 10 x 10 x 2 mm. These are inserted into a 3D printed housing as described in Figure 17:

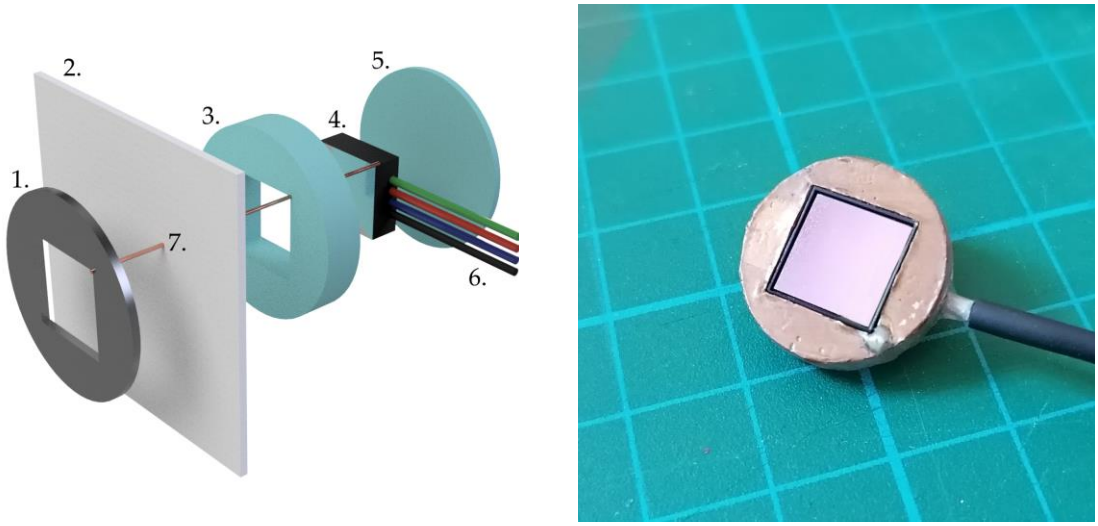

Figure 17: Left, exploded view of sensor: 1) deposited reference electrode material (conductive polymer ink or conductive textile fabric), 2) cotton substrate, 3&5) 3D printed housing, 4) EPS ASIC, 6) power & signal connections, 7) single strand copper connection to the sensor ground. Right, assembled EPS sensor, with standard copper electrode, without cotton layer attachment

A single strand of copper wire (diameter ≈ 0.08 mm) was threaded through the cotton and connected to the EPS sensor reference (Figure 17 feature 7), and the patient facing side was covered with an additional layer of the respective electrode material to ensure no copper was present at the skin-electrode interface. The sensor housing was then held in place on the cotton to avoid relative movement between the sensor and reference electrode.

Two materials were considered for embedding the sensors within a NICU mattress in this work. A silver conductive polymer ink (Fabink-TC-C4001) and a self-adhesive conductive textile fabric (MOS TitanRF). The silver conductive polymer ink has a resistance of 30 mΩ/sq when applied to polyester cotton with interface inks, and the conductive textile fabric has a resistance of approximately 0.5 Ω/sq.

Figure 18 shows these two materials deposited on a cotton substrate, with a central cut out of 10 x 10 mm where the EPS electrode was located underneath the cotton.

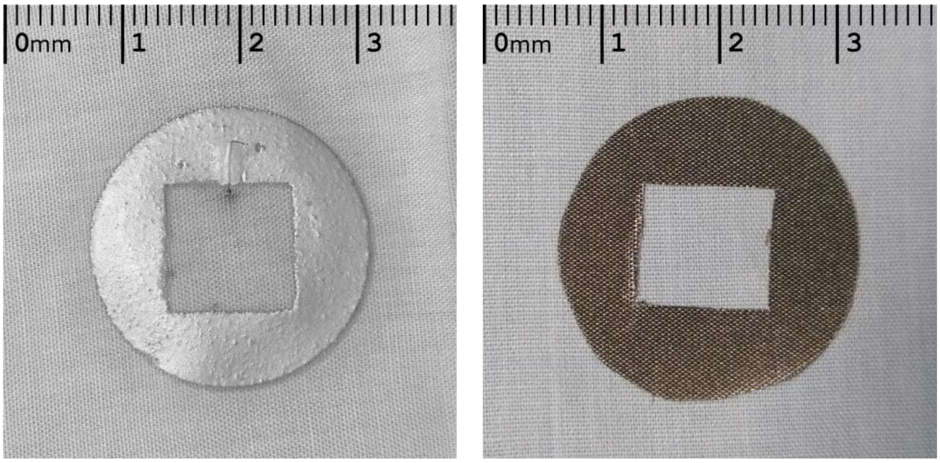

Figure 18: Textile based EPS electrodes, silver conductive ink (left) and conductive textile (right)

Considering the inverse linear relationship between electrode size and impedance [122], each electrode had an equal area of 410 mm^2 to minimise variation in impedance due to electrode geometry. The conductive textile tape was 0.08 mm thick as supplied by the manufacturer, and the silver ink was deposited to a similar average thickness of 0.1 mm to make a reasonable comparison between the two electrodes. The conductive polymer ink consists of biocompatible silver flakes suspended in a vinyl resin, and perform as well as commercial silver chloride electrodes when screen printed onto fabric [102], and have also been shown to be durable when subjected to washing and abrasion [101].

The silver conductive ink electrodes were screen printed on the cotton substrate and cured at 120° C for 10 minutes to evaporate unwanted solvents and improve conductivity. For the conductive textile fabric, a pattern was printed and the electrode shape was cut out following this. The electrode was then attached to the cotton substrate using the self-adhesive backing.

The conductive textile fabric is composed of a polyester fiber with metallic copper and nickel composition. These types of commercially available conductive fabrics are shown to be biocompatible and to have low resistance and to keep electrical durability when subjected to repeated washing cycles [123].

The noise induced by the capacitive components of the skin-electrode interface have been shown to dominate the thermal and resistive noise from the electrode alone [124], therefore AC impedance measurement of the electrodes was conducted. Figure 19 shows the impedance measurement schematics to assess the skin-electrode interface & tissue model:

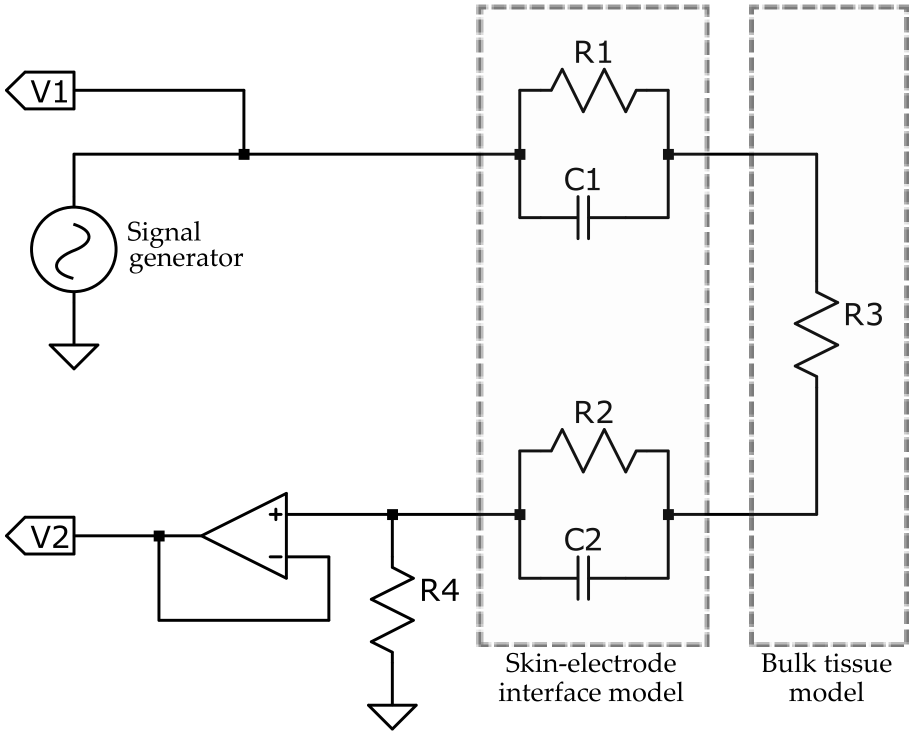

Figure 19: Skin-electrode interface & tissue model for impedance measurement setup

A Keysight Infiniivision oscilloscope & signal generator was used to calculate electrode impedances at 10, 50, 100, 500, and 1000 Hz. A measurement of impedance at the skin-electrode interface was taken using the IV method described in [125]. Figure 20 shows the calculated impedances & mismatch between electrode pairs from the voltage measurements:

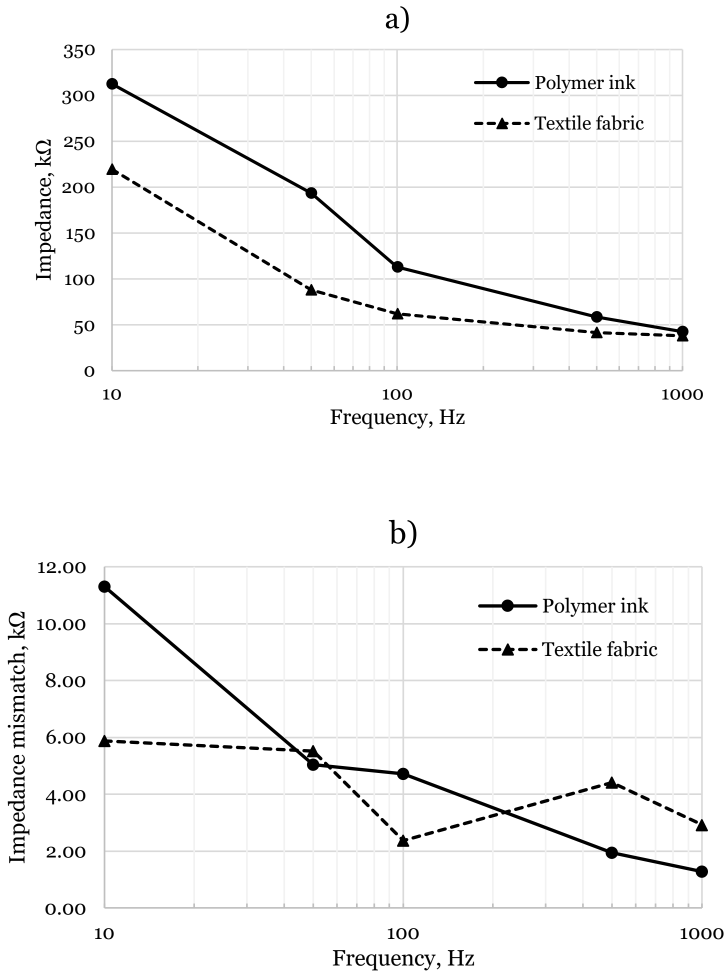

Figure 20: a) Measured impedance of the skin electrode interface, b) impedance mismatch between electrode pairs

The polymer ink electrodes showed marginally an increased impedance across all frequencies than the textile fabric electrodes, but both had a similar impedance profile. The maximum impedance recorded was 300 kΩ at 10 Hz for the polymer ink electrode. Previous works of dry textile ECG electrodes recorded a comparable maximum impedance of 200 kΩ [126] at low frequencies for a polyester/silver textile fabric, dropping off to an average of 50 kΩ for the 500 to 1 kHz range which correlates with the results obtained in Figure 20a.

In Figure 20b the mismatch between the two electrodes of each evaluated material is shown. As it is observed, a maximum mismatch of ~ 11 kΩ for the polymer ink material and 6 kΩ for the textile fabric was measured displaying a maximum mismatch of < 5% of the total impedance for each frequency. This close impedance matching serves to increase the CMRR and reduce noise.

The relationship between mismatch impedances to common mode rejection ratio (CMRR) is defined using Equation 4 and Equation 5, where *X1, X2, R1* and *R2* correspond to the associated reactance and resistance respectively:

$$\Delta \boldsymbol{V} = \boldsymbol{V1}_{+} + \boldsymbol{V1}_{-} = \boldsymbol{V}_{cm} \times \left(\frac{\boldsymbol{X1}}{(\boldsymbol{X1} + \boldsymbol{R1})} - \frac{\boldsymbol{X2}}{(\boldsymbol{X2} + \boldsymbol{R2})} \right)$$

Equation 4

$$\boldsymbol{CMRR}(\boldsymbol{dB}) = \mathbf{20} \times \boldsymbol{Log}\mathbf{10} \left(\frac{\mathbf{1}}{\Delta \boldsymbol{V}} \right)$$

Equation 5

Although impedance mismatch between pairs of electrodes could reduce the CMRR and therefore increase the effect of motion artefacts and power line noise on the recordings [127] the EPS sensor is designed with an external bias circuitry in a way that does not compromise the input impedance of the sensor. Its design includes associated feedback loops providing the functions of guarding, bootstrapping, and neutralization to enhance the input impedance, reduce the input capacitance, and maintain the electronic stability of the sensor [7].

3.2.2 Filtering stage

Electrometer based sensors such as the EPS are highly sensitive and susceptible to noise, predominantly 50 Hz power line noise and movement artefacts. The proposed application for this system is a busy NICU where many devices with unknown levels of electromagnetic shielding will be in use and the subject may be in motion due to resuscitation procedures. A dual filtering approach is used employing both hardware and software filters to ensure the 50 Hz noise is sufficiently attenuated to enable an accurate HR measurement. Figure 21 shows the signal conditioning and filtering section of Figure 16 in isolation, with the split between hardware and software stages highlighted:

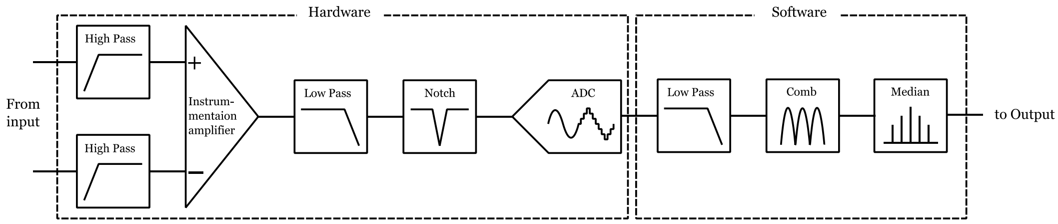

Figure 21: Filtering stage block diagram identifying hardware and software stages

Initially a pair of passive high pass filters (corner frequency, f_c = *0.5 Hz*) remove baseline wander. Next, a subtraction is performed using a precision instrumentation amplifier between both sensor signals to remove common noise. An active 2nd order low pass (f_c = *200 Hz*) and an active 2nd order twin-T form notch filter (f_c = *50 Hz*) remove high frequency and power line noise respectively. The full details of the hardware filter stages are shown in Table 5 below:

Type	f_c **(Hz)** [(1)]	**Operation**
High pass (×2)	0.05	Passive
Low pass	200	2nd order active
Notch	50	2nd order active twin-T, variable Q

(1) f_c = Corner frequency / frequency of interest

Table 5: Hardware filter specifications

Signal conditioning circuitry then scales the signal to ensure the full range of the 12-bit analog to digital convertor (ADC) is used. This ADC bit depth is sufficient to represent the acquired signal with enough detail to identify the QRS waves required for HR detection.

The serial peripheral interface (SPI) output of the ADC is read at 1000 samples per second by a quad-core ARM Cortex-A53 based platform (Raspberry Pi 3 Model A+) which performs additional software filtering with a modified Pan Tompkins algorithm [128] for peak detection and heart rate acquisition. The software filtering consists of a forwards form comb filter (f_c = *50, 100 & 150 Hz*), a low pass 20th order finite impulse response filter (f_c = *200 Hz*), and a variable median filter for signal smoothing. The software filters are coded in C++ avoiding any external dependencies and to minimise system resource usage, and the details of the implementation are summarized below:

Type	f_c **(Hz)** [(1)]	**Operation**
Comb	50	Forwards form
Low pass	200	20th order
Averaging window	-	5 samples (variable)

(1) f_c = Corner frequency / frequency of interest

Table 6: Software filter specifications

For the filter validation, the EPS sensors were removed, and a generated signal employing a NI USB 6009 and LabVIEW biomedical toolkit providing the combined ECG and 50 Hz noise signal was injected to the inverting and noninverting terminals of the instrumentation amplifier. Figure 22a shows the frequency response analysis (FRA) of both the hardware and software stages, and Figure 22b shows the power spectral density (PSD):

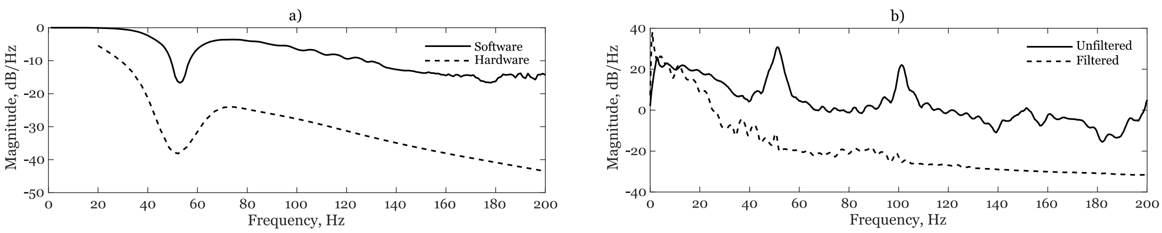

Figure 22: a) (left) Frequency response analysis of hardware and software stages, b) (right) power spectral density showing the combined effect of hardware and software filtering on a noisy test ECG signal injected directly into the front end

The majority of the ECG signal power is within the 0.5 to 40 Hz range, and the filter corner frequencies are chosen to match the specifications recommended by the American Heart Association, the American College of Cardiology and the Heart

Rhythm Society [129], and to minimize uncertainty in the measurement of the R-R peak intervals used to calculate the HR [130]. Figure 22b shows that the peak at 50 Hz which represents the mains electrical hum, in our measurements, the system-induced power line noise is reduced by 40 dB, and the subsequent peak at 100 Hz is also not present. This shows the system capacity for filtering 50 Hz and higher harmonic frequency noise that are most common in ECG recordings.

3.2.3 Output stage

A custom graphical user interface (GUI) coded in C++ running on Raspbian Linux OS displays the output of the EPS sensors after the filtering stages on a 7" capacitive touch screen display (Official Raspberry Pi 7" Touchscreen Display ACGGD070-004-CG-B, resolution 800 x 480 pixels). See Figure 23.

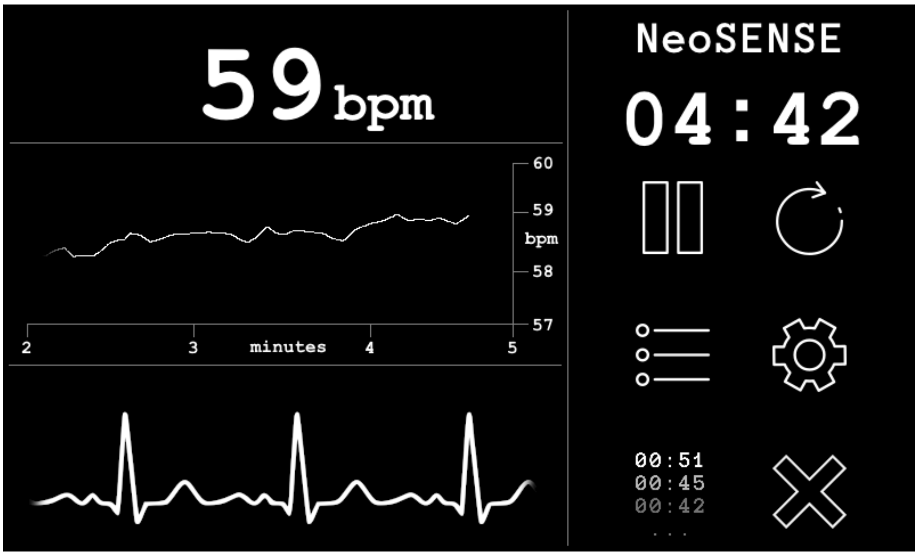

Figure 23: Screenshot of prototype graphical user interface with clinician statistics display (instantaneous HR, HR variation with time & idealised waveform) on the left and user controls on the right.

The GUI allows for real time inspection of the cardiac signal and heart rate. The layout and information presented on the GUI was informed both by the existing literature and by consultation with our clinical partners. The principle that certain values and trends relevant to the specific clinical use of the device should be emphasised is employed here [131]. The key information for the clinician (instantaneous HR) is displayed in large type in the top left, with a historical measure of HR spanning the last 3 minutes below for identification of longer term HR trends during interventions. Data is stored on the device memory and can be timestamped and reset from within the GUI using the controls on the right hand side. These controls also include a large and easily legible stopwatch function, which was identified by our clinical partners as a vital tool. Examples of the use of stopwatches include timing the elapsed period from birth, or between resuscitation attempts.

The system is portable and can be powered by a standard 5V DC USB power bank, giving a running time of 4 hours from a 10,000 mAh battery. Considering IEC 60601 the prototype presented here is classified as an IP (internal power supply) device. The use of a battery DC supply removes the possibility of 50 Hz power line noise contamination of the signal that is often common in devices powered by mains switch mode power supplies that convert AC to DC. Please note that under the classification of patient applied parts the EPS sensors, being non-contact and isolated behind a dielectric material, are not covered under IEC 60601, however the reference electrodes are considered as patient applied part floating - surface conductor. In this prototype, the device was designed so that it cannot be operated during the battery charging cycle.

3.3 Experimental Results

The goal of our experimental tests is to assess the suitability of the manufactured textile-based electrodes for use in a full end to end non-contact ECG acquisition system. In order to evaluate these, two ECG recording scenarios were investigated:

- A simulated cardiac signal employing a neonatal simulation environment
- A real cardiac signal from an adult volunteer

The neonate simulation environment is used to form an initial comparison of ECG reproduction and a baseline comparison of the different electrodes. Then the human volunteer serves to establish a proof of concept for the end to end system. Three electrode configurations were evaluated in each of the two scenarios:

- baseline copper electrodes
- conductive polymer ink
- conductive textile fabric

To simulate signal acquisition of the heartbeat of a neonate a simulated ECG signal was radiated from a premature infant mannequin, with an internal antenna (3 cm^2). The bio signals were generated in a custom LabVIEW GUI using a USB 6009 National Instruments DAQ with a 16-bit digital to analog converter (DAC). This test ECG signal was radiated across an air gap of 2 cm and through 2 mm of the electrically insulating plastic of the mannequin having an amplitude of 200 mV peak-to-peak (PP) at 140 bpm. A human ECG was also taken from a male adult volunteer as a proof of concept trial, with the subject sat in a comfortable upright position and the sensor attached to the chest using an additional 5 cm layer of foam padding on the reverse to simulate the delivery room mattress material. Figure 24 shows the position of the sensors and interference layers for both scenarios.

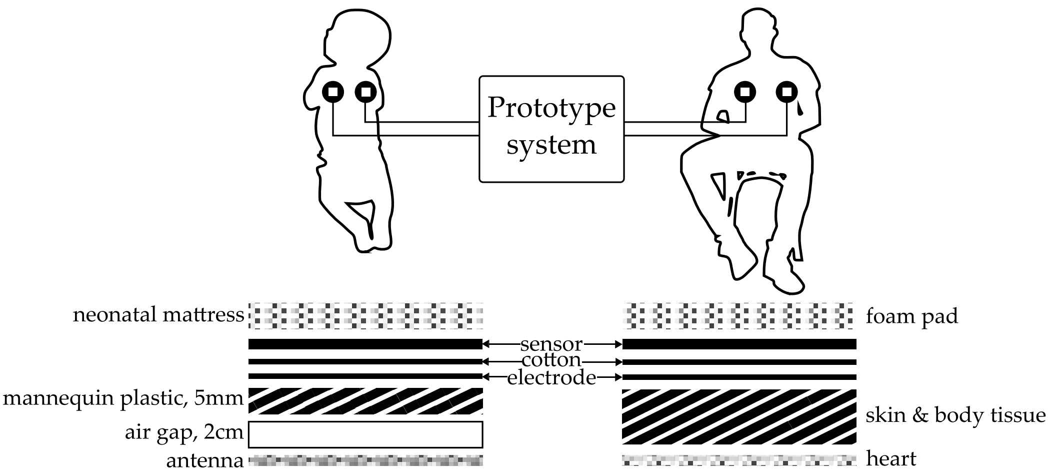

Figure 24: Experimental set up - electrode placement and interference layers for simulated and human ECG readings, left neonate mannequin, right human volunteer

After signal acquisition was carried out, multiple readings of 60 second segments were taken for the simulated mannequin signal and the human volunteer. These were exported from the data acquisition system and imported into MatLab for analysis.

3.3.1 Neonatal simulation environment

The mannequin providing the simulated ECG signal was used as a control to create a baseline of ECG reproduction regarding the comparison of copper electrodes with the manufactured textile-based electrodes.

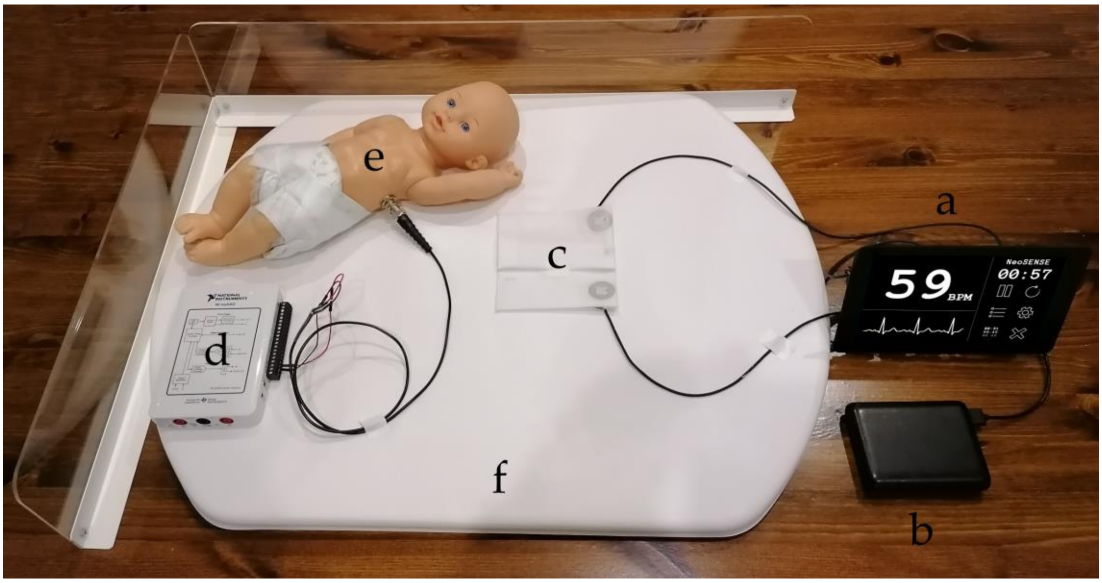

Figure 25: Photograph of prototype system hardware in neonate simulation environment: a) front end and GUI (Dimensions 195x100x90mm); b) USB 5V power bank; c) EPS sensors & textile based electrodes; d) digital to analog converter for test signal generation; e) neonate mannequin with internal antenna; f) commercial delivery room mattress

Figure 25 shows the neonatal simulation environment and test setup for the initial signal characterisation providing the simulated ECG signal. The neonate mannequin was placed on top of the electrodes and sensors to perform the recordings. Figure 26 shows a representative sample of 5 seconds of simulated signal ECG recording.

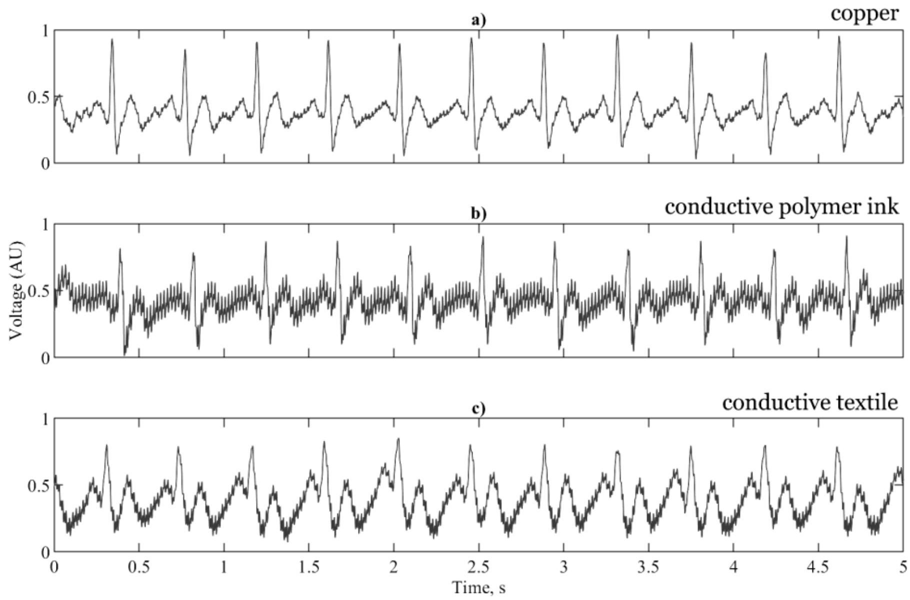

Figure 26: 5 seconds segments of a simulated ECG signal for a) baseline copper electrodes; b) conductive polymer ink; c) conductive textile fabric

Figure 26a shows the signal reproduction of the simulated test signal using the copper electrodes, the conductive polymer ink and conductive textile fabric. For accurate HR calculation the R peak of the ECG signal must be clearly visible above the baseline. For each of the three sensor configurations the R peak is prominent and suitable for RR interval calculation. Figure 26b shows the T and P waves of the ECG clearly reproduced, with the same timing as the reference copper electrodes having an increase in the noise components. For the conductive textile fabric electrodes shown in Figure 26c the waveform is distorted with the T waves elevated, the R peak and subsequent characteristic dip truncated, and the amplitude of the P waves increased. High frequency noise is present in the conductive textile fabric electrodes, but at a lower amplitude than the conductive polymer ink electrodes.

Analysis of a single beat and power spectral density (PSD) of the recorded signals is presented in Figure 27:

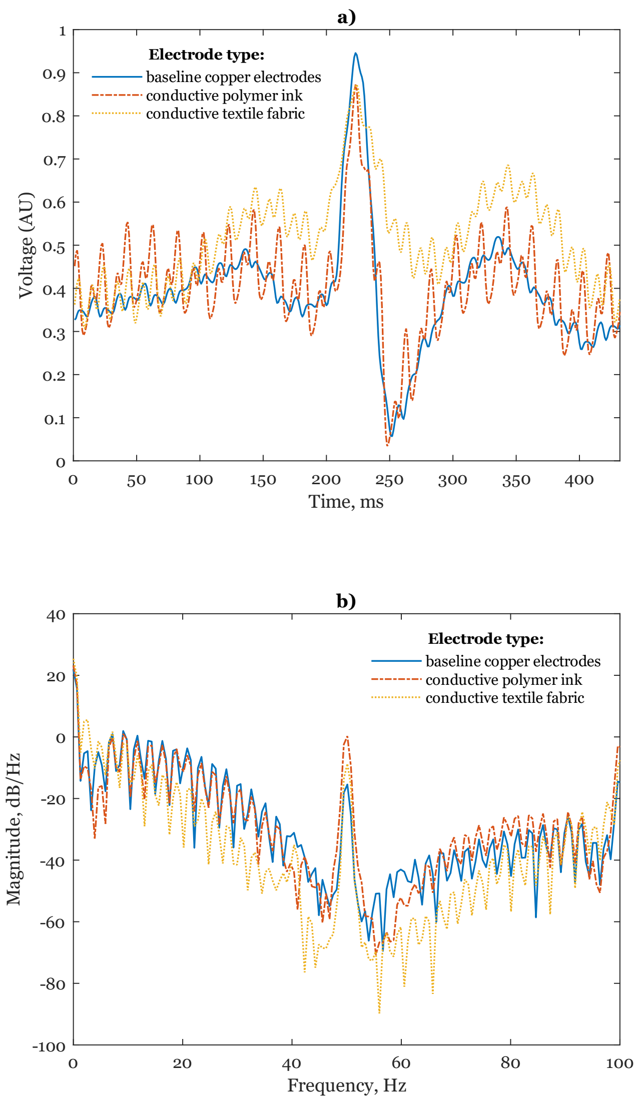

Figure 27: a) Single beat waveform and b) PSD of a simulated ECG simulated from the test mannequin for each electrode configuration

50 Hz noise is visible for both the polymer ink and conductive textile electrodes. This is more pronounced for the polymer ink electrode. The air gap between the antenna and mannequin body has a capacitance that dominates the total electrode capacitance in the series connection [132] with the insulating layer of the EPS sensor, so any noise in this gap will be amplified in the final signal.

Data from the simulated cardiac signal in a neonatal simulation environment was processed using the Pan Tompkins algorithm for HR calculation, and a mean RR interval and average bpm was calculated. Considering the precise bpm of the simulated signal, these results can then be used as a measure of the accuracy of the sensor acquisition and ECG recording stages.

140 bpm simulated signal:

Electrode	Mean RR interval, ms	Average bpm
baseline copper	428.6	140.2
conductive polymer ink	431.6	139.0
conductive textile fabric	428.3	140.0

60 bpm simulated biosignal:

Electrode	Mean RR interval, ms	Average bpm
baseline copper	999	60.1
conductive polymer ink	1001	59.9
conductive textile fabric	1004	59.8

Table 7: RR interval & calculated bpm comparison of the mannequin simulated signal for each electrode case at 140 bpm and 60 bpm generated test signals

The mean RR intervals as shown in Table 7 are within 0.5 % of the expected RR interval of 432 ms for a heart rate of 140 bpm, the heart rate for the normal neonate being between 120 to 160 bpm [106]. The average bpm recorded by the system are with 1 bpm of the simulated signal, which compares favourably with pulse oximeters which commonly have a stated accuracy of ± 2 bpm. An additional test signal at 60 bpm confirmed the suitability of the device for recording low heart rates and showed RR intervals within 0.4 % of the expected RR interval of 1000 ms and an average within ± 0.2 bpm.

3.3.2 Proof of concept with human volunteer

The prototype system was then used to characterize a human cardiac signal. The weight of the heart of an infant is ~ 14 times smaller than that of an adult [133], resulting in a reduction of the ECG signal amplitude falling within the micro to millivolts range. Nevertheless, EPS sensors have proved to record high quality ECGs from a young infant [89].

The sensors, front end and power bank (Figure 25 a, b and c) were removed from the neonatal simulation environment and applied to an adult volunteer. The proof of concept trial showed more accurate signal reproduction for the fabricated electrodes compared to the baseline copper electrode than in the mannequin tests. A 15 second sample of each test case is show in Figure 28:

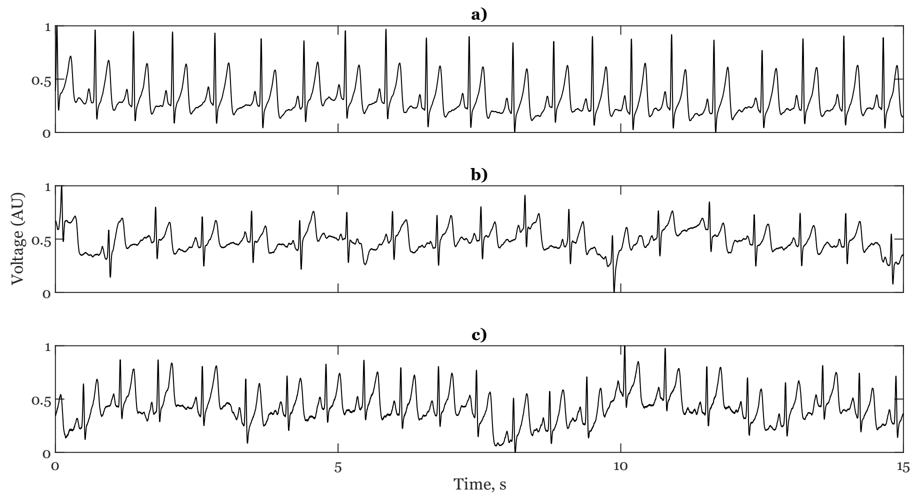

Figure 28: 15 seconds segments of a human signal ECG signal recorded with a) baseline copper electrodes; b) conductive polymer ink; c) conductive textile fabric

The R peak is visible in each ECG trace having a suitable amplitude for HR calculation, along with the P and T waves. Despite the high pass filtering, baseline wander caused by the EPS susceptibility to movement artefacts (such as respiration) are more prominent in the conductive polymer ink and conductive textile fabric electrode cases.

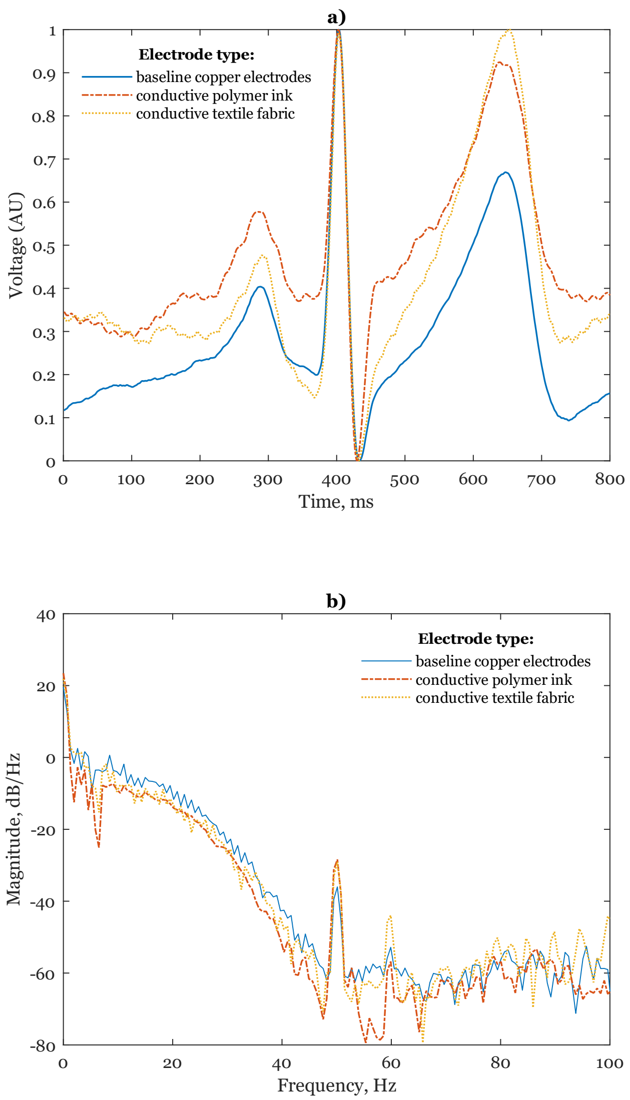

Figure 29: a) Single beat waveform and b) PSD of a human ECG for each electrode configuration

The power spectral density for the 3 test cases (Figure 29b) shows that again, as in the mannequin test, the ink and conductive textile fabric electrodes pick up more 50 Hz noise than the copper electrodes. This peak, however, is substantially lower than the peak previously recorded (-30 dB/Hz compared to -10 dB/Hz for the mannequin). The thickness and relative permittivity of the cotton layer, which is not present in the baseline copper electrodes, alters the capacitance of the skin-electrode interface being responsible for this increase in noise in agreement with [134].

Discrepancies in the amplitude of the P and T waves visible in Figure 29a are likely caused by slight differences in the locations of the sensors on the subjects torso from test to test, however the P, R and T waves are of equal width with matching peaks indicating that the ECG is faithfully reproduced. The peak of the T wave for the conductive textile electrode is as large in magnitude as the R peak for this particular beat, however this will not affect the R peak detection as the detection algorithm uses the derivative of the signal. Given this, the gradual slope of the P wave will not be considered as a peak candidate.

3.3.3 Signal quality assessment

There is no single standardized metric for defining ECG signal quality, therefore, to provide a robust analysis for both the silver conductive and textile conductive electrodes, in comparison with the baseline copper electrodes, three methods have been considered. These are waveform averaging, wavelet-based ECG delineation, and pSQI/kSQI (relative power in the baseline and the kurtosis of the signal respectively).

3.3.3.1 Waveform averaging

A waveform averaging approach as described in [135] has been used for signal quality assessment and the identification of heartbeats. Irrespective of the actual morphology of the ECG features for a given signal, this technique considers the regularity of a signal and can be used as a strong indicator of the repeatability and reliability of the ECG recording method, as any artefacts introduced in the recording or processing would result in morphological irregularities. The following approach was applied in the human ECG recordings, and the results of this analysis are presented in Figure 30 and Table 8 below.

1. R-peaks were detected using the Pan-Tompkins algorithm, and an average R-R interval was calculated.
2. Individual heart beats were extracted using a window with a number of samples equal to that of the average R-R interval and centered on each detected R peak.

3. An average of the extracted heart beats was calculated, which was used to derive the correlation coefficient of each beat using the following formula:

$$CorrXY = \frac{\sum_{i=1}^{n_{window}} (x(i) - \mu_x) \cdot (y(i) - \mu_y)}{\sqrt{\sum_{i=1}^{n_{window}} (x(i) - \mu_x)^2} \sqrt{\sum_{i=1}^{n_{window}} (y(i) - \mu_y)^2}}$$

Equation 6

Where n_{window} is the number of samples in the individual beat window (in this case 800), *x(i)* is the ECG signal, *y(i)* is the average heartbeat signal and μx and μy are the means of *x(i)* and *y(i)*. An average of these correlation co-efficients ($\mu CorrXY$) was taken to obtain a total average correlation coefficient for each test case.

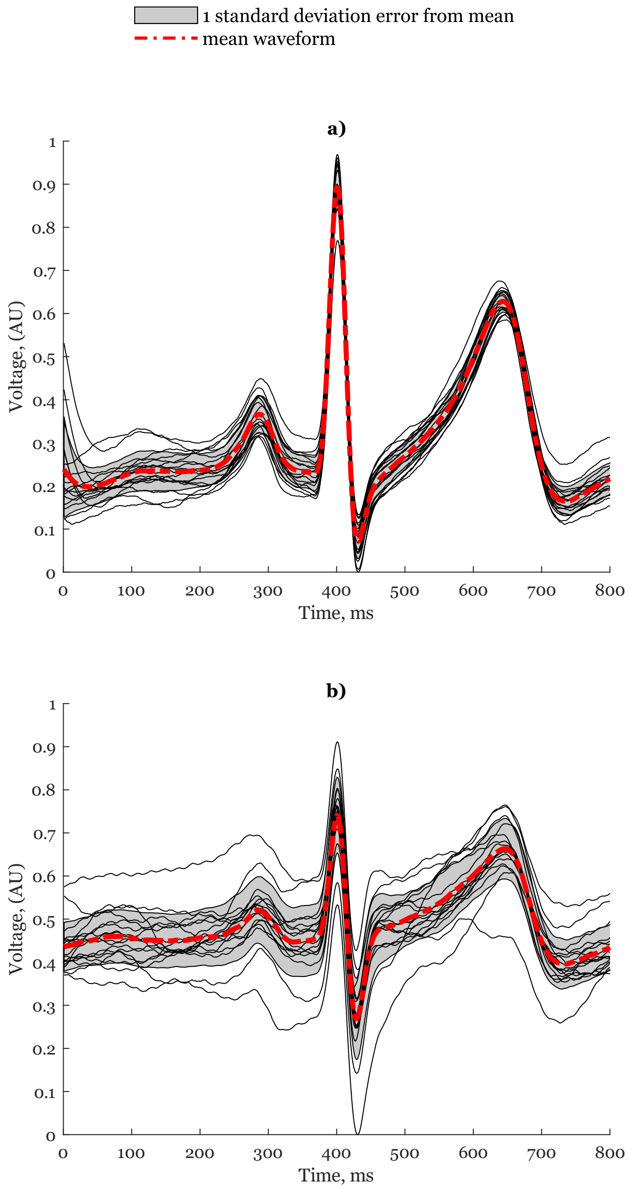

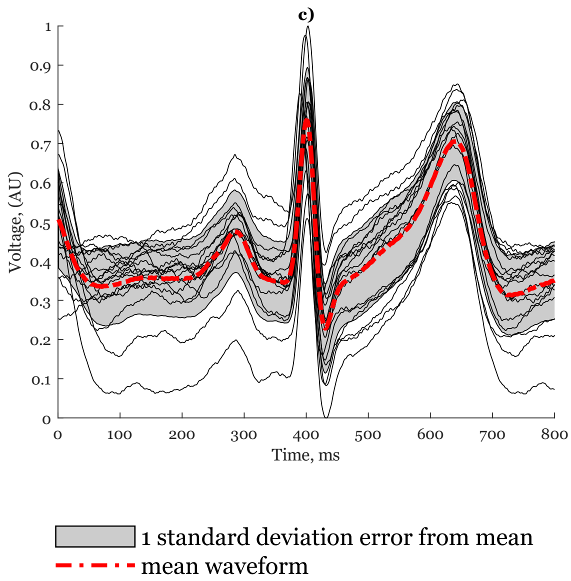

Figure 30: Waveform averaging of the human ECG for a) baseline copper electrodes; b) conductive polymer ink; c) conductive textile fabric

The regularity of the waveforms in Figure 30a show that the copper electrodes provide a reliable baseline for comparison using the manufactured electrodes, with 80% of the waveforms residing within 1 standard deviation of the mean. This is evidenced by the high correlation co-efficient displayed in Table 8:

Electrode type	Average correlation co-efficient, μ_{CorrXY}:
baseline copper electrodes	0.987
conductive polymer ink	0.865
conductive textile fabric	0.902

Table 8: Average correlation coefficients

Both fabricated electrodes (Figure 30b and c) show the P and T waves broadly represented correctly in terms of peak position and width. The R peaks were correctly identified for all beats by the Pan Tompkins algorithm, but there is more variation than in the baseline case. The conductive polymer ink electrodes (Figure 30c) showed the worst beat to beat signal reproduction, with the lowest correlation co-efficient and clearly deformed features of the ECG. Despite the effects of baseline wander affecting the amplitude of the signal, the conductive textile fabric electrodes produced regular and repeatable waveforms, with only 25% of the beats falling outside one standard deviation from the mean. This observation is confirmed by the higher correlation coefficient score obtained by the conductive textile fabric electrodes in comparison to the conductive polymer ink electrodes (see Table 8).

3.3.3.2 Wavelet-based ECG delineation

While there is no standardized consensus on delineating the location of the components of the ECG wave, the repeatability and similarity of individual ECG readings for each of the electrode cases can still be compared. The duration of the P, QRS and T waves of the ECG can be used as an indicator of the signal quality of the reading, as any unwanted noise or phase shift introduced by the electrodes would alter the length and location of these features. A wavelet-based delineation algorithm [136] separates and identifies the features of the ECG, as demonstrated with one of the recorded signals in Figure 31:

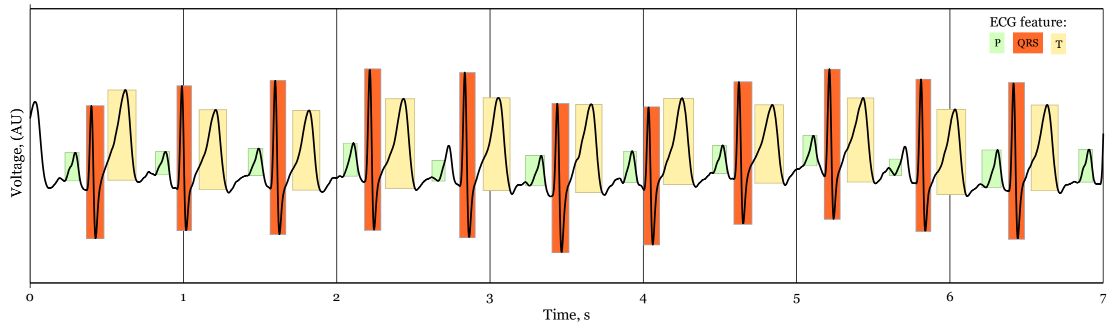

Figure 31: Wavelet delineation of a 7 second sample of recorded ECG, showing the location and duration of the waveform features

This algorithm was implemented in MatLab using the PhysioNet ECGKIT toolbox [137] to compare the duration of the ECG features, as well as the RR intervals, for each of the five 60 second recordings for the three electrode cases. The pooled mean for each case is shown in Figure 32, with an error of 1 standard deviation of the individual means:

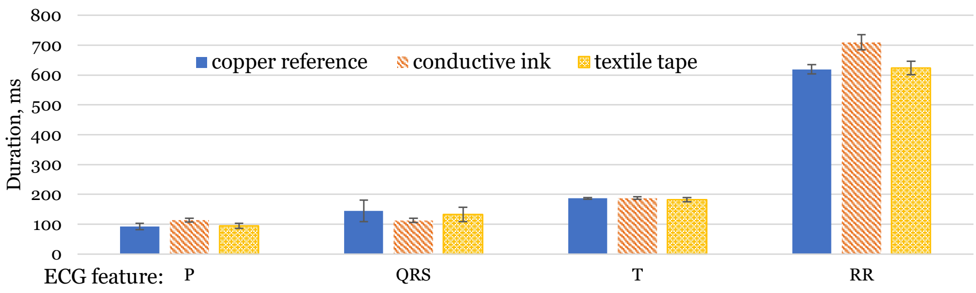

Figure 32: mean P QRS and T lengths and RR intervals for each electrode case

The calculated P, QRS and T wave lengths are closely grouped, showing that the electrodes did not introduce any major variation into the waveforms that altered the output of the delineation algorithm. The conductive ink electrodes showed the largest deviations, notably a reduction of 23% in the mean length of the QRS feature compared to the copper reference electrode. Small variations in the feature lengths can be attributed to small variations in the placement of the sensors for each data set but are broadly compensated for by the sample size.

3.3.3.3 Relative power & kurtosis

Two additional signal quality indicators (SQI) are considered for evaluating the proposed electrodes, the relative power in the baseline (pSQI) and the kurtosis of the signal (kSQI). These SQIs are used as indicators of the clinical acceptability of ECGs for HR calculation and further interpretation [138].

pSQI considers the fact that the energy of the QRS feature is concentrated between 5 and 15 Hz [139] and the QRS feature is the main feature used in determining HR, therefore a comparison of the ratio of power in this band with the band power of the total signal provides a quantifiable measure of ECG quality. pSQI is defined as:

$$baseline\ relative\ power, \qquad pSQI = \frac{\int_{f=5\ Hz}^{f=15\ Hz} P\ (f)df}{\int_{f=5\ Hz}^{f=40\ Hz} P(f)df}$$

Equation 7

Low pSQI is an indicator of high frequency noise in the ECG, such as the electric potential generated by muscle cells, whereas high pSQI is the result of artefacts such as electrode motion due to subject movement. pSQI values should be within a range of 0.5 – 0.8 for clinically acceptable ECG recordings.

kSQI is a measure of the correlation of the ECG signal. The central limit theorem shows that random signals such as noise tend towards gaussian distributions, and correlated signals, such as the repeating pattern of an ECG, tend towards non-gaussian distributions. kSQI is a simple measure of how gaussian-like a signal appears to be, as defined by:

$$kurtosis, \qquad kSQI = \frac{E(x-\mu_x)^4}{\sigma^4}$$

Equation 8

A clean ECG signal generally has a kurtosis of more than 5, and artefacts such as baseline wander and power line interference reduce the overall kSQI. The kSQI was measured for 10 second segments of the ECG and average across the readings.

From the results in Table 9 we can see that all three cases displayed a high pSQI, within the bounds of clinically acceptable ECGs but towards the upper limit. This suggests that electrode motion is present in these recordings, which is clear from the baseline wander shown in Figure 28b and c where it is clearly more pronounced in the textile-based electrodes than in the copper reference electrodes.

Electrode:	**pSQI**	**kSQI**
baseline copper	0.79	4.9
conductive polymer ink	0.74	3.8
conductive textile fabric	0.74	4.2

Table 9: Signal quality indices for each of the electrode cases

The kSQI results clearly show the influence of 50 Hz noise in the recordings (also visible in the noise peaks in the power spectral density in Figure 29b) with a reduction of 22% and 15% respectively for the conductive ink and textile fabric electrode in comparison with the reference case.

The waveform averaging, wavelet-based delineation and signal quality indices all show strong correlation between the baseline copper electrodes and the textile based electrodes. In particular the main feature of interest (the R peak) is reproduced allowing for accurate HR calculation in both textile-based electrodes.

3.3.4 Heart rate acquisition time

One of the primary requirements of a device for monitoring during resuscitation is that HR readings should be displayed within a time frame below 30 seconds to avoid oxygen deprivation consequences such as cerebral palsy, impaired motor skills etc. In this section, one of the main advantages of the proposed system is the reduced time from birth to HR measurement. This is assessed in Figure 33 which shows a typical connection event from the proof of concept trial considering the adult participant:

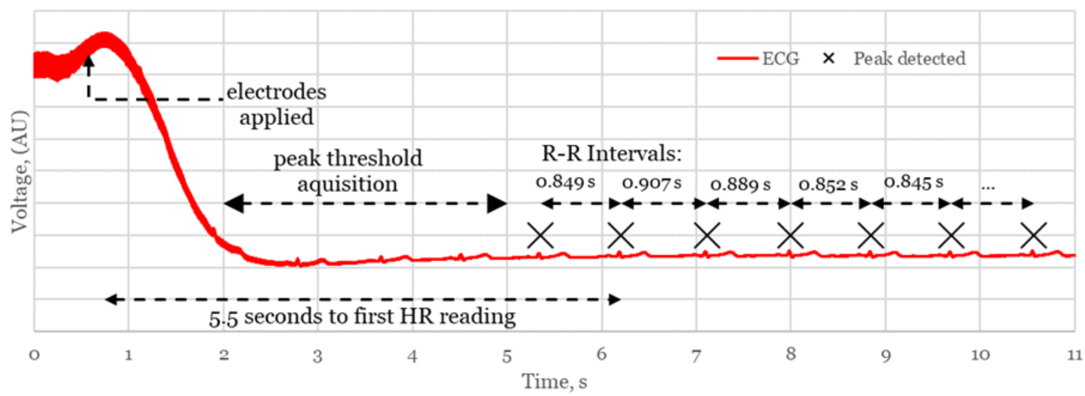

Figure 33: Connection event showing time from sensor application to first HR measurement

The system takes ~5.5 seconds to register an RR interval, after a 3 second delay for the Pan Tompkins algorithm to establish a threshold for R peaks. An averaged heart rate is compiled from the subsequent measured RR intervals to generate a stable reading in situations where there may be a loss of connection or incorrectly registered peaks in the presence of noise. Different competing systems use various sizes of window to generate the HR, dependent on technology and manufacturer. In our case, a stable and accurate heart rate was consistently measured using a window of 5 RR intervals, suggesting a minimum time from application to HR of around 8 seconds for a typical neonate with a HR of 140 bpm. This confirms the potential of the device to compete with, and surpass, existing delivery room technologies in rapidity of HR measurement.

3.4 Discussion & Conclusions

This work showed that the complete prototype system with novel EPS sensors and textile-based electrodes successfully recorded electrocardiograms from both a simulated and human source. Signal conditioning and filtering in the analog and digital stages removed unwanted noise and produced a high-quality ECG suitable for heart rate measurement.

Both fabricated silver and conductive fabric electrodes accurately reproduced the R peak timing of the simulated ECG signal to ~ 0.5% of the baseline copper electrodes. The human ECG was also successfully reproduced using the textile based electrodes, and in comparison with the baseline copper electrodes where the temporal features of the ECG (QRS complex and P T wave) were correctly located, and the width of the QRS complex was within 1 ms of the copper reference electrode for both cases. Both implementations of textile-based electrode generated reliable and repeatable signals, with correlation coefficients of 0.90 and 0.87 for the conductive textile fabric and conductive silver ink electrodes respectively, compared to 0.99 for the reference copper electrode. The regularity of the signal acquired from the textile-based electrodes combined with their high signal quality gave a 100% detection confidence for each of the five 60 second human recordings, confirming their suitability to be used for ECG recordings.

A foam pad was used in the human trial to ensure both sensors were located at a repeatable position, however small deviations in body and sensor position translated to amplitude changes in the ECG waveform which limited the amplitude feature analysis in comparison to the baseline copper electrode ECG features. Further investigations could be performed using a range of textile based electrodes simultaneously to investigate amplitude effects, or in simultaneous comparison with a traditional AgCl electrode to determine any RR interval variations induced by different electrode configurations.

In comparison with the reference copper electrodes, the larger surface area and materials of the fabricated textile-based electrodes are more prone to picking up ambient 50 Hz noise. Therefore, the conductive polymer ink and conductive textile fabric electrodes collected larger amounts of 50 Hz noise added to the resultant signal of the human ECG by 30% (-40 dB compared with -30dB for the copper electrodes), where the output signal contained visible 50 Hz noise despite large amounts of frequency specific filtering capacity. The resultant reduction in signal to noise ratio is in part due to the sensing of the ECG through a layer of cotton fabric as well as the alteration of the skin-electrode capacitance, and the electrodes being prone to receive ambient 50 Hz noise. Despite this increased noise level, both test cases still produced a signal of sufficient quality for the calculation of HR from RR interval data.

The prototype system described here uses 2 electrodes. Future work on the prototype system could involve increasing the number of sensors to reduce the 50 Hz noise and providing a greater contact area for readings for the case when the neonate is moved during resuscitation efforts.

This work provides a strong proof of concept for the embedding of textile-based electrodes in a delivery room mattress for ECG measurement, as well as the demonstration of a complete standalone system for HR assessment, data acquisition and display. The extensive characterisation of conductive textile fabric and conductive silver ink electrodes in comparison with a standard reference copper electrode confirms their suitability for use in such a device. These novel flexible electrodes are suitable for embedding in a delivery room mattress and provide the benefits of conformity for increased signal quality and a reduction in the chance of abrasive damage to delicate newborn skin. Signal quality assessment confirmed that high quality ECG recording was achieved in the presence of interference layers and an air gap, with reliable and repeatable ECG waveforms. The device described here could conceivably be used to automatically acquire the HR of a newborn immediately after delivery without the need to attach additional sensors in a safe, rapid and reliable way.

Chapter 4: Model based Wiener filtering for electric potential sensing ECGs: a phantom study

4.1 Introduction

The cardiac biopotentials measured from the skin are of the order of 1 mV, and the majority of the power spectrum of the ECG is concentrated in the 1-40 Hz band [140]. The low amplitude and narrow band of the ECG signal makes it highly susceptible to both external noise and noise inherent in the signal itself. The predominant noise is power line interference (50/60 Hz depending on country) but low frequency (LF) components such as motion induced artefacts from breathing or muscle action and high frequency (HF) components from RF signals [141] are also present. The standard filtering method (implemented in either in hardware or software) specifies linear 0.5 Hz high pass and 200 Hz low pass filters to remove LF & HF noise [142] respectively and produces ECGs suitable for diagnosing arrhythmias and informing interventions.

The initial clinical application of the ECG was in the detection of acute myocardial injury and later in the identification of atrial fibrillation, but improvements in signal processing and the introduction of novel sensors have expanded the potential applications of the ECG. The ECG is now included in personal eHealth devices such as smart watches and smart mattresses for neonatal monitoring [143], and the ECG is routinely used as security biometric [144]. With the introduction of new applications and new sensing methods there is a demand for improved signal processing for the reduction of noise. The higher frequencies components (150 to 250 Hz) of the ECG can improve detection of coronary artery occlusion [145] and myocardial ischemia [146]. Artificial Intelligence based interpretation systems can now find signals in the ECG that may be invisible to the human eye [147]. Many of these new applications would benefit from a higher signal to noise ratio a signal range outside the commonly used band pass range of 0.5 – 200 Hz which is largely a relic from the limitations of legacy technologies' sample rate and bit depth.

Traditional filters used in signal processing are designed for a certain response (e.g. low pass, high pass etc.) at a target frequency. In contrast, the Wiener filter takes a statistical approach, and given the known spectral properties (the power distribution of the signal in the frequency domain) of the original signal and the added noise, attempts to approximate the linear time invariant filter that has an output most closely matching the original signal. Ideal Wiener filtering requires an accurate knowledge of the noise level or the original signal.

Wiener filtering has been shown to be effective in reducing noise and improving the signal quality of the ECG [148, 149] however these methods rely on an estimation of the noise. In the case of the ECG and other biopotentials the signal is also unknown, and will differ depending on many variables including the physiology of the patient, placement of sensors etc. An improved “a Posteriori” Wiener filtering [150] has been used in the noise reduction of biosignals, however the limitations of using an estimated spectrum for subtraction with its inherent variabilities and the problem of overlapping signal and noise spectra causing suppression of signal components limit its effectiveness.

For traditional AgCl electrodes the common types of noise in a clinical setting are well understood, but in the case of novel electrodes and in non-clinical settings the types and levels of noise can vary during ECG collection. Cellular and Wi-Fi transceivers [151] as well as RFID equipment [152] have been also shown to cause interference in ECG recordings which could potentially lead to misdiagnosis.

In this work we consider the use of electric potential sensors (EPS) [13]. EPS sensors do not require galvanic contact with the skin and instead operate with displacement currents. In this way, high resolution ECGs can be recorded without the need for sensor attachment allowing for rapid and accurate infant HR calculation. EPS sensors are more susceptible to ambient noise (predominantly 50/60 Hz power line interference) than AgCl electrodes and can also pick up other frequencies that would not be considered in the traditional filtering schemes [153].

As Wiener filtering requires an accurate knowledge of the noise level or the original signal, to overcome the problem of the ECG as a blind source and unknown or varying noise levels this work proposes the use of a known injected signal recorded alongside the ECG from which an accurate noise reading can be taken, as opposed to a noise estimate, leading to improved and adaptive Wiener filtering. This method has been shown to be effective in removing power line and short electromagnetic interference (such as the bursts characteristic of cellular and Wi-Fi data transmission) in geophysical magnetic resonance sounding measurements [154], and this technique is adapted in this work for use in electric potential electrocardiography. The method is validated using a cardiac phantom using both generated and human biosignals in a real world setting to provide a robust proof of concept.

4.2 Materials and Methods

4.2.1 Wiener filtering

Consider an idealised ECG signal described as:

$$x(t) = s(t) + n(t)$$

Equation 9

Where $x(t)$ is the ECG waveform recorded from the sensor composed of $s(t)$ the electrical signal of the heart and $n(t)$ being the noise component. The optimal filter to reconstruct signal $s(t)$ is calculated by:

$$H(f) = \frac{P_{ss}(f)}{P_{ss}(f) + P_{nn}(f)}$$

Equation 10

Where *H(f)* is the transfer function of the filter, *Pss(f)* and *Pnn(f)* are the known power spectral densities of the signal and noise respectively.

Given full knowledge of the underlying cardiac signal *s(t)* the noise component *n(t)* this can be easily determined by simple subtraction, and the Wiener filtering process produces an accurate reproduction of the original signal, minimising the mean square error. However, in the real world it is not possible to know the original signal or the noise, as described previously. To overcome the problem of unknown signal and noise components this work proposes the injection of a known signal for the calculation of noise via subtraction. Figure 34 shows an idealised Wiener filtering process using generated signals:

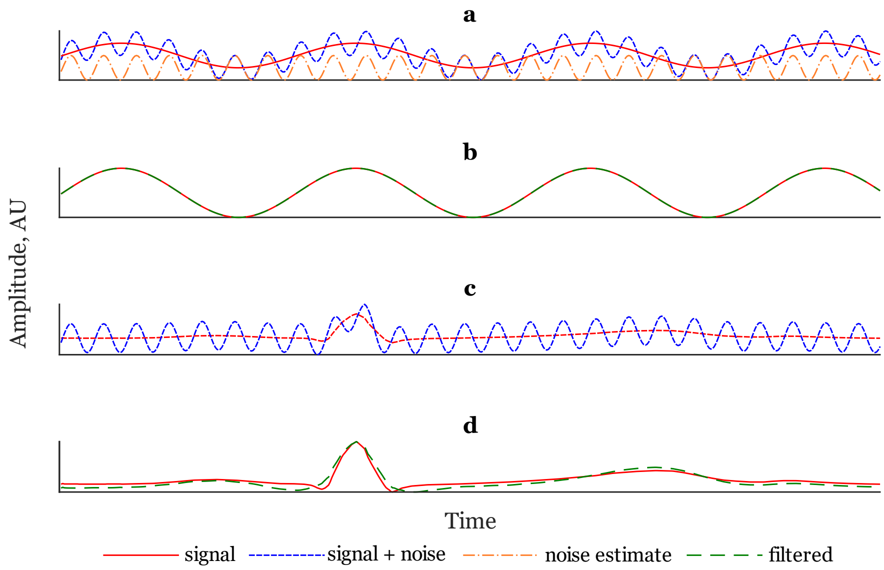

Figure 34: An example of ECG Wiener filtering: (a) reference signal & noise estimation; (b) reference filtering; (c) Idealised ECG & sensor output; (d) ECG filtering

In Figure 34a, we see a 7 Hz sine signal and the same signal with added 50 Hz noise, by simple subtraction we get the calculated noise. From this the ideal filter H(f) is calculated, and the original and filtered signals are shown in Figure 34b, with a minimal mean square error. Figure 34c shows an idealised ECG signal and the same signal with 50Hz noise added. Applying the filter H(f) derived from the sine wave gives us the filtered ECG signal in Figure 34d. Whilst there is more error in the filtered ECG than the filtered sine, the 50 Hz noise is entirely removed, improving the quality of the ECG.

4.2.2 Phantom

To provide meaningful and repeatable data, a cardiac phantom was developed for testing. This phantom serves two purposes: to mimic the interference layer of tissue between signal source and sensor, and to provide a signal ground path with similar conductivity to human tissue. It consists of a stack of layers modelling the voltage of the heart and the signal propagation through the human tissue. The phantom will act as both simulated neonate cardiac signal and destination of injected signal for noise calculation.

Agarose gel is routinely used to mimic brain tissue in phantoms for magnetic resonance (MR) and nuclear magnetic resonance (NMR) imaging [155]. Pharmaceutical-grade agar powder (Intralabs, UK) was mixed with a saline solution at various concentrations to increase the conductivity. When cast into a known volume, the conductivity at a range of frequencies can be determined using Equation 11, aiming for a conductivity ≈ 0.5 Siemens/m as described in [156]:

$$Conductivity, \qquad \sigma = \frac{1}{\rho} = \frac{l}{R \times A}$$

Equation 11

where, σ is the electrical conductivity in Siemens/m, ρ is the electrical resistivity (Ohms-m), R is the electrical resistance (Ohms), A is the cross-sectional area of the gel sample in m^2 and l is the length of gel sample in meters. Agar formulations with a range of salt concentrations were cast into 20 mm diameter ABS tubing. After cooling and solidification samples were placed in a test jig and subjected to a 10 V peak to peak voltage at room temperature (~25° C), with the resulting measured voltage and current values being used to calculate resistance. The results are shown in Figure 35, leading to a final concentration of 1 mg/100 ml for an approximate conductivity of ≈ 0.5 Siemens/m.

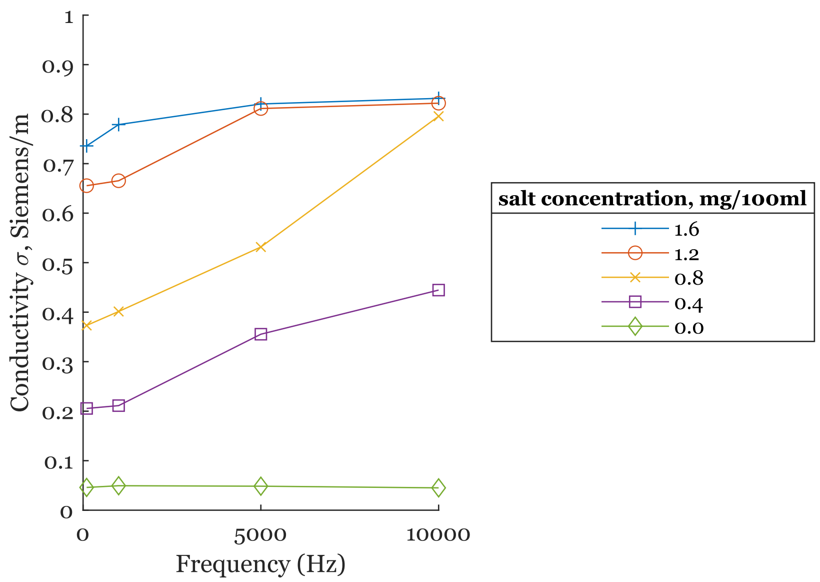

Figure 35: Salt doping of agar phantom

Agar castings were then placed on top of an insulating base with a copper ground loop and voltage source emitter connected to a signal generator as shown in Figure 36.

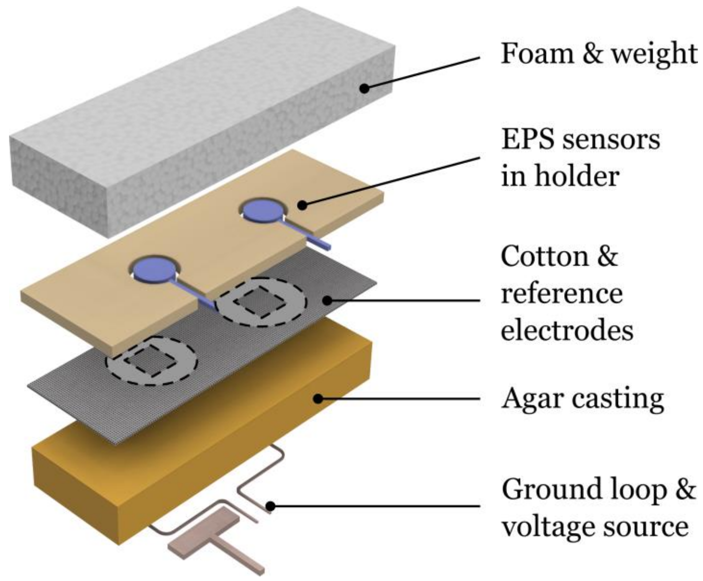

Figure 36: Fabrication of neonate phantom stack

The EPS are held in place by an insulating central layer to constrain any movement of the sensors and ensure repeatable placement. Each layer has dimensions of 50 x 120 mm (width x length). The agar casting was 10 mm thick to approximate the distance from thorax to the heart in a neonate, and the holder and foam layers were 5 mm and 20 mm thick respectively.

Phantom stiffness and sensor contact pressure has a direct effect on signal quality which is highly dependent on the distance between EPS and voltage source, therefore any deformation of the phantom will decrease distance and increase signal quality. Typically, agarose powder is used at 1% concentration, but this leads to a casting with insufficient stiffness. The combined Young's modulus of bulk tissue in the body varies from around 0.4 to 1.5 MPa[157], therefore following the recommendations in [158] a 4% agarose concentration was used to approximate a modulus in the middle of this range of approximately 1MPa. Contact pressure was controlled using a 50g weight placed on top of a foam block for even distribution on the phantom stack (contact area of 0.05 X 0.05 cm) to generate a pressure of 196 Pa, this corresponds to a light pressure similar to manually pressing the sensors to human skin, which is sufficient to achieve sensor coupling without causing excessive indentation.

4.2.3 Experimental setup

Three tests are considered in this study: a system characterisation using simulated signals, an analysis using real world signals taken from an ECG waveform database, and a limited test using the researcher's own biosignals. The simulated signal test system is described in Figure 37.

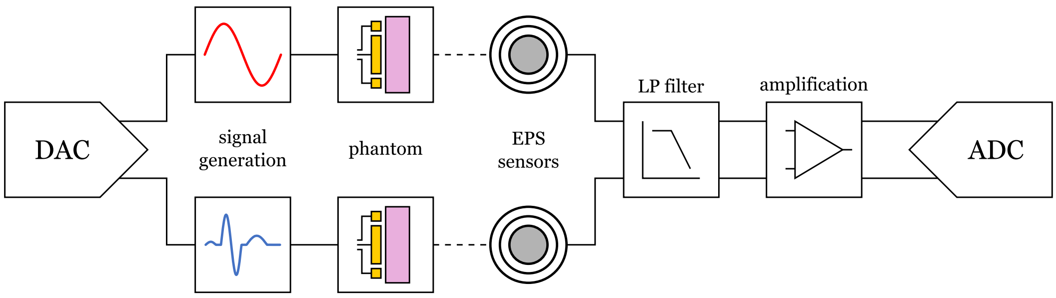

Figure 37: Block diagram of test system

Sine reference and simulated biosignal data are transmitted to a pair of phantoms by the DAC at 12 bit, 1 kHz. An accurate signal amplitude to simulate a human ECG was derived by observing the voltage output of the EPS sensors when reading a normal adult ECG in previous works. The output of the EPS sensors when attached to the phantom was matched to this observed value by varying the amplitude of the generated signals, resulting in a generation amplitude of 10 mV PP for both the sine and biosignal. These signals are picked up by the EPS sensors and processed by an analog front end consisting of a 2nd order antialiasing low pass filter (cutoff frequency fc = 500 Hz) and amplification for full ADC utilisation. Digitization and signal generation is performed by a National Instruments myDAQ (National Instruments, TX, USA). Signal generation and acquisition is performed at a sample rate of 1kHz at 16bit resolution. For the human test the second phantom was replaced with an EPS sensor attached to the researcher's chest by an elasticated band. The resulting data is then processed in MatLab using the algorithm described in Figure 38.

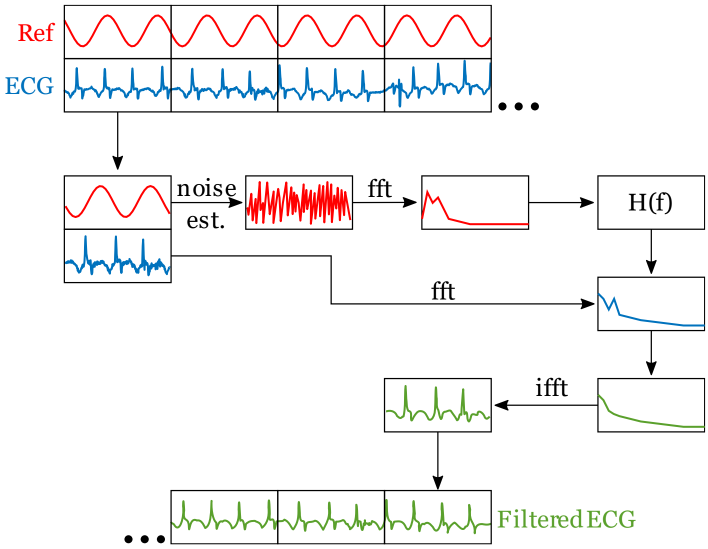

Figure 38: Filtering algorithm

To reduce computational power and allow for online filtering the data is not continuously filtered but instead windowed into 1 second segments. The reference sine wave with known frequency is amplitude matched to a generated sine wave and phase corrected in case of any system lag, then subtracted to give a noise estimate. The ECG and noise estimates are both fast Fourier transformed and, being sampled at 1 kHz give an FFT frequency resolution of 1 Hz. Two main metrics are considered to evaluate signal quality of the filtered ECG: mean square error (MSE) and 50 Hz attenuation. MSE is calculated as the averaged squared difference between the generated biosignal and the filtered EPS reading using Equation 12:

$$MSE = \frac{1}{n}\sum_{i=1}^{n}(Y_i - \hat{Y}_i)^2$$

Equation 12

where Y_i is the filtered EPS reading, $\hat{Y}_i$ is the generated signal broadcast from the phantom, and $n = 1000$ for the 1 second window sampled at 1 kHz. These MSE values are then averaged across all windows for each individual test to get a window averaged MSE. 50 Hz attenuation is considered significant as it is the predominant ambient noise that the EPS sensors pick up in operation. This is calculated by subtraction of the power at 50 Hz for the frequency domain transforms of the filtered and unfiltered signals, as these are available from the FFT of each window. Again, these 50 Hz attenuation values are averaged across all windows for each test.

4.3 Results

4.3.1 Reference sine wave frequency

A study was performed to determine the optimal frequency of the reference sine signal. Figure 39 shows a sample of the results from this testing:

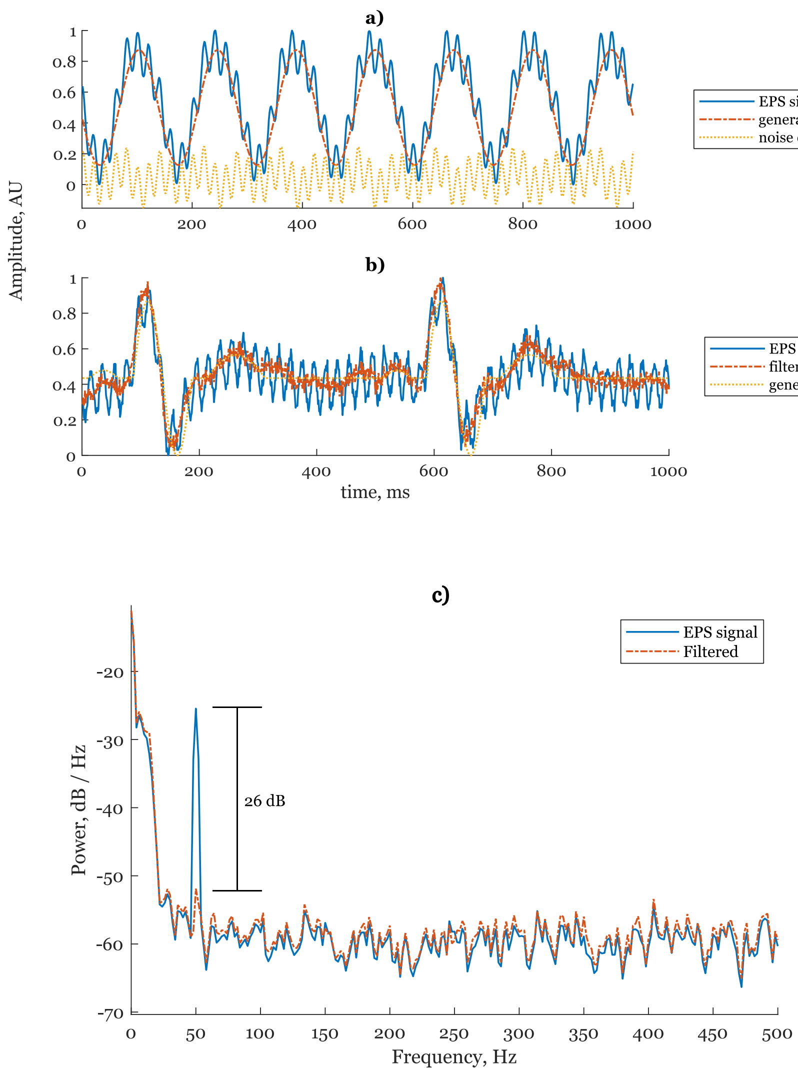

Figure 39: Sample data from the Wiener filtering algorithm: a) reference sine wave and noise estimate; b) ECG signal filtering; c) PSD of ECG signal pre and post filtering showing 26 dB reduction in 50 Hz noise

In Figure 39a the reference sine signal is shown at a frequency of 7 Hz. Phase matching is performed on the EPS signal to remove any errors in transmission in the signal chain, and amplitude matching to remove the amplification and attenuation effects of the phantom and EPS sensors. Then by subtraction of the EPS and generated signals the noise estimate is calculated and used to generate the ideal Wiener filter. Figure 39b shows a sample of the EPS data output as well as the wiener filtered signal and phase & amplitude matched input signal. The mean square error (MSE) is calculated from the filtered and generated signals. Figure 39c shows the PSD of the filtered and unfiltered EPS recordings of the generated biosignals, and the quantity of 50 Hz attenuation is calculated from the subtraction of these two peaks.

Theory would suggest that the optimal reference sine wave is in the same frequency band as that of the ECG signal itself – therefore somewhere between 5-40 Hz, as the Wiener filter should recognize frequencies within this band to be passed, and outside of this band to be attenuated. As biosignals are not homogenous amongst the humans (the frequency being subject to minor variations due to different HR) there is a range of frequencies available in this frequency band for the reference sine wave. Therefore the optimal frequency was derived experimentally. The results of testing a range of reference sine frequencies from 1 to 200 Hz are summarised in Figure 40a & b in terms of 50 Hz attenuation and MSE compared to the generated biosignal. For these tests the phantom signals (both reference sine and generated biosignal) were transmitted with an amplitude of 5 mV, with 5 minutes of data recorded for each frequency tested. Mean MSE and attenuation values were then calculated from 1 second windows of each recording. The results of these test are shown in Figure 40:

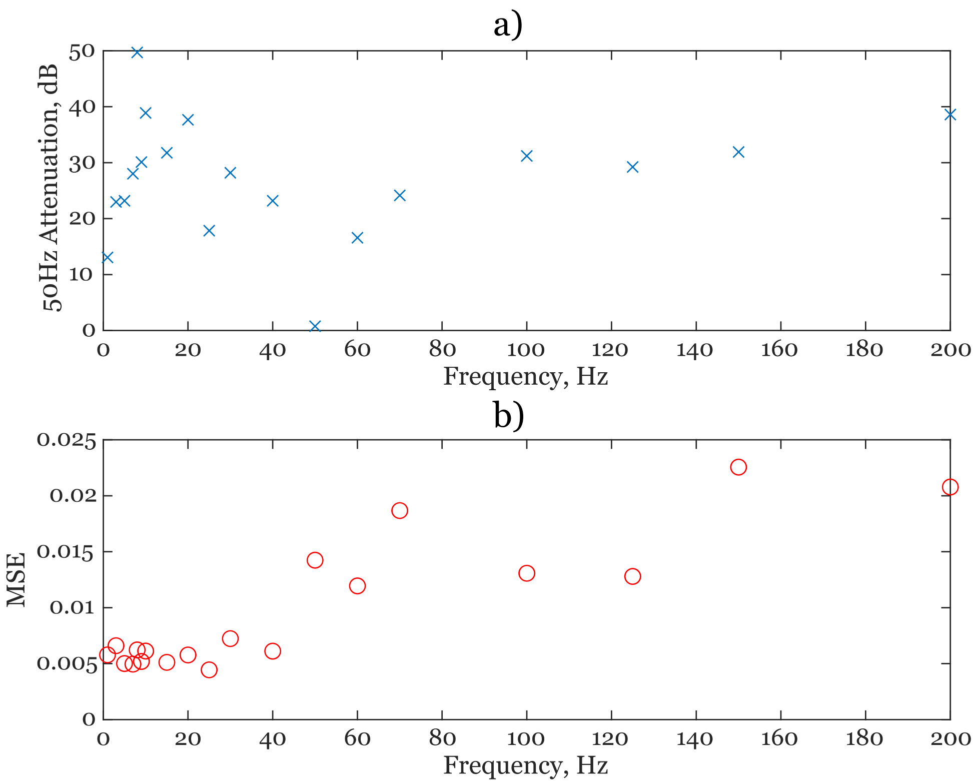

Figure 40: 50 Hz attenuation (a) and MSE (b) for a range of reference sine wave frequencies

In Figure 40a the maximum attenuation of 50 Hz noise (50 dB) is seen at a reference frequency of 8 Hz. All reference frequencies achieve some degree of attenuation apart from the 50 Hz reference frequency, where the wiener filter effectively passes the 50Hz noise as it is not considered noise, which is to be expected. Figure 40b shows the level of mean squared error, with the lowest error in the frequency band 1 to 40 Hz. This is where the majority of the ECG power is located, and therefore it is shown that a reference frequency within the frequency of interest is desirable for high quality signal reconstruction. At higher reference frequencies the mean square error increases, as the ECG signal becomes considered as noise and is altered by the Wiener filter.

4.3.2 Variable signal amplitude

To examine the adaptive nature of the Wiener filter the amplitude of the generated phantom ECG and sine signals was varied. A range of 5 to 100 mVpp was used and recordings were taken for 60 seconds, then the filtering algorithm was applied. The results are shown in Figure 41.

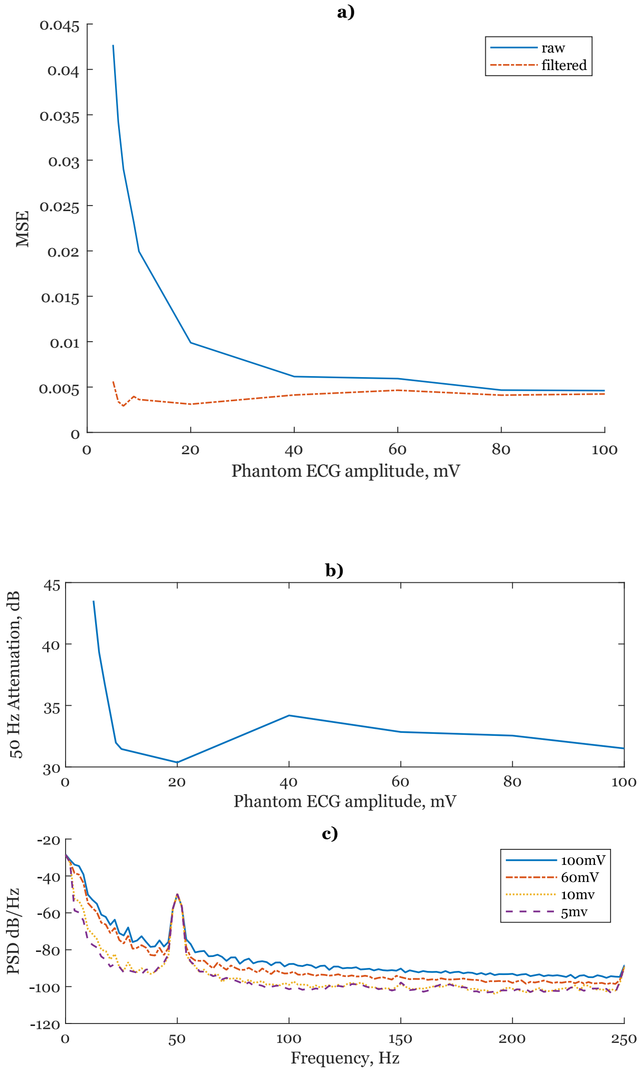

Figure 41: Wiener filtered generated ECGs with varying amplitudes: (a) Mean square error; (b) 50 Hz attenuation; (c) PSD of unfiltered EPS signals

The 50 Hz noise in the phantom is introduced only ambiently by the environment (unshielded electronics, mains power lines etc.) and therefore is independent of the amplitude of either the simulated biosignal or the reference sine wave. Assuming the magnitude of 50 Hz noise is broadly constant, by reducing the amplitude of the phantom signals the amount of noise is increased. This is seen in Figure 41c where the 50 Hz peak remains the same across all phantom voltage levels. This leads to much greater MSE in the lower amplitude tests (5 to 20 V range) seen in Figure 41a. The correlation between Figure 41a and b shows that as the level of noise increases the amount of 50 Hz attenuation also increases, showing the adaptive nature of this method of filtering.

4.3.3 MIT-BIH arrythmia database

The phantom setup and filtering algorithm was tested using a known set of real world electrocardiograms taken from the MIT-BIH arrythmia database [159]. The arrythmia of the ECGs in these recordings is not the point of interest for these tests, but the database has been widely studied in the literature and is routinely used for ECG denoising and signal processing, so provides an appropriate data set for comparison with other works. MIT-BIH database records were originally recorded at 360 samples/s, so these were resampled to 1000 samples/s before transmission. 5 minute samples of the first 8 records in the database (labelled m100 to m107) were transmitted at an amplitude of 10 mVpp, and mean values for MSE and 50Hz attenuation were calculated from 1 second windows. The reference sine wave signal was chosen to be Hz following the results described in Figure 40. The results of these test are shown in Figure 42:

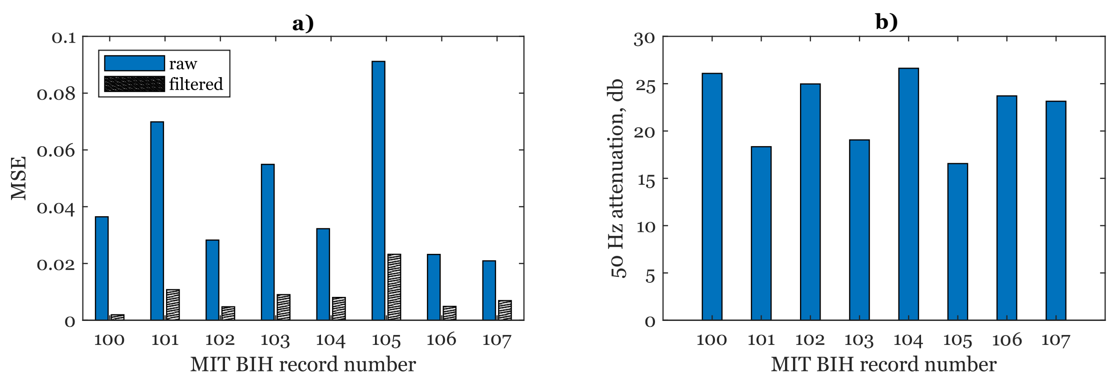

Figure 42: (a) MSE and (b) 50 Hz attenuation for Wiener filtered MIT-BIH arrythmia database records

Figure 42a shows the reduction in MSE for each record. The filtering improved the signal quality for all cases, with a maximum reduction of 95% MSE for record 100 and minimum 67% for record 107. The averaged MSE across the filtered records was 0.0087. In Figure 42b the level of 50 Hz attenuation is shown, with all records showing at least 16 dB of attenuation with an average across all records of 22.3 dB.

Record 100 is widely used in other works by virtue of being the first record in the database, so points of comparison are widely available. Table 10 shows a comparison of different filtering and noise reduction techniques applied to this record, and the resulting MSE & SNR improvement (where available) compared to this work:

Method	Reference	Noise (source)	SNR improvement, dB	MSE
This work	-	50 Hz PLI+ WGN (ambient)	10.7	0.0019
Infinite impulse response (FIR)	[160]	WGN (simulated)	N/A	0.0018
Normalised least mean square (NLMS)	[161]	50 Hz (simulated)	N/A	0.002
Empirical mode decomposition (EMD)	[162]	WGN (simulated)	8.82	N/A
Discrete wavelet transform (DWT)	[162]	WGN (simulated)	7.32	N/A

Table 10: Comparison of different filtering methods for record #100 of MIT-BIH database

All the comparative studies surveyed used simulated data, with either 50 Hz power line interference (PLI) or white gaussian noise (WGN) added to varying unspecified degrees, whereas this work considered ambient noise which included both PLI and WGN. The MSE is comparable with the results of both the FIR filtering and NLMS method, and the improvement in SNR is marginally higher than that of either the EMD or DWT methods presented. All methods referenced in Table 10 were simulated studies as no comparable phantom studies could be found. The phantom method presented here inherently introduces more error as it considers real rather than ideal signals and noise, and is therefore a more demanding test of the capability of the filter.

4.3.4 Human test

As a final proof of concept, the ECG broadcasting phantom was replaced with the researcher's own ECG via an EPS sensor attached by an elasticated band to the chest. The phantom was used to record the reference sine wave at 7 Hz, and was placed in close proximity to the subject to minimise any variation in environment and therefore ambient noise. Figure 43 shows the results of this ECG recording and the effect of the wiener filtering:

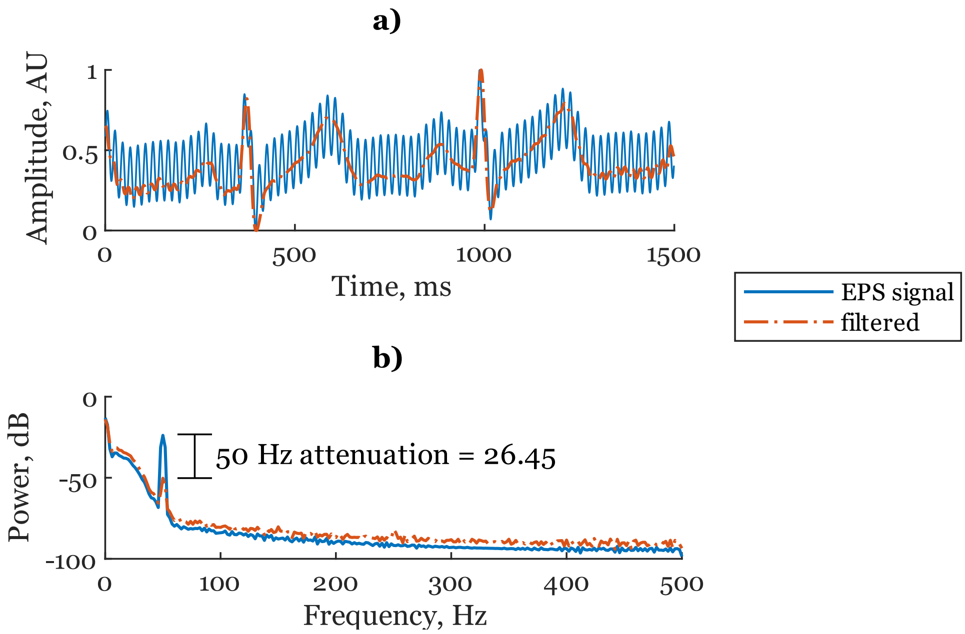

Figure 43: The 50 Hz attenuation effect of Wiener filtering an EPS recording of a human ECG

In Figure 43a a representative sample of the 5 minute recording is shown. The major features of the ECG, R peak & P and T waves, are clearly defined. The noise is visibly attenuated although there is still an amount of 50 Hz distortion, predominantly in the ST segment (the flat section of the ECG between ventricular depolarization and repolarization). From the PSD of the entire recording in Figure 43b we can see the attenuation of the 50 Hz noise peak, with a reduction of 26.5 dB. Across the other frequencies the power spectrum of the filtered and raw signal is well correlated, especially in the 1 to 40 Hz range where the ECG power is located, indicating that no significant alteration to the ECG is introduced by the filtering.

4.4 Discussion

This experimental work shows that the proposed method is suitable for the de-noising of EPS recorded electrocardiograms. An average reduction in mean square error of 80% was recorded across 40 minutes of test data from multiple records in the MIT-BIH arrythmia database. The predominant noise (50 Hz powerline interference) was attenuated by an average of 22.3 dB for these data sets, and 26.45 dB in the limited human trial. Examination of the ECG waveforms and power spectral density components showed no significant alteration of the morphology of the ECG, with all the main features intact suggesting that these ECGs could be used for clinical diagnosis as well as HR calculation.

Error reduction after filtering was shown to be directly related to the choice of sine wave reference signal, reference frequencies outside the range of the signal of interest (in the case of the ECG a band of approximately 1 to 40 Hz) causing signal wander and distortion. The level of 50 Hz attenuation was not affected by the choice of sine wave reference frequency, except in the case of 50 Hz reference frequency. This suggests a limitation of this method as it is shown here any noise in the ECG at the same frequency as the reference would not be removed by the Wiener filter. Therefore, some knowledge of the environment in which this method might be implemented could reduce the chance of reference/noise correlation.

The limitations of the experimental setup in this study mean that only the predominant 50 Hz powerline noise was investigated, as no effort to shield or isolate the phantom was made in order to better simulate real world signals. It can be strongly inferred that this method would have similar results in an environment where the utility frequency is 60 Hz. Noise above the 500 Hz range can be discounted due to the analog filtering present in the input stage, but other frequencies especially those in 1 to 40 Hz range should be a subject for further investigation. Additionally, EPS sensors have the capacity to record other electrophysiological signals such as the electromyogram (EMG) electro-oculogram (EOG). Initial investigation into these signals shows the same noise profile and subsequent signal improvements as with the ECG, indicating that this method could have broader applications than just the ECG and should also be considered for further study.

This works shows the application of a geophysical filtering technique to the domain of biosignals. Adaptative noise cancelling using model-based removal of powerline noise by Wiener filtering is validated using both idealised and pre-recorded ECGs. The use of a simple but effective phantom test rig which allows for repeatable and accurate experimentation and measurement takes this study out of the theoretical domain and instead considers real world signals and noise sources.

Chapter 5: Conclusions

The use of textile electrodes with EPS sensors is comprehensively explored in Chapter 3, where a comparison of dry and flexible electrode materials for use as a ground reference for EPS sensing ECGs is presented. Conductive textile fabric (nickel/copper polyester) was contrasted with silver conductive polymer ink, as well as the standard copper reference electrodes, and a method was defined for calculating sensor impedance. A neonate simulation environment, was employed and a wide range of signal quality indices were used to characterise the 3 electrode configurations, including waveform averaging, wavelet based ECG delineation and numerical methods such as relative power and kurtosis calculations.

Both types of textile electrode were able to reproduce the R peak timing of the simulated ECG signal to ~0.5% of the reference electrodes, with a 100% detection confidence across 5 minutes of human ECG recording. Between the two textile electrodes the nickel/copper polyester had a significantly reduced impedance mismatch, and outperformed the silver conductive polymer ink across all signal quality indices. The increased signal quality produced clinical quality ECGs with minimal morphological variation, as seen in the high average correlation coefficient (0.9) and average durations of the P, QRS and T waves corresponding with those recorded by the reference electrodes, as seen in the wavelet feature delineation. Additionally, this work also established a minimum time of 5.5 seconds from sensor application to HR reading by RR interval measurement, confirming the rapid acquisition capability of EPS sensors. These improvements in characterization, filtering and signal quality demonstrate the capacity of EPS with textile electrodes demonstrate to rapidly record high-quality electrocardiograms.

Chapter 3 also demonstrates a wide range of signal quality metrics that have not been previously applied to electric potential sensing ECGs, and presents a comparison of novel textile electrode materials compared to a known baseline.

Furthermore, this work demonstrates a prototype of the smart mattress system, furthering the case for the use of such a device in the neonatal intensive care unit.

Further work in this area should investigate a broader range of electrode types, using the impedance calculation methods and signal quality indices presented here. Additionally, a planned clinical study using a prototype smart mattress and a cohort of infants was planned but had to be abandoned due to the global Covid pandemic, therefore moving forwards this should be initiated to provide real world data with neonate biosignals. Not only would a clinical study further the case for EPS ECG use in the NICU, it would also generate a database of high quality EPS recordings of infants (similar to widely used databases such as the MIT-BIH Arrhythmia Database) which could be used to investigate EPS specific filtering methods.

A novel application of an adaptive ECG filtering method is presented in Chapter 4. EPS sensors are susceptible to ambient noise, and in operation in a clinical setting this noise may vary in magnitude and be of unknown origin. These noise sources may be electronics, radio frequency devices, LED lighting, large exotic medical devices (e.g., X-ray computed tomography scanners) or from procedures applied to patients. The combination of a wide range of noise sources and the susceptibility of the EPS sensor to noise form a strong case for the use of adaptive filtering. This method involves injecting a known sine wave signal input and recording the output using EPS sensors, then calculating a noise estimate from the subtraction of input and output. From the spectral properties of this noise estimate a statistical approach is used, via the minimum mean square method, to define the filter that approximates the original injected signal as closely as possible. As this method requires accurate signal generation and recording, a neonate phantom technique was developed from simple inexpensive agar castings to emulate the behaviour of human tissue and improve the correlation of the tests with a real world scenario.

The Wiener filter method was characterised at a range of sine injection frequencies, the most favourable for signal quality being those in the frequency band 1 to 40 Hz, as expected considering this is the frequency range of the majority of the main power band of the ECG. It was also shown to have variable 50 Hz attenuation based on the level of noise present. Testing using real neonate biosignal data in the form of 8 records from the MIT-BIH arrythmia database showed that 50 Hz noise was reduced by an average of 22.3 dB and a minimum of 16 dB across the dataset, proving the effectiveness of the filter in removing the predominant noise. Mean squared error (MSE) was reduced by an average of 80% across the simulated neonate tests. Record 100 in the MIT-BIH database is widely used for comparison, and this method compare favourably with the reported results of other methods such as Normalised least mean square (NLMS) and Discrete wavelet transform (DWT), with the similar or improved noise reduction and MSE reduction. Additionally, in a limited human trial, there was seen to be a 26.5 dB reduction in 50 Hz noise, with no morphological variation.

This is the first known application of this method to EPS sensors, it is shown to be both adaptive and effective in noise removal for ECGs. Improvements in signal quality via methods such as this can help to facilitate the wider adoption of EPS technology.

5.1 Concluding statement

In summary, this thesis develops the two key areas of textile electrodes and advanced signal processing techniques for sensing the electrocardiogram with electric potential sensors. The smart mattress concept is demonstrated and verified in two prototypes using both generated ECGs signals and recorded ECGs from databases broadcast via neonate phantoms, and also employing real human biosignals. High resolution EPS ECGs are recorded, and are shown to be suitable for the rapid acquisition of heart rate. Improvements in signal quality and stability are practically demonstrated through advances in textile electrodes and signal processing techniques targeted specifically at EPS ECGs. These encouraging results and proof of incremental development provide a strong case for the continued development of this novel sensor technology into applications such as the smart mattress and beyond.

Chapter 6: Appendices

6.1 Appendix 1: “Neo-Sense: a real time data processing & acquisition unit for monitoring neonatal ECG in the delivery room” (conference poster)

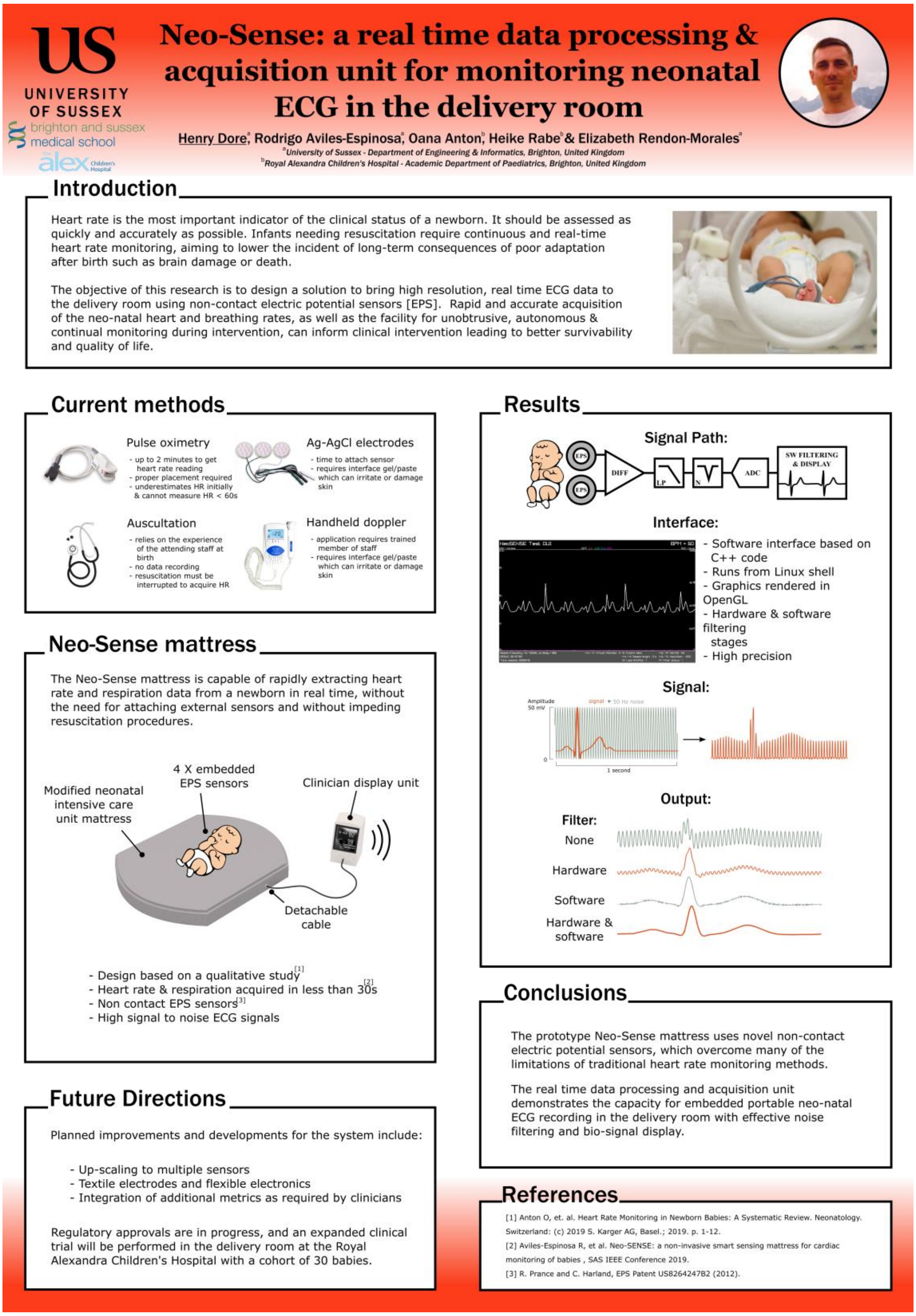

6.2 Appendix 2: Prototype #1 schematic

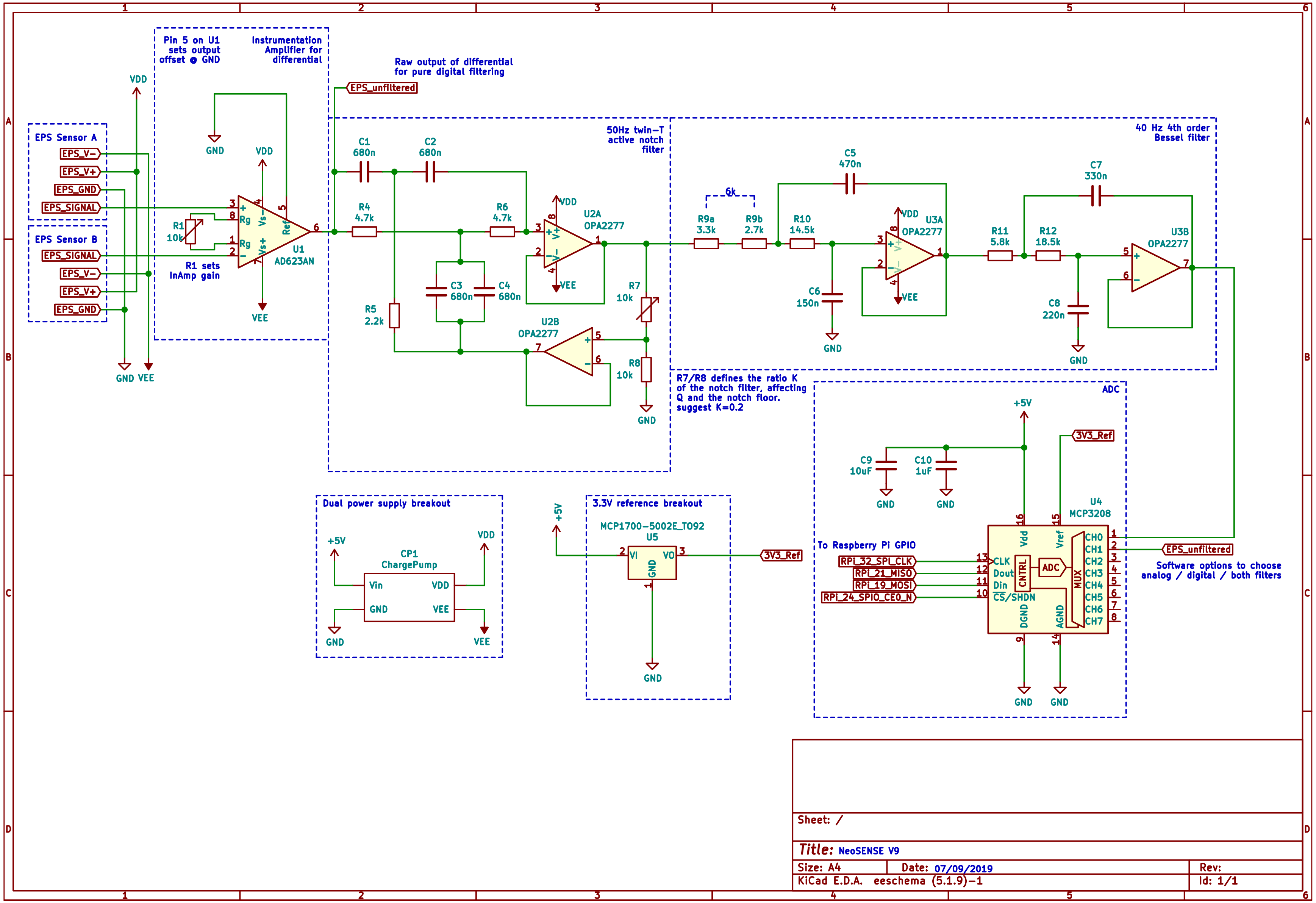

6.3 Appendix 3: Prototype #2 schematic

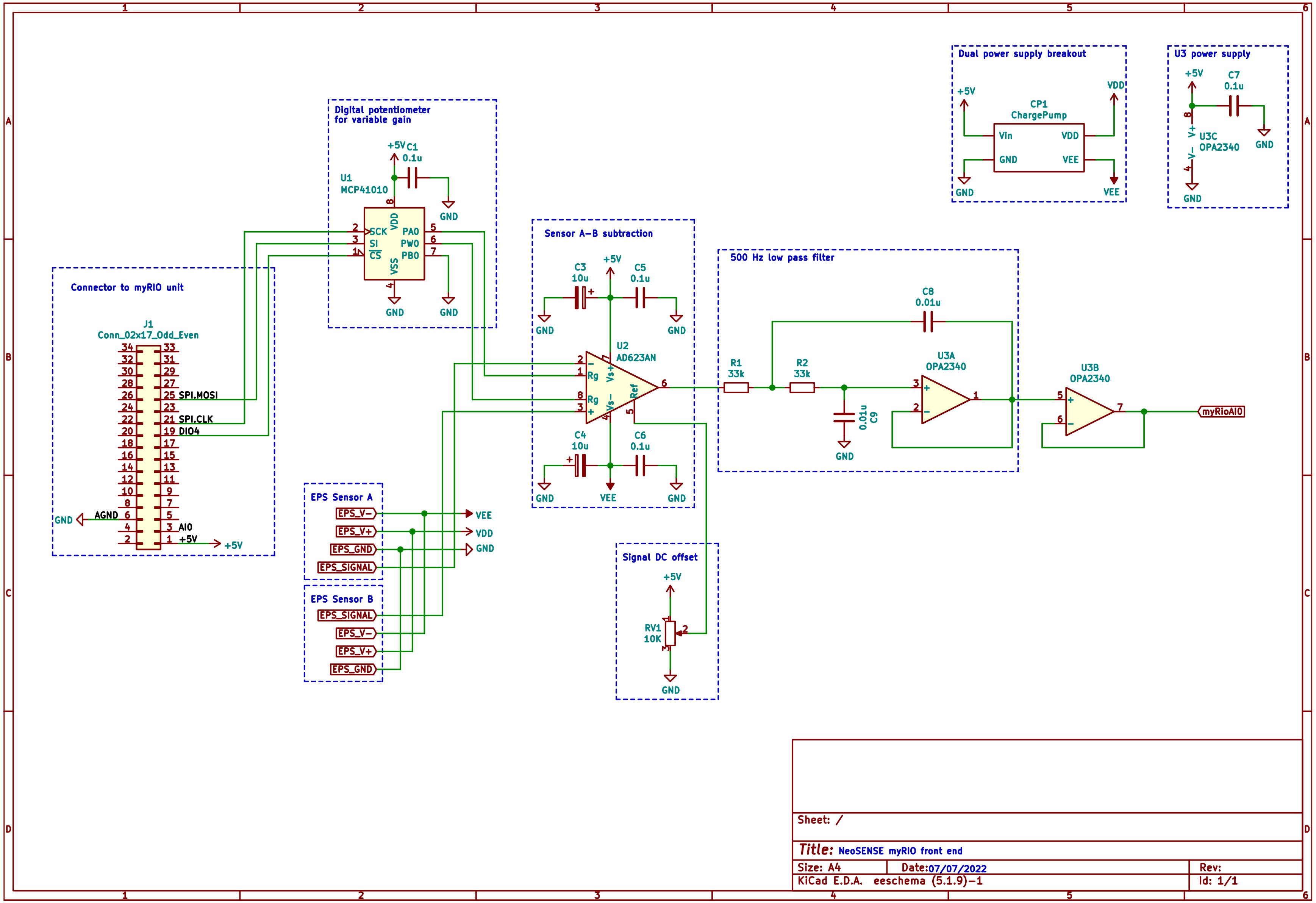

Chapter 7: References

[1] N. H. Hillman, S. G. Kallapur, and A. H. Jobe, "Physiology of transition from intrauterine to extrauterine life," (in eng), *Clin Perinatol,* vol. 39, no. 4, pp. 769-83, Dec 2012, doi: https://doi.org/10.1016/j.clp.2012.09.009.

[2] H. Lagercrantz and T. A. Slotkin, "The stress of being born," *Scientific American,* vol. 254, no. 4, pp. 100-107, 1986.

[3] O. D. Saugstad, S. Ramji, T. Rootwelt, and M. Vento, "Response to resuscitation of the newborn: early prognostic variables," (in eng), *Acta paediatrica (Oslo, Norway : 1992),* vol. 94, no. 7, pp. 890-5, Jul 2005, doi: https://doi.org/10.1080/08035250510036507.

[4] L. Hug, M. Alexander, D. You, and L. Alkema, "National, regional, and global levels and trends in neonatal mortality between 1990 and 2017, with scenario-based projections to 2030: a systematic analysis," *The Lancet Global Health,* vol. 7, no. 6, pp. e710-e720, 2019, doi: https://doi.org/10.1016/S2214-109X(19)30163-9.

[5] J. M. Perlman *et al.*, "Neonatal resuscitation: 2010 international consensus on cardiopulmonary resuscitation and emergency cardiovascular care science with treatment recommendations," *Pediatrics,* vol. 126, no. 5, pp. e1319-e1344, 2010, doi: https://doi.org/10.1542/peds.2010-2972B.

[6] World Health Organization, "World health statistics 2019." [Online]. Available: https://apps.who.int/iris/rest/bitstreams/1237162/retrieve

[7] R. J. Prance *et al.*, "An Ultra Low Noise Electric Potential Probe for Human Body Scanning," *Meas Sci Technol,* vol. 11, no. 3, pp. 291-297, 2000, doi: https://doi.org/10.1088/0957-0233/11/3/318.

[8] W. H. Ko, M. R. Neuman, R. N. Wolfson, and E. T. Yon, "Insulated Active Electrodes," *IEEE Transactions on Industrial Electronics and Control Instrumentation,* vol. IECI-17, no. 2, pp. 195-198, 1970, doi: https://doi.org/10.1109/TIECI.1970.230763.

[9] P. C. Richardson, "The insulated electrode: a pasteless electrocardiographic technique," in *Annual Conference on Engineering in Medicine and Biology*, 1967, vol. 15, p. 7, doi: https://doi.org/10.1007/BF02477385.

[10] J. Roman, "Flight research program--3. High impedance electrode techniques," *Aerospace medicine,* vol. 37, no. 8, pp. 790-795, 1966.

[11] M. E. Griffith, W. M. Portnoy, L. J. Stotts, and J. L. Day, "Improved capacitive electrocardiogram electrodes for burn applications," *Medical and Biological Engineering and Computing,* vol. 17, no. 5, pp. 641-646, 1979/09/01 1979, doi: https://doi.org/10.1007/BF02440910.

[12] Plessey Semiconductors. "EPIC Ultra High Impedance ECG Sensor PS25101." http://www.plesseysemiconductors.com/wp-content/uploads/ps25101-epic-sensor-development-sensor-high-gain-datasheet.pdf (accessed.

[13] C. J. Harland, R. J. Prance, and T. D. Clark, "Electric Potential Probes - New Directions in the Remote Sensing of the Human Body," *Meas Sci Technol,* vol. 13, no. 2, pp. 163-169, 2002, doi: https://doi.org/10.1088/0957-0233/13/2/304.

[14] N. V. Thakor, J. G. Webster, and W. J. Tompkins, "Estimation of QRS complex power spectra for design of a QRS filter," *IEEE Transactions on Biomedical Engineering,* no. 11, pp. 702-706, 1984, doi: https://doi.org/10.1109/TBME.1984.325393.

[15] M. B. Weil, M. Oehler, M. Schilling, and L. S. Maier, "First clinical evaluation of a novel capacitive ECG system in patients with acute myocardial infarction," *Clinical Research in Cardiology,* vol. 101, no. 3, pp. 165-174, 2012/03/01 2012, doi: https://doi.org/10.1007/s00392-011-0377-1.

[16] L. Atallah *et al.*, "Unobtrusive ECG monitoring in the NICU using a capacitive sensing array," *Physiological Measurement,* vol. 35, no. 5, pp. 895-913, 2014/04/17 2014, doi: https://doi.org/10.1088/0967-3334/35/5/895.

[17] Y. Varabyova, C. R. Blankart, A. L. Greer, and J. Schreyögg, "The determinants of medical technology adoption in different decisional systems: A systematic literature review," *Health Policy,* vol. 121, no. 3, pp. 230-242, 2017/03/01/ 2017, doi: https://doi.org/10.1016/j.healthpol.2017.01.005.

[18] K. R. Foster and J. Torous, "The opportunity and obstacles for smartwatches and wearable sensors," *IEEE pulse,* vol. 10, no. 1, pp. 22-25, 2019, doi: https://doi.org/10.1109/MPULS.2018.2885832.

[19] J. Sakuma, D. Anzai, and J. Wang, "Performance of human body communication-based wearable ECG with capacitive coupling electrodes," *Healthcare technology letters,* vol. 3, no. 3, pp. 222-225, 2016, doi: https://doi.org/10.1049/htl.2016.0023.

[20] Y. M. Chi and G. Cauwenberghs, "Wireless Non-contact EEG/ECG Electrodes for Body Sensor Networks," in *2010 International Conference on Body Sensor Networks*, 7-9 June 2010 2010, pp. 297-301, doi: 10.1109/BSN.2010.52.

[21] C. J. Harland, R. J. Prance, and H. Prance, "Remote monitoring of biodynamic activity using eletric potential sensors," *Journal of Physics: Conference Series,* vol. 142, no. 1, 2008, doi: https://doi.org/10.1088/1742-6596/142/1/012042.

[22] R. J. Prance, S. T. Beardsmore-Rust, P. Watson, C. J. Harland, and H. Prance, "Remote detection of human electrophysiological signals using electric potential sensors," *Applied Physics Letters,* vol. 93, no. 3, p. 0339061, 2008, doi: https://doi.org/10.1063/1.2964185.

[23] MarketsAndMarkets, "Wearable Electronics and Technology Market by Applications," vol. 2022, no. 17/05. [Online]. Available: https://www.marketsandmarkets.com/Market-Reports/wearable-electronics-market-983.html

[24] J. Dunn, R. Runge, and M. Snyder, "Wearables and the medical revolution," *Personalized medicine,* vol. 15, no. 5, pp. 429-448, 2018, doi: https://doi.org/10.2217/pme-2018-0044.

[25] L. A. Geddes and L. E. Baker, *Principles of applied biomedical instrumentation*. John Wiley & Sons, 1975.

[26] H. P. Schwan and C. F. Kay, "Specific resistance of body tissues," *Circulation Research,* vol. 4, no. 6, pp. 664-670, 1956, doi: https://doi.org/10.1161/01.RES.4.6.664.

[27] H. P. Schwan and C. F. Kay, "Capacitive properties of body tissues," *Circulation Research,* vol. 5, no. 4, pp. 439-443, 1957, doi: https://doi.org/10.1161/01.RES.5.4.439.

[28] M. Chen *et al.*, "A 400 GΩ Input-Impedance Active Electrode for Non-Contact Capacitively Coupled ECG Acquisition With Large Linear-Input-Range and High CM-Interference-Tolerance," *IEEE Transactions on Biomedical Circuits and Systems,* vol. 13, no. 2, pp. 376-386, 2019, doi: 10.1109/TBCAS.2019.2895660.

[29] Y. M. Chi, T. Jung, and G. Cauwenberghs, "Dry-Contact and Noncontact Biopotential Electrodes: Methodological Review," *IEEE Reviews in Biomedical Engineering,* vol. 3, pp. 106-119, 2010, doi: https://doi.org/10.1109/RBME.2010.2084078.

[30] B. Babusiak, S. Borik, and L. Balogova, "Textile electrodes in capacitive signal sensing applications," *Measurement,* vol. 114, pp. 69-77, 2018, doi: https://doi.org/10.1016/j.measurement.2017.09.024.

[31] H. Li *et al.*, "Textile-based ECG acquisition system with capacitively coupled electrodes," *Transactions of the Institute of Measurement and Control,* vol.

39, no. 2, pp. 141-148, 2017, doi: https://doi.org/10.1177%2F0142331215600254.
[32] A. Ankhili, X. Tao, C. Cochrane, V. Koncar, D. Coulon, and J.-M. Tarlet, "Comparative Study on Conductive Knitted Fabric Electrodes for Long-Term Electrocardiography Monitoring: Silver-Plated and PEDOT:PSS Coated Fabrics," *Sensors,* vol. 18, p. 3890, 2018, doi: https://doi.org/10.3390/s18113890.
[33] M. Weder *et al.*, "Embroidered electrode with silver/titanium coating for long-term ECG monitoring," *Sensors,* vol. 15, no. 1, pp. 1750-1759, 2015, doi: https://doi.org/10.3390/s150101750.
[34] J. S. Lee, J. Heo, W. K. Lee, Y. G. Lim, Y. H. Kim, and K. S. Park, "Flexible capacitive electrodes for minimizing motion artifacts in ambulatory electrocardiograms," *Sensors,* vol. 14, no. 8, pp. 14732-14743, 2014, doi: https://doi.org/10.3390/s140814732.
[35] M. K. Yapici and T. E. Alkhidir, "Intelligent medical garments with graphene-functionalized smart-cloth ECG sensors," *Sensors,* vol. 17, no. 4, p. 875, 2017, doi: https://doi.org/10.3390/s17040875.
[36] S. Fuhrhop, S. Lamparth, and S. Heuer, "A textile integrated long-term ECG monitor with capacitively coupled electrodes," in *2009 IEEE Biomedical Circuits and Systems Conference*, 2009: IEEE, pp. 21-24, doi: https://doi.org/10.1109/BIOCAS.2009.5372095.
[37] A. Boehm, X. Yu, W. Neu, S. Leonhardt, and D. Teichmann, "A novel 12-lead ECG T-shirt with active electrodes," *Electronics,* vol. 5, no. 4, p. 75, 2016, doi: https://doi.org/10.3390/electronics5040075.
[38] A. Aleksandrowicz and S. Leonhardt, "Wireless and non-contact ECG measurement system–the "Aachen SmartChair"," *Acta Polytechnica,* vol. 47, no. 4-5, 2007, doi: https://doi.org/10.14311/974.
[39] J. M. Warnecke, J. Wang, T. Cakir, N. Spicher, N. Ganapathy, and T. M. Deserno, "Registered report protocol: Developing an artifact index for capacitive electrocardiography signals acquired with an armchair," *PLoS One,* vol. 16, no. 7, p. e0254780, 2021, doi: https://doi.org/10.1371/journal.pone.0254780.
[40] B. Chamadiya, K. Mankodiya, M. Wagner, and U. G. Hofmann, "Textile-based, contactless ECG monitoring for non-ICU clinical settings," *Journal of Ambient Intelligence and Humanized Computing,* vol. 4, no. 6, pp. 791-800, 2013, doi: https://doi.org/10.1007/s12652-012-0153-8.
[41] M. Takano, S. Yamagishi, T. Ohmuta, Y. Fukuoka, and A. Ueno, "Non-contact simultaneous measurements of electrocardiogram and respiratory movements using capacitive sheet electrodes," *Advanced Biomedical Engineering,* vol. 6, pp. 28-36, 2017, doi: https://doi.org/10.14326/abe.6.28.
[42] H. J. Lee, S. H. Hwang, H. N. Yoon, W. K. Lee, and K. S. Park, "Heart rate variability monitoring during sleep based on capacitively coupled textile electrodes on a bed," *Sensors,* vol. 15, no. 5, pp. 11295-11311, 2015, doi: https://doi.org/10.3390/s150511295.
[43] Y. G. Lim, K. K. Kim, and K. S. Park, "ECG recording on a bed during sleep without direct skin-contact," *IEEE Transactions on Biomedical Engineering,* vol. 54, no. 4, pp. 718-725, 2007, doi: https://doi.org/10.1109/tbme.2006.889194.
[44] B. Feng *et al.*, "Sleeping Heart Monitoring Using Hydrogel-Textile Capacitive ECG Electrodes," *IEEE Sensors Journal,* vol. 22, no. 10, pp. 9255-9267, 2022, doi: https://doi.org/10.1109/JSEN.2022.3164076.
[45] D. R. Illová, Ľ. Balogová, K. Ščasníková, M. Gála, B. Babušiak, and Š. Borik, "Smart mattress topper with enhanced hygienic properties for ECG measurement and detection of position," *Vlakna a Textil,* vol. 27, no. 4, pp. 81-86, 2020.

[46] J. Weeks, M. Elsaadany, M. Lessard-Tremblay, L. Targino, M. Liamini, and G. Gagnon, "A Novel Sensor-Array System for Contactless Electrocardiogram Acquisition," in *2020 42nd Annual International Conference of the IEEE Engineering in Medicine & Biology Society (EMBC)*, 20-24 July 2020 2020, pp. 4122-4125, doi: https://doi.org/10.1109/EMBC44109.2020.9175666.

[47] H. Lee, S. Lee, and K. Park, "Evaluation of three mattress designs for capacitive ecg measurement from conductive textiles on bed," in *10th IASTED International Conference on Biomedical Engineering, BioMed 2013*, 2013, pp. 62-66, doi: https://doi.org/10.2316/P.2013.791-136.

[48] L. Atallah *et al.*, "Unobtrusive ECG monitoring in the NICU using a capacitive sensing array," *Physiological measurement,* vol. 35, no. 5, p. 895, 2014, doi: https://doi.org/10.1088/0967-3334/35/5/895.

[49] J. Werth, A. Serteyn, P. Andriessen, R. M. Aarts, and X. Long, "Automated preterm infant sleep staging using capacitive electrocardiography," *Physiological Measurement,* vol. 40, no. 5, p. 055003, 2019/06/04 2019, doi: https://doi.org/10.1088/1361-6579/ab1224.

[50] T. Kato, A. Ueno, S. Kataoka, H. Hoshino, and Y. Ishiyama, "An Application of Capacitive Electrode for Detecting Electrocardiogram of Neonates and Infants," in *2006 International Conference of the IEEE Engineering in Medicine and Biology Society*, 30 Aug.-3 Sept. 2006 2006, pp. 916-919, doi: https://doi.org/10.1109/IEMBS.2006.260362.

[51] P. H. T. Cartlidge, "Newborn skin," *Current Paediatrics,* vol. 1, no. 3, pp. 153-154, 1991/09/01/ 1991, doi: https://doi.org/10.1016/0957-5839(91)90008-2.

[52] S. Peng, K. Xu, S. Bao, Y. Yuan, C. Dai, and W. Chen, "Flexible Electrodes-Based Smart Mattress for Monitoring Physiological Signals of Heart and Autonomic Nerves in a Non-Contact Way," *IEEE Sensors Journal,* vol. 21, no. 1, pp. 6-15, 2021, doi: 10.1109/JSEN.2020.3012697.

[53] M. Takano and A. Ueno, "Noncontact in-bed measurements of physiological and behavioral signals using an integrated fabric-sheet sensing scheme," *IEEE journal of biomedical and health informatics,* vol. 23, no. 2, pp. 618-630, 2018, doi: https://doi.org/10.1109/JBHI.2018.2825020.

[54] R. Joshi, B. Bierling, L. Feijs, C. Van Pul, and P. Andriessen, "Monitoring the respiratory rate of preterm infants using an ultrathin film sensor embedded in the bedding: a comparative feasibility study," *Physiological measurement,* vol. 40, no. 4, p. 045003, 2019, doi: https://doi.org/10.1088/1361-6579/ab1595.

[55] G. Cay *et al.*, "An E-Textile Respiration Sensing System for NICU Monitoring: Design and Validation," *Journal of Signal Processing Systems,* vol. 94, no. 6, pp. 543-557, 2022/06/01 2022, doi: https://www.doi.org/10.1007/s11265-021-01669-9.

[56] B. Johansson, "A history of the electrocardiogram," *Dansk Medicinhistorisk Arbog,* pp. 163-176, 2001.

[57] W. B. Fye, "A History of the origin, evolution, and impact of electrocardiography," *The American Journal of Cardiology,* vol. 73, no. 13, pp. 937-949, 1994/05/15/ 1994, doi: https://doi.org/10.1016/0002-9149(94)90135-X.

[58] M. J. Cattermole, "The Cambridge Scientific Instrument Company from 1881 to 1968," *IEE Proceedings A (Physical Science, Measurement and Instrumentation, Management and Education, Reviews),* vol. 134, no. 4, pp. 351-358, 1987, doi: https://doi.org/10.1049/ip-a-1.1987.0054.

[59] W. C. Roberts and M. A. Silver, "Norman Jefferis Holter and ambulatory ECG monitoring," *The American journal of cardiology,* vol. 52, no. 7, pp. 903-906, 1983, doi: https://doi.org/10.1016/0002-9149(83)90439-3.

[60] L. Taback, E. Marden, H. L. Mason, and H. V. Pipberger, "Digital Recording of Electrocardiographic Data for Analysis by a Digital Computer," *IRE*

Transactions on Medical Electronics, vol. ME-6, no. 3, pp. 167-171, 1959, doi: https://doi.org/10.1109/IRET-ME.1959.5007946.

[61] P. M. Rautaharju, "Eyewitness to history: Landmarks in the development of computerized electrocardiography," *Journal of Electrocardiology,* vol. 49, no. 1, pp. 1-6, 2016/01/01/ 2016, doi: https://doi.org/10.1016/j.jelectrocard.2015.11.002.

[62] E. Drazen, N. Mann, R. Borun, M. Laks, and A. Bersen, "Survey of computer-assisted electrocardiography in the United States," *Journal of electrocardiology,* vol. 21, pp. S98-S104, 1988, doi: https://doi.org/10.1016/0022-0736(88)90068-4.

[63] A. Baldassarre *et al.*, "The Role of Electrocardiography in Occupational Medicine, from Einthoven's Invention to the Digital Era of Wearable Devices," *International Journal of Environmental Research and Public Health,* vol. 17, no. 14, p. 4975, 2020, doi: https://doi.org/10.3390/ijerph17144975.

[64] N. Faruk *et al.*, "A comprehensive survey on low-cost ECG acquisition systems: Advances on design specifications, challenges and future direction," *Biocybernetics and Biomedical Engineering,* vol. 41, no. 2, pp. 474-502, 2021/04/01/ 2021, doi: https://doi.org/10.1016/j.bbe.2021.02.007.

[65] N. Saghir, A. Aggarwal, N. Soneji, V. Valencia, G. Rodgers, and T. Kurian, "A comparison of manual electrocardiographic interval and waveform analysis in lead 1 of 12-lead ECG and Apple Watch ECG: A validation study," *Cardiovascular Digital Health Journal,* vol. 1, no. 1, pp. 30-36, 2020/07/01/ 2020, doi: https://doi.org/10.1016/j.cvdhj.2020.07.002.

[66] N. Isakadze and S. S. Martin, "How useful is the smartwatch ECG?," *Trends in Cardiovascular Medicine,* vol. 30, no. 7, pp. 442-448, 2020/10/01/ 2020, doi: https://doi.org/10.1016/j.tcm.2019.10.010.

[67] C. Assambo and M. Burke, "Low-Frequency Response and the Skin-Electrode Interface in Dry-Electrode Electrocardiography," 2012.

[68] C. Levkov, G. Mihov, R. Ivanov, I. Daskalov, I. Christov, and I. Dotsinsky, "Removal of power-line interference from the ECG: a review of the subtraction procedure," *BioMedical Engineering OnLine,* vol. 4, no. 1, p. 50, 2005/08/23 2005, doi: https://www.doi.org/10.1186/1475-925X-4-50.

[69] L. Frølich and I. Dowding, "Removal of muscular artifacts in EEG signals: a comparison of linear decomposition methods," *Brain Informatics,* vol. 5, no. 1, pp. 13-22, 2018/03/01 2018, doi: https://www.doi.org/10.1007/s40708-017-0074-6.

[70] H. Rakshit and M. A. Ullah, "A new efficient approach for designing FIR low-pass filter and its application on ECG signal for removal of AWGN noise," *IAENG International Journal of Computer Science,* vol. 43, no. 2, pp. 176-183, 2016.

[71] R. He *et al.*, "Reducing false arrhythmia alarms in the ICU using novel signal quality indices assessment method," in *2015 Computing in Cardiology Conference (CinC)*, 2015: IEEE, pp. 1189-1192, doi: https://doi.org/10.1109/CIC.2015.7411129.

[72] M. M. Butt, U. Akram, and S. A. Khan, "Denoising practices for electrocardiographic (ECG) signals: A survey," in *2015 International Conference on Computer, Communications, and Control Technology (I4CT)*, 21-23 April 2015 2015, pp. 264-268, doi: https://doi.org/10.1109/I4CT.2015.7219578.

[73] S. Luo and P. Johnston, "A review of electrocardiogram filtering," *Journal of Electrocardiology,* vol. 43, no. 6, pp. 486-496, 2010/11/01/ 2010, doi: https://doi.org/10.1016/j.jelectrocard.2010.07.007.

[74] D. Cindrić, A. Stanešić, and M. Cifrek, "Analog Frontend for ECG/EMG Capacitive Electrodes," in *2021 44th International Convention on Information, Communication and Electronic Technology (MIPRO)*, 27

Sept.-1 Oct. 2021 2021, pp. 363-366, doi: http://doi.org/10.23919/MIPRO52101.2021.9597199.
[75] M. Oehler, V. Ling, K. Melhorn, and M. Schilling, "A multichannel portable ECG system with capacitive sensors," *Physiological measurement,* vol. 29, no. 7, p. 783, 2008, doi: https://doi.org/10.1088/0967-3334/29/7/007.
[76] L. Smolarik, A. Libosvarova, D. Mudroncik, and P. Schreiber, "Non-contact ECG signal processing," in *2012 6th IEEE International Conference Intelligent Systems*, 2012: IEEE, pp. 349-354, doi: https://doi.org/10.1109/IS.2012.6335241.
[77] T. Komensky, M. Jurcisin, K. Ruman, O. Kovac, D. Laqua, and P. Husar, "Ultra-wearable capacitive coupled and common electrode-free ECG monitoring system," in *2012 Annual International Conference of the IEEE Engineering in Medicine and Biology Society*, 2012: IEEE, pp. 1594-1597, doi: https://doi.org/10.1109/EMBC.2012.6346249.
[78] B. Eilebrecht, T. Wartzek, J. Willkomm, A. Schommartz, M. Walter, and S. Leonhardt, "Motion artifact removal from capacitive ECG measurements by means of adaptive filtering," in *5th European conference of the international federation for medical and biological engineering*, 2011: Springer, pp. 902-905, doi: https://doi.org/10.1007/978-3-642-23508-5_234.
[79] V. P. Rachim, S.-C. Kang, W.-Y. Chung, and T.-H. Kwon, "Implementation of extended kalman filter for real-time noncontact ecg signal acquisition in android-based mobile monitoring system," *Journal of Sensor Science and Technology,* vol. 23, no. 1, pp. 7-14, 2014, doi: https://doi.org/10.5369/JSST.2014.23.1.7.
[80] R. Vullings, B. De Vries, and J. W. Bergmans, "An adaptive Kalman filter for ECG signal enhancement," *IEEE Transactions on Biomedical Engineering,* vol. 58, no. 4, pp. 1094-1103, 2010, doi: https://doi.org/10.1109/TBME.2010.2099229.
[81] B. Yang, Y. Dong, C. Yu, and Z. Hou, "Singular Spectrum Analysis Window Length Selection in Processing Capacitive Captured Biopotential Signals," *IEEE Sensors Journal,* vol. 16, no. 19, pp. 7183-7193, 2016, doi: https://doi.org/10.1109/JSEN.2016.2594189.
[82] S. Peng, K. Xu, and W. Chen, "Comparison of Active Electrode Materials for Non-Contact ECG Measurement," (in eng), *Sensors,* vol. 19, no. 16, p. 3585, 2019, doi: https://doi.org/10.3390/s19163585.
[83] S. M. Lee, K. K. Kim, and K. S. Park, "Wavelet approach to artifact noise removal from Capacitive coupled Electrocardiograph," in *2008 30th Annual International Conference of the IEEE Engineering in Medicine and Biology Society*, 2008, vol. 2008, 2009/01/24 ed., pp. 2944-7, doi: https://doi.org/10.1109/iembs.2008.4649820.
[84] S. Peng, S. Bao, and W. Chen, "Capacitive coupled electrodes based non-contact ECG measurement system with real-time wavelet denoising algorithm," in *2019 41st Annual International Conference of the IEEE Engineering in Medicine and Biology Society (EMBC)*, 2019: IEEE, pp. 6587-6590, doi: https://doi.org/10.1109/EMBC.2019.8856885.
[85] V. Ravichandran *et al.*, "Deep network for capacitive ECG denoising," in *2019 IEEE International Symposium on Medical Measurements and Applications (MeMeA)*, 2019: IEEE, pp. 1-6, doi: https://doi.org/10.1109/MeMeA.2019.8802155.
[86] J. S. Lee, S. J. Lee, M. Choi, M. Seo, and S. W. Kim, "QRS detection method based on fully convolutional networks for capacitive electrocardiogram," *Expert Systems with Applications,* vol. 134, pp. 66-78, 2019, doi: https://doi.org/10.1016/j.eswa.2019.05.033.
[87] K. Kido *et al.*, "A novel CNN-based framework for classification of signal quality and sleep position from a capacitive ECG measurement," *Sensors,* vol. 19, no. 7, p. 1731, 2019, doi: https://doi.org/10.3390/s19071731.

[88] A. H. Association, "AHA guidelines update for CPR and ECC," *Circulation,* vol. 132, no. 18, 2015, doi: https://doi.org/10.1161/CIR.0000000000000265.

[89] R. Aviles-Espinosa *et al.*, "Neo-SENSE: a non-invasive smart sensing mattress for cardiac monitoring of babies," in *2019 IEEE Sensors Applications Symposium (SAS)*, 11-13 March 2019 2019, pp. 1-5, doi: 10.1109/SAS.2019.8705971.

[90] C. P. F. O'Donnell, C. O. F. Kamlin, P. G. Davis, and C. J. Morley, "Feasibility of and Delay in Obtaining Pulse Oximetry during Neonatal Resuscitation," *The Journal of Pediatrics,* vol. 147, no. 5, pp. 698-699, 2005/11/01/ 2005, doi: https://doi.org//10.1016/j.jpeds.2005.07.025.

[91] H. Mizumoto *et al.*, "Electrocardiogram shows reliable heart rates much earlier than pulse oximetry during neonatal resuscitation," (in eng), *Pediatr Int,* vol. 54, no. 2, pp. 205-7, Apr 2012, doi: https://doi.org/10.1111/j.1442-200X.2011.03506.x.

[92] D. Finn, G. Boylan, A. C. Ryan, and E. Dempsey, "Enhanced Monitoring of the Preterm Infant during Stabilization in the Delivery Room," *Frontiers in Pediatrics,* vol. 4, 03/31 2016, doi: https://doi.org/10.3389/fped.2016.00030.

[93] A. C. Kevat, D. V. R. Bullen, P. G. Davis, and C. O. F. Kamlin, "A systematic review of novel technology for monitoring infant and newborn heart rate," *Acta Paediatrica,* vol. 106, no. 5, pp. 710-720, 2017, doi: https://doi.org/10.1111/apa.13786.

[94] R. Prance and C. Harland, "Electric potential sensor, Patent Number: US8264247B2," Patent US8264247B2, 2012.

[95] W. Gebrial, R. J. Prance, T. D. Clark, C. J. Harland, H. Prance, and M. Everitt, "Non-invasive Imaging of Signals in Digital Circuits," *Review of Scientific Instruments,* vol. 73, no. 3, pp. 1293-1298, 2002, doi: https://doi.org/10.1063/1.1447302.

[96] E. Rendon-Morales, R. Prance, H. Prance, and R. Aviles-Espinosa, "Non-invasive electrocardiogram detection of in vivo zebrafish embryos using electric potential sensors," *Applied Physics Letters,* vol. 107, no. 19, pp. 193701-1-193701-4, 2015, doi: https://doi.org/10.1063/1.4935249.

[97] P. Watson, R. J. Prance, S. T. Beardsmore-Rust, and H. Prance, "Imaging electrostatic fingerprints with implications for a forensic timeline," *Forensic Science International,* vol. 209, no. 1, pp. e41-e45, 2011/06/15/ 2011, doi: https://doi.org/10.1016/j.forsciint.2011.02.024.

[98] W. Gebrial, R. Prance, C. J. Harland, and T. D. Clark, "Noninvasive imaging using an array of electric potential sensors," *Review of Scientific Instruments,* vol. 77, 2006, doi: https://doi.org/10.1063/1.2213219.

[99] R. J. P. E. Rendon-Morales, and R. Aviles-Espinosa, "Noninvasive recordings of fetal electrocardiogram during pregnancy using electric potential sensors," *AIP Advances,* vol. 8, p. 105114, 2018, doi: https://doi.org/10.1063/1.5042358.

[100] G. Acar, O. Ozturk, A. J. Golparvar, T. A. Elboshra, K. Böhringer, and M. K. Yapici, "Wearable and Flexible Textile Electrodes for Biopotential Signal Monitoring: A review," *Electronics,* vol. 8, no. 5, p. 479, 2019, doi: https://doi.org/doi:10.3390/electronics8050479.

[101] K. Yang, R. Torah, Y. Wei, S. Beeby, and J. Tudor, "Waterproof and durable screen printed silver conductive tracks on textiles," *Textile Research Journal,* vol. 83, no. 19, pp. 2023-2031, 2013/11/01 2013, doi: https://doi.org/10.1177/0040517513490063.

[102] A. Chlaihawi, B. Narakathu, S. Emamian, B. J. Bazuin, and M. Atashbar, "Development of printed and flexible dry ECG electrodes," *Sensing and Bio-Sensing Research,* vol. 20, 05/01 2018, doi: https://doi.org/10.1016/j.sbsr.2018.05.001.

[103] R. M. Kliegman, R. E. Behrman, H. B. Jenson, and B. M. Stanton, *Nelson textbook of pediatrics*. Elsevier Health Sciences, 2007.

[104] M. K. Marks, M. South, and J. B. Carlin, "Reference ranges for respiratory rate measured by thermistry (12-84 months)," *Archives of disease in childhood,* vol. 69, no. 5, pp. 569-572, 1993, doi: https://doi.org/10.1136/adc.69.5.569.

[105] L. Fanucci *et al.*, "Sensing Devices and Sensor Signal Processing for Remote Monitoring of Vital Signs in CHF Patients," *IEEE Transactions on Instrumentation and Measurement,* vol. 62, no. 3, pp. 553-569, 2013, doi: https://doi.org/10.1109/TIM.2012.2218681.

[106] G. M. Z. Weiner, J.; Kattwinkel, J.; Ades, A., *Textbook of Neonatal Resuscitation*, 7th ed. Elk Grove Village, IL, USA,: American Academy of Pediatrics, 2016.

[107] J. Wyllie, J. Bruinenberg, C. C. Roehr, M. Rüdiger, D. Trevisanuto, and B. Urlesberger, "European Resuscitation Council Guidelines for Resuscitation 2015: Section 7. Resuscitation and support of transition of babies at birth," *Resuscitation,* vol. 95, pp. 249-263, 2015, doi: https://doi.org/10.1016/j.resuscitation.2015.07.029.

[108] J. M. Perlman *et al.*, "Part 7: Neonatal Resuscitation," *Pediatrics,* vol. 136, no. Supplement 2, p. S120, 2015, doi: https://doi.org/10.1542/peds.2015-3373D.

[109] K. G. Voogdt, A. C. Morrison, F. E. Wood, R. M. van Elburg, and J. P. Wyllie, "A randomised, simulated study assessing auscultation of heart rate at birth," (in eng), *Resuscitation,* vol. 81, no. 8, pp. 1000-3, Aug 2010, doi: https://doi.org/10.1016/j.resuscitation.2010.03.021.

[110] R. Chitkara, A. K. Rajani, J. W. Oehlert, H. C. Lee, M. S. Epi, and L. P. Halamek, "The accuracy of human senses in the detection of neonatal heart rate during standardized simulated resuscitation: implications for delivery of care, training and technology design," (in eng), *Resuscitation,* vol. 84, no. 3, pp. 369-72, Mar 2013, doi: https://doi.org/10.1016/j.resuscitation.2012.07.035.

[111] M. Finster, M. Wood, and Srinivasa N. Raja, "The Apgar Score Has Survived the Test of Time," *Anesthesiology,* vol. 102, no. 4, pp. 855-857, 2005, doi: https://doi.org/10.1097/00000542-200504000-00022.

[112] J. Dawson, P. Davis, C. O'Donnell, C. O. Kamlin, and C. Morley, "Pulse oximetry for monitoring infants in the delivery room: A review," *Archives of disease in childhood. Fetal and neonatal edition,* vol. 92, pp. F4-7, 02/01 2007, doi: https://doi.org/10.1136/adc.2006.102749.

[113] O. Anton, R. Fernandez, E. Rendon-Morales, R. Aviles-Espinosa, H. Jordan, and H. Rabe, "Heart Rate Monitoring in Newborn Babies: A Systematic Review," *Neonatology,* vol. 116, pp. 1-12, 06/27 2019, doi: 10.1159/000499675.

[114] J. J. van Vonderen *et al.*, "Pulse Oximetry Measures a Lower Heart Rate at Birth Compared with Electrocardiography," *The Journal of Pediatrics,* vol. 166, no. 1, pp. 49-53, 2015/01/01/ 2015, doi: https://doi.org/10.1016/j.jpeds.2014.09.015.

[115] P. A. Johnson, P. Y. Cheung, T. F. Lee, M. O'Reilly, and G. M. Schmölzer, "Novel technologies for heart rate assessment during neonatal resuscitation at birth - A systematic review," (in eng), *Resuscitation,* vol. 143, pp. 196-207, Oct 2019, doi: https://doi.org/10.1016/j.resuscitation.2019.07.018.

[116] J. E. Linde *et al.*, "Normal Newborn Heart Rate in the First Five Minutes of Life Assessed by Dry-Electrode Electrocardiography," *Neonatology,* vol. 110, no. 3, pp. 231-237, 2016, doi: https://doi.org/10.1159/000445930.

[117] S. B. Choi *et al.*, "Conformable, Thin, and Dry Electrode for Electrocardiography Using Composite of Silver Nanowires and Polyvinyl

Butyral," *Electronic Materials Letters,* vol. 15, no. 3, pp. 267-277, 2019/05/01 2019, doi: https://doi.org/10.1007/s13391-019-00125-y.
[118] Q. Qin, J. Li, S. Yao, C. Liu, H. Huang, and Y. Zhu, "Electrocardiogram of a Silver Nanowire Based Dry Electrode: Quantitative Comparison With the Standard Ag/AgCl Gel Electrode," *IEEE Access,* vol. PP, pp. 1-1, 02/05 2019, doi: https://doi.org/10.1109/ACCESS.2019.2897590.
[119] L. Zhang *et al.*, "Fully organic compliant dry electrodes self-adhesive to skin for long-term motion-robust epidermal biopotential monitoring," *Nature Communications,* vol. 11, no. 1, p. 4683, 2020/09/17 2020, doi: https://doi.org/10.1038/s41467-020-18503-8.
[120] Y. Mei *et al.*, "Biocompatibility of sorbitol-containing polyesters. Part I: Synthesis, surface analysis and cell response in vitro," *Biomaterials,* vol. 25, no. 18, pp. 4195-4201, 2004/08/01/ 2004, doi: https://doi.org/10.1016/j.biomaterials.2003.10.087.
[121] Y. Gao *et al.*, "Heart Monitor Using Flexible Capacitive ECG Electrodes," *IEEE Transactions on Instrumentation and Measurement,* vol. 69, no. 7, pp. 4314-4323, 2020, doi: https://doi.org/10.1109/TIM.2019.2949320.
[122] L. A. Geddes and L. E. Baker, "The relationship between input impedance and electrode area in recording the ECG," *Medical and biological engineering,* vol. 4, no. 5, pp. 439-450, 1966/09/01 1966, doi: https://doi.org/10.1007/BF02476166.
[123] C. Jayoung, M. Jihye, J. Keesam, and C. Gilsoo, "An exploration of electrolessly Cu/Ni plated polyester fabrics as e-textiles," in *Ninth IEEE International Symposium on Wearable Computers (ISWC'05)*, 18-21 Oct. 2005 2005, pp. 206-207, doi: https://doi.org/10.1109/ISWC.2005.9.
[124] S. Yacoub, E. Novakov, P. Gumery, C. Gondran, and E. Siebert, "Noise analysis of NASICON ceramic dry electrodes," in *Proceedings of 17th International Conference of the Engineering in Medicine and Biology Society*, 20-23 Sept. 1995 1995, vol. 2, pp. 1553-1554 vol.2, doi: https://doi.org/10.1109/IEMBS.1995.579823.
[125] C. Assambo, A. Baba, R. Dozio, and M. Burke, "Determination of the parameters of the skin-electrode impedance model for ECG measurement," in *Proceedings of the 6th WSEAS Int. Conf. on Electronics, Hardware, Wireless and Optical Communications*, 2007, pp. 90-95.
[126] L. Rattfält, M. Lindén, P. Hult, L. Berglin, and P. Ask, "Electrical characteristics of conductive yarns and textile electrodes for medical applications," (in eng), *Med Biol Eng Comput,* vol. 45, no. 12, pp. 1251-7, Dec 2007, doi: https://doi.org/10.1007/s11517-007-0266-y.
[127] T. Degen and T. Loeliger, "An improved Method to continuously monitor the Electrode-Skin Impedance during Bioelectric Measurements," in *2007 29th Annual International Conference of the IEEE Engineering in Medicine and Biology Society*, 22-26 Aug. 2007 2007, pp. 6294-6297, doi: https://doi.org/10.1109/IEMBS.2007.4353794.
[128] J. Pan and W. J. Tompkins, "A Real-Time QRS Detection Algorithm," *IEEE Transactions on Biomedical Engineering,* vol. BME-32, no. 3, pp. 230-236, 1985, doi: https://doi.org/10.1109/TBME.1985.325532.
[129] F. Parola and J. García-Niebla, "Use of High-Pass and Low-Pass Electrocardiographic Filters in an International Cardiological Community and Possible Clinical Effects," *Advanced Journal of Vascular Medicine,* vol. 2, pp. 34-38, 12/01 2017.
[130] A. A. Fedotov, "Selection of Parameters of Bandpass Filtering of the ECG Signal for Heart Rhythm Monitoring Systems," *Biomedical Engineering,* journal article vol. 50, no. 2, pp. 114-118, July 01 2016, doi: https://doi.org/10.1007/s10527-016-9600-8.
[131] Y. G. Weiss and C. L. Sprung, "Patient data management systems in critical care," *Current Opinion in Critical Care,* vol. 2, no. 3, pp. 187-192, 1996.

[132] S. N. Asl, M. Oehler, and M. Schilling, "Noise Model of Capacitive and Textile Capacitive Noncontact Electrodes for Bioelectric Applications," *IEEE Transactions on Biomedical Circuits and Systems,* vol. 12, no. 4, pp. 851-859, 2018, doi: https://doi.org/10.1109/TBCAS.2018.2832287.

[133] C. E. Friedman and T. Lewis, "The Normal Size of the Heart Muscle Weight," *Acta Medica Scandinavica,* vol. 139, no. S257, pp. 15-19, 1951, doi: https://doi.org/10.1111/j.0954-6820.1951.tb13194.x.

[134] C. L. Ng and M. B. I. Reaz, "Characterization of Textile-Insulated Capacitive Biosensors," (in eng), *Sensors,* vol. 17, no. 3, p. 574, 2017, doi: https://doi.org/10.3390/s17030574.

[135] H. L. Chan, G. U. Chen, M. A. Lin, and S. C. Fang, "Heartbeat Detection Using Energy Thresholding and Template Match," in *2005 IEEE Engineering in Medicine and Biology 27th Annual Conference*, 17-18 Jan. 2006 2005, pp. 6668-6670, doi: https://doi.org/10.1109/IEMBS.2005.1616032.

[136] J. P. Martinez, R. Almeida, S. Olmos, A. P. Rocha, and P. Laguna, "A wavelet-based ECG delineator: evaluation on standard databases," *IEEE Transactions on Biomedical Engineering,* vol. 51, no. 4, pp. 570-581, 2004, doi: https://doi.org/10.1109/TBME.2003.821031.

[137] A. L. Goldberger *et al.*, "PhysioBank, PhysioToolkit, and PhysioNet: components of a new research resource for complex physiologic signals," (in eng), *Circulation,* vol. 101, no. 23, pp. E215-20, Jun 13 2000, doi: https://doi.org/10.1161/01.cir.101.23.e215.

[138] G. D. Clifford, J. Behar, Q. Li, and I. Rezek, "Signal quality indices and data fusion for determining clinical acceptability of electrocardiograms," *Physiological measurement,* vol. 33, pp. 1419-33, 08/17 2012, doi: https://doi.org/10.1088/0967-3334/33/9/1419.

[139] I. S. Murthy and G. S. Prasad, "Analysis of ECG from pole-zero models," (in eng), *IEEE Trans Biomed Eng,* vol. 39, no. 7, pp. 741-51, Jul 1992, doi: https://doi.org/10.1109/10.142649.

[140] J. G. Webster, *The physiological measurement handbook*. CRC Press, 2014.

[141] G. D. Clifford, F. Azuaje, and P. Mcsharry, *ECG statistics, noise, artifacts, and missing data* (Advanced methods and tools for ECG data analysis, no. 1). 2006, p. 18.

[142] P. Kligfield *et al.*, "Recommendations for the Standardization and Interpretation of the Electrocardiogram: Part I: The Electrocardiogram and Its Technology A Scientific Statement From the American Heart Association Electrocardiography and Arrhythmias Committee, Council on Clinical Cardiology; the American College of Cardiology Foundation; and the Heart Rhythm Society Endorsed by the International Society for Computerized Electrocardiology," *Journal of the American College of Cardiology,* vol. 49, no. 10, pp. 1109-1127, 2007/03/13/ 2007, doi: https://doi.org/10.1016/j.jacc.2007.01.024.

[143] H. Dore, R. Aviles-Espinosa, Z. Luo, O. Anton, H. Rabe, and E. Rendon-Morales, "Characterisation of Textile Embedded Electrodes for Use in a Neonatal Smart Mattress Electrocardiography System," *Sensors,* vol. 21, no. 3, p. 999, 2021, doi: https://doi.org/10.3390/s21030999.

[144] I. Odinaka, P. Lai, A. D. Kaplan, J. A. O. Sullivan, E. J. Sirevaag, and J. W. Rohrbaugh, "ECG Biometric Recognition: A Comparative Analysis," *IEEE Transactions on Information Forensics and Security,* vol. 7, no. 6, pp. 1812-1824, 2012, doi: https://doi.org/10.1109/TIFS.2012.2215324.

[145] J. Pettersson *et al.*, "Changes in high-frequency QRS components are more sensitive than ST-segment deviation for detecting acute coronary artery occlusion," *Journal of the American College of Cardiology,* vol. 36, no. 6, pp. 1827-1834, 2000, doi: https://doi.org/10.1016/S0735-1097(00)00936-0.

[146] E. Pueyo, L. Sornmo, and P. Laguna, "QRS slopes for detection and characterization of myocardial ischemia," *IEEE transactions on Biomedical Engineering,* vol. 55, no. 2, pp. 468-477, 2008, doi: https://doi.org/10.1109/TBME.2007.902228.

[147] Z. I. Attia *et al.*, "An artificial intelligence-enabled ECG algorithm for the identification of patients with atrial fibrillation during sinus rhythm: a retrospective analysis of outcome prediction," *The Lancet,* vol. 394, no. 10201, pp. 861-867, 2019/09/07/ 2019, doi: https://doi.org/10.1016/S0140-6736(19)31721-0.

[148] N. Nikolaev, Z. Nikolov, A. Gotchev, and K. Egiazarian, "Wavelet domain Wiener filtering for ECG denoising using improved signal estimate," in *2000 IEEE International Conference on Acoustics, Speech, and Signal Processing. Proceedings (Cat. No.00CH37100)*, 5-9 June 2000 2000, vol. 6, pp. 3578-3581 vol.6, doi: https://doi.org/10.1109/ICASSP.2000.860175.

[149] L. Smital, M. Vítek, J. Kozumplík, and I. Provazník, "Adaptive Wavelet Wiener Filtering of ECG Signals," *IEEE Transactions on Biomedical Engineering,* vol. 60, no. 2, pp. 437-445, 2013, doi: https://doi.org/10.1109/TBME.2012.2228482.

[150] J. P. C. D. Weerd, "Facts and Fancies About a Posteriori "Wiener" Filtering," *IEEE Transactions on Biomedical Engineering,* vol. BME-28, no. 3, pp. 252-257, 1981, doi: https://doi.org/10.1109/TBME.1981.324697.

[151] A. Baranchuk *et al.*, "Electromagnetic interference of communication devices on ECG machines," (in eng), *Clin Cardiol,* vol. 32, no. 10, pp. 588-92, Oct 2009, doi: https://doi.org/10.1002/clc.20459.

[152] R. van der Togt, E. Jan van Lieshout, R. Hensbroek, E. Beinat, J. M. Binnekade, and P. J. M. Bakker, "Electromagnetic Interference From Radio Frequency Identification Inducing Potentially Hazardous Incidents in Critical Care Medical Equipment," *JAMA,* vol. 299, no. 24, pp. 2884-2890, 2008, doi: https://doi.org/10.1001/jama.299.24.2884.

[153] S. T. Beardsmore-Rust, R. J. Prance, A. Aydin, H. Prance, C. J. Harland, and P. B. Stiffell, "Signal specific electric potential sensors for operation in noisy environments," *Journal of Physics: Conference Series,* vol. 178, no. 1, 2009, doi: https://doi.org/10.1088/1742-6596/178/1/012011.

[154] J. J. Larsen, E. Dalgaard, and E. Auken, "Noise cancelling of MRS signals combining model-based removal of powerline harmonics and multichannel Wiener filtering," *Geophysical Journal International,* vol. 196, no. 2, pp. 828-836, 2013, doi: https://doi.org/10.1093/gji/ggt422.

[155] M. Kandadai, J. Raymond, and G. Shaw, "Comparison of electrical conductivities of various brain phantom gels: Developing a 'Brain Gel Model'," *Materials science & engineering. C, Materials for biological applications,* vol. 32, pp. 2664-2667, 12/01 2012, doi: https://doi.org/10.1016/j.msec.2012.07.024.

[156] S. Gabriel, R. Lau, and C. Gabriel, "The dielectric properties of biological tissues: II. Measurements in the frequency range 10 Hz to 20 GHz," *Physics in medicine & biology,* vol. 41, no. 11, p. 2251, 1996, doi: https://doi.org/10.1088/0031-9155/41/11/002.

[157] M. Griffin, B. Leung, Y. Premakumar, M. Szarko, and P. Butler, "Comparison of the mechanical properties of different skin sites for auricular and nasal reconstruction," *Journal of Otolaryngology-Head & Neck Surgery,* vol. 46, no. 1, pp. 1-6, 2017, doi: https://doi.org/10.1186/s40463-017-0210-6.

[158] V. Normand, D. L. Lootens, E. Amici, K. P. Plucknett, and P. Aymard, "New insight into agarose gel mechanical properties," *Biomacromolecules,* vol. 1, no. 4, pp. 730-738, 2000, doi: https://doi.org/10.1021/bm005583j.

[159] G. B. Moody and R. G. Mark, "The impact of the MIT-BIH arrhythmia database," (in eng), *IEEE Eng Med Biol Mag,* vol. 20, no. 3, pp. 45-50, May-Jun 2001, doi: https://doi.org/10.1109/51.932724.

[160] S. Chouakri, F. Bereksi-Reguig, S. Ahmaidi, and O. Fokapu, "Wavelet denoising of the electrocardiogram signal based on the corrupted noise estimation," in *Computers in Cardiology, 2005*, 2005: IEEE, pp. 1021-1024, doi: https://doi.org/10.1109/CIC.2005.1588284.

[161] S. Saxena, R. Jais, and M. K. Hota, "Removal of powerline interference from ECG signal using FIR, IIR, DWT and NLMS adaptive filter," in *2019 International Conference on Communication and Signal Processing (ICCSP)*, 2019: IEEE, pp. 0012-0016, doi: https://doi.org/10.1109/ICCSP.2019.8698112.

[162] G. Tang and A. Qin, "ECG de-noising based on empirical mode decomposition," in *2008 The 9th International Conference for Young Computer Scientists*, 2008: IEEE, pp. 903-906, doi: https://doi.org/10.1088/0031-9155/41/11/002.